INFORMATION TO USERS

This manuscript has been reproduced from the microfilm master. UMI films the text directly from the original or copy submitted. Thus, some thesis and dissertation copies are in typewriter face, while others may be from any type of computer printer.

The quality of this reproduction is dependent upon the quality of the copy submitted. Broken or indistinct print, colored or poor quality illustrations and photographs, print bleedthrough, substandard margins, and improper alignment can adversely affect reproduction.

In the unlikely event that the author did not send UMI a complete manuscript and there are missing pages, these will be noted. Also, if unauthorized copyright material had to be removed, a note will indicate the deletion.

Oversize materials (e.g., maps, drawings, charts) are reproduced by sectioning the original, beginning at the upper left-hand corner and continuing from left to right in equal sections with small overlaps. Each original is also photographed in one exposure and is included in reduced form at the back of the book.

Photographs included in the original manuscript have been reproduced xerographically in this copy. Higher quality 6" x 9" black and white photographic prints are available for any photographs or illustrations appearing in this copy for an additional charge. Contact UMI directly to order.

UMI®

Bell & Howell Information and Learning
300 North Zeeb Road, Ann Arbor, MI 48106-1346 USA
800-521-0600

d-MUSIC: An Algorithm for Single Snapshot Direction-of-Arrival Estimation

by

Randy Keith Howell
B. Eng., Memorial University of Newfoundland, 1986
M. Eng., Memorial University of Newfoundland, 1990

A Dissertation Submitted in Partial Fulfillment of the
Requirements for the Degree of

DOCTOR OF PHILOSOPHY

in the Department of Electrical and Computer Engineering

We accept this dissertation as conforming
to the required standard

Dr. R. L. Kirlin, Supervisor (Department of Electrical and Computer Engineering)

Dr. P. Dreissen, Departmental Member (Department of Electrical and Computer Engineering)

Dr. F. El Guibaly, Departmental Member (Department of Electrical and Computer Engineering)

Dr. R. Chapman, Outside Member (School of Earth and Ocean Sciences)

Dr. F. Li, External Examiner (Department of Electrical and Computer Engineering, Portland State University)

Supervisor: Dr. R. L. Kirlin

ABSTRACT

The d-MUSIC algorithm estimates the direction-of-arrival of two closely spaced sources using a single array snapshot. To make the problem full rank, d-MUSIC utilizes additional information, specifically the derivative of the input snapshot vector. The combined vector set yields a rank two signal space projector that can be used to estimate the source directions. To construct this projector, an estimate for the center of the target cluster is required. In many radar low angle tracking problems involving distant aircraft, the center of the target plus multipath cluster is known *a priori* (flat earth approximation). Otherwise, d-MUSIC estimates the source bearings for a grid of center angles and selects the grid point where the signal space of the solution is most consistent with the input vector.

Following the approach of Stoica and Nehorai [10], a theoretical estimate for the d-MUSIC error variance is derived and compared to the Cramér-Rao bound for the case of a known cluster centroid (typical air traffic control problem). The algorithm nearly attains the Cramér-Rao bound, displaying a low sensitivity to signal correlation. A number of Monte Carlo tests are also performed to compare the performance of MUSIC to the two d-MUSIC algorithms (cluster center known or unknown). These tests demonstrate that both versions of d-MUSIC is highly resilient to signal correlation whereas MUSIC is not.

The algorithm is field tested using data from a X-band radar tracking a low flying helicopter. The receive array is a 6 channel vertical linear array of horns with an array aperture of nearly 19 wavelengths. As the flat earth approximation is not appropriate to this experiment the grid search version of d-MUSIC is employed (unknown cluster center). The array is calibrated using the method of Wylie *et al.* [30] to restore the Toeplitz structure of the covariance matrix.

With a spacing of 16% to 35% of a beamwidth between the direct and multipath signals, the d-MUSIC rms error for the source spacing is 9.6% of a beamwidth for the 4 data collections while MUSIC resolved the two signals for 2 of the 4 cases with a rms error of 18.1%.

Examiners:

Dr. R. L. Kirlin, Supervisor (Department of Electrical and Computer Engineering)

Dr. P. Dreissen, Departmental Member (Department of Electrical and Computer Engineering)

Dr. F. El Gaibaly, Departmental Member (Department of Electrical and Computer Engineering)

Dr. R. Chapman, Outside Member (School of Earth and Ocean Sciences)

Dr. F. Li, External Examiner (Department of Electrical and Computer Engineering, Portland State University)

TABLE OF CONTENTS

ABSTRACT ii

TABLE OF CONTENTS iv

LIST OF TABLES vii

LIST OF FIGURES viii

LIST OF SYMBOLS x

LIST OF ACRONYMS xiv

ACKNOWLEDGMENTS xv

DEDICATION xvi

1 INTRODUCTION 1

1.1 Problem Outline: Low Angle Tracking 1

1.2 d-MUSIC Objectives 4

1.3 Array Calibration 7

1.4 Thesis Organization 9

2 THE d-MUSIC ALGORITHM 10

2.1 Preamble 10

2.2 The Linear Array Signal Model 10

2.3 MUSIC 13

2.4 The Linear Array Direction Vector Derivative 17

2.5 d-MUSIC 19

2.6 Application to the Multi-Source Multipath Problem 25

2.7 Notes on the Single Source Problem 26

3 PERFORMANCE ANALYSIS **27**

3.1 Preamble 27

3.2 Performance in the Noiseless Case 29

3.3 Signal Model 34

3.4 The Statistics of the d-MUSIC Null Spectrum 36

3.5 Error Statistics 39

3.6 The Cramér-Rao Bound (CRB) and MUSIC Errors 42

3.7 Error Analysis: Comparison to MUSIC and the CRB 43

3.8 Simulation Tests 52
3.8.1 Setup 52
3.8.2 Known Cluster Centroid 54
3.8.3 Unknown Cluster Centroid 56

4 ARRAY CALIBRATION **61**

4.1 Preamble: Sources of Array Errors 61

4.2 Toeplitz Approximation 65

4.3 Blind Calibration via the Toeplitz Property 66

4.4 Simulation Examples 69

5 EVALUATION TESTS USING EARS **73**

5.1 Overview 73

5.2 The EARS Radar 74

5.3 Osborne Head Experiment 75
5.3.1 Experiment Setup 75
5.3.2 Range Response 76
5.3.3 Doppler Analysis 78

5.4 Calibration Analysis 81
5.4.1 Need for Calibration 81
5.4.2 Calibration Issues 82
5.4.3 Calibration Results 84

5.5 d-MUSIC and MUSIC Analysis 88

6 CONCLUSIONS **93**

6.1 Summary 93

6.2 Achievements 95

6.3 Recommendations 95

BIBLIOGRAPHY **97**

A APPLICATION TO PLANAR ARRAYS **102**

A.1 Problem Outline 102

A.2 Rectangular Planar Array Geometry 103

A.3 The Rectangular Planar Array Direction Vector Derivative 106

A.4 Low Angle Specular Multipath 108
A.4.1 Array Parallel to Surface 108
A.4.2 Array Perpendicular to Surface 109

B CRAMÉR-RAO BOUND DERIVATION **110**

B.1 Preamble 110

B.2 Problem Statement 111

B.3 List of Modifications to Derive the CRB 112

B.4 Conversion to Thesis Notation 115

LIST OF TABLES

Table 2-1 d-MUSIC Algorithm 24

Table 3-1 Mean and Standard Deviation of $\dot{S}(\gamma_n)$ and $\ddot{S}(\gamma_n)$ for $K = 100$ snapshots of a 10 element array with $d = \lambda/2$, source spacing of 2°, signal weights $k_1 = k_2 = 1$ and no array or ϕ errors 40

Table 3-2 Linear array structure for the theoretical error analysis 44

Table 3-3 Simulation Model 53

Table 3-4 Summary of Simulation Results 54

Table 4-1 Array Model for Array Calibration Tests 69

Table 5-1 List of EARS Data Files 76

Table 5-2 RMS Calibration Errors 87

Table 5-3 d-MUSIC and MUSIC error summary (% BW denotes % of a beamwidth) 91

LIST OF FIGURES

Figure 1.1 Specular multipath geometry 2

Figure 2-1 Linear array geometry 11

Figure 3.1 Taylor series amplitude distortion for a 10 sensor array with array spacing $d = \lambda/2$. 33

Figure 3.2 MUSIC and d-MUSIC spectra for a 10 sensor array, $d = \lambda/2$, and a 2° source spacing. 34

Figure 3.3 First and second derivative of $S(\theta)$ for a 10 sensor array ($d=\lambda/2$) and a 2° source spacing 40

Figure 3.4 d-MUSIC variance and $var(\varepsilon)_{CR,\,\phi=0}$ for $\sigma^2 = 0.1$ 46

Figure 3.5 MUSIC variance and $var(\varepsilon)_{CR}$ for $\sigma^2 = 0.1$ 46

Figure 3.6 d-MUSIC variance and $var(\varepsilon)_{CR,\,\phi=0}$ for $\sigma^2 = 1$ 48

Figure 3.7 MUSIC variance and $var(\varepsilon)_{CR}$ for $\sigma^2 = 1$ 48

Figure 3.8 d-MUSIC variance and $var(\varepsilon)_{CR,\,\phi=0}$ for $\sigma^2 = 10$ 49

Figure 3.9 MUSIC variance and $var(\varepsilon)_{CR}$ for $\sigma^2 = 10$ 49

Figure 3.10 d-MUSIC and MUSIC variance for $\sigma^2 = 0.1$ and $\chi = 160°$ (signals nearly subtract) 51

Figure 3.11 d-MUSIC variance with array errors for $\sigma^2 = 0.1$ and $\chi = 0°$ 52

Figure 3.12 d-MUSIC analysis of simulated EARS data for $\chi = 90°$ and $\sigma^2 = 0.1$ 55

Figure 3.13 MUSIC analysis of simulated EARS data for $\chi = 90°$ and $\sigma^2 = 0.1$ 55

Figure 3.14 d-MUSIC analysis of simulated EARS data for $\chi = 0°$ and $\sigma^2 = 0.1$ 55

Figure 3.15 d-MUSIC analysis of simulated EARS data for $\chi = 90°$ and $\sigma^2 = 0.5$ 57

Figure 3.16 MUSIC analysis of simulated EARS data for $\chi = 90°$ and $\sigma^2 = 0.5$ 57

Figure 3.17 d-MUSIC analysis of simulated EARS data for $\chi = 0°$ and $\sigma^2 = 0.5$ 57

Figure 3.18 d-MUSIC analysis of simulated EARS data for $\chi = 0°$ and $\sigma^2 = 1$ 58

Figure 3.19 d-MUSIC analysis of simulated EARS data for $\chi = 90°$ and $\sigma^2 = 4$ 58

Figure 3.20 d-MUSIC analysis with unknown ϕ for simulated EARS data with $\chi = 90°$ and $\sigma^2 = 0.5$ 58

Figure 3.21 d-MUSIC analysis with unknown ϕ for simulated EARS data with $\chi = 0°$ and $\sigma^2 = 0.5$ 60

Figure 3.22 d-MUSIC analysis with unknown ϕ for simulated EARS data with $\chi = 90°$ and $\sigma^2 = 1$ 60

Figure 3.23 d-MUSIC analysis with unknown ϕ for simulated EARS data with $\chi = 0°$ and $\sigma^2 = 1$ 60

Figure 4.1 Calibration magnitude estimate for one run with 20 dB SNR 71

Figure 4.2 Calibration phase estimate for one run with 20 dB SNR 71

Figure 4.3 RMS error of magnitude estimate for 100 runs at 20 dB SNR 72

Figure 4.4 RMS error of phase estimate for 100 runs at 20 dB SNR 72

Figure 5.1 EARS radar plus Sea King helicopter 74

Figure 5.2 EARS 8-element vertical receive array of horns aimed at a cylindrical reflector 75

Figure 5.3 Range plot of channel 3 IF data power for each 100 pulse block of file fort.7 77

Figure 5.4 Range plot of I/Q data power of the 0° beam for each 100 pulse block of file fort.7 77

Figure 5.5 Doppler versus range of the 0° beam for block 19 of file fort.7 79

Figure 5.6 Velocity (Doppler) spectrum of range bin 98 (target) 80

Figure 5.7 Velocity (Doppler) spectrum of range bins 37 to 57 (clutter) 80

Figure 5.8 Phase of the principal eigenvector of file fort.7 for blocks of 100 pulses 82

Figure 5.9 Estimate of array errors for file fort.6: a) magnitude versus channel for each data block (19 curves); b) phase versus data block for channels 4 to 8 (5 curves). 85

Figure 5.10 Estimate of array errors for file fort.7: a) magnitude versus channel for each data block (19 curves); b) phase versus data block for channels 4 to 8 (5 curves). 85

Figure 5.11 Estimate of array errors for file fort.18: a) magnitude versus channel for each data block (19 curves); b) phase versus data block for channels 4 to 8 (5 curves). 86

Figure 5.12 Estimate of array errors for file fort.19: a) magnitude versus channel for each data block (19 curves); b) phase versus data block for channels 4 to 8 (5 curves). 86

Figure 5.13 Source spacing estimates for file fort.6: a) d-MUSIC; b) MUSIC. 89

Figure 5.14 Source spacing estimates for file fort.7: a) d-MUSIC; b) MUSIC. 89

Figure 5.15 Source spacing estimates for file fort.18: a) d-MUSIC; b) MUSIC. 90

Figure 5.16 Source spacing estimates for file fort.19: a) d-MUSIC; b) MUSIC. 90

Figure A.1 Rectangular planar array geometry 103

LIST OF SYMBOLS

Mathematical Functions and Operators

$(\bullet)^T$	Transpose
$(\bullet)^*$	Complex conjugate
$(\bullet)^H$	Hermitian transpose (complex conjugate transpose)
$\angle x$	Phase angle of x
$\mathbf{A} \bullet \mathbf{B}$	Hadamard (element-by-element) product of matrices **A** and **B**
(:, n)	Notation denoting the *n*th column of a matrix
$[\bullet]_{n,n}$	Notation representing element (n,n) of a matrix
diag{•}	Converts a vector into a diagonal matrix
e^x	Exponential function, $e^1 = 2.7182818$
E{•}	Statistical expectation operator
$\log_{10}(x)$	Base 10 logarithm of x
$O\{\|x\|^n\}$	Denotes order with respect to nth power of x
Re{•}	Real component of a complex quantity
std{•}	Standard deviation
tr{•}	Matrix trace (sum of main diagonal)
var{•}	Variance

Latin Symbols

$\boldsymbol{\theta}$	N × 1 vector of ones
1	N x 1 vector of ones
$\mathbf{a}(\theta)$	Direction vector (Array response to a signal arriving along θ)
$\dot{\mathbf{a}}(\theta)$	Derivative of $\mathbf{a}(\theta)$ with respect to α, $\dot{\mathbf{a}}(\theta) = \frac{d\,\mathbf{a}(\theta)}{d\,\alpha} = \mathbf{D}\,\mathbf{a}(\theta)$
$\ddot{\mathbf{a}}(\theta)$	Second derivative of with respect to α, $\ddot{\mathbf{a}}(\theta) = \mathbf{D}\,\mathbf{D}\,\mathbf{a}(\theta)$
A	$\mathbf{A} = \left[\mathbf{a}(\theta_1)\ \mathbf{a}(\theta_2)\ \ldots\ \mathbf{a}(\theta_L)\right]$, set of L steering vectors for L sources
$\mathbf{a}_M(\theta)$	Array manifold, $\mathbf{a}_M(\theta) = \mathbf{G}(\theta)\mathbf{a}(\theta)$ represents the array response to a signal arriving along direction θ with array calibration error weights $\mathbf{G}(\theta)$

c	$c = (\mathbf{u}^H\mathbf{u})(\dot{\mathbf{u}}^H\dot{\mathbf{u}})$ where $\mathbf{u}$ and $\dot{\mathbf{u}}$ are the d-MUSIC signal space vectors (see equations (3-19) and (3-20))
C	Velocity of light
$\mathbf{c}_A$	Array calibration vector
$\mathbf{C}_A$	Array calibration matrix, $\mathbf{C}_A = \text{diag}\{\mathbf{c}_A\}$
d	Sensor spacing for a vertical linear array
D	Linear array derivative operator, $\mathbf{D} = j\,\text{diag}\{(N-1)/2 - [0\ 1 \cdots N-1]^T\}$
$E\{\varepsilon_n\}_{d-MU}$	d-MUSIC error (bias)
$\mathbf{g}$	Array calibration error vector (complex),
$\mathbf{G}$	Diagonal matrix of array error weights, $\mathbf{G} = \text{diag}(\mathbf{g})$
$\mathbf{I}$	Identity matrix
j	Imaginary number, j = sqrt(-1)
$\mathbf{J}$	Reverse permutation matrix (ones along anti-diagonal, zeros elsewhere)
k_1, k_2	Complex gain constants for the direct path and multipath signals, i.e., combined signal is $\mathbf{v} = k_1\mathbf{a}(\theta_T) + k_2\mathbf{a}(\theta_R)$
K	Number of array snapshots
L	Number of sources
$\mathbf{n}(t)$	N×1 array noise vector at time t
$\mathbf{n}$	N x 1 array noise vector for either a single snapshot or a single snapshot after coherent processing of a K sample long time series
$\mathbf{n}_d$	d-MUSIC noise vector, $\mathbf{n}_d = (\mathbf{I} + \mathbf{J})\mathbf{n}$ (spatially correlated)
N	Number of vertical linear array sensors
p	Rank of $\mathbf{R}$
$\mathbf{P}_S$	d-MUSIC signal space projector
$\hat{\mathbf{P}}_S$	Estimate for P_S
$\hat{\mathbf{P}}_N$	d-MUSIC null space projector estimate, $\hat{\mathbf{P}}_N = c\,\mathbf{I} - c\,\hat{\mathbf{P}}_S$
$\mathbf{q}_i$	Eigenvector i of $\mathbf{R}$ (unitary)
$\mathbf{Q}$	Eigenvectors of $\mathbf{R}$. $\mathbf{QQ}^H = \mathbf{Q}^H\mathbf{Q} = \mathbf{I}$ and $\mathbf{Q} = [\mathbf{q}_1\ \mathbf{q}_2 \cdots \mathbf{q}_N]$
$\mathbf{R}$	Array covariance matrix, $\mathbf{R} = E\{\mathbf{x}\,\mathbf{x}^H\}$
$\mathbf{R}_C$	Calibrated covariance matrix, $\mathbf{R}_C = \mathbf{C}_A\mathbf{R}\mathbf{C}_A^H$

$\mathbf{R}_{fb}$	$\mathbf{R}_{fb} = (\mathbf{R} + \mathbf{J}\,\mathbf{R}^{*}\mathbf{J})/2$
$s_R(t)$	Target signal arriving from direction θ_R
$s_T(t)$	Target signal arriving from direction θ_T
$\mathbf{s}(t)$	$\mathbf{s}(k) = [s_1(k)\ s_2(k)\ \ldots\ s_L(k)]^T$, set of L waveforms for L sources
$\mathbf{S}$	Signal covariance matrix, $\mathbf{S} = E\{\mathbf{s}\,\mathbf{s}^H\}$
$\mathbf{S}_{fb}$	$\mathbf{S}_{fb} = (\mathbf{S} + \mathbf{J}\,\mathbf{S}^{*}\mathbf{J})/2$
$S_{MUSIC}(\theta)$	MUSIC spectrum
$S(\theta)$	d-MUSIC null spectrum, $S(\theta) = \mathbf{a}^H(\theta)(\mathbf{I} - \mathbf{P}_s)\mathbf{a}(\theta)$
$\dot{S}(\theta)$	First derivative of d-MUSIC null spectrum, $\dot{S}(\theta) = \frac{dS(\theta)}{d\alpha}$
$\ddot{S}(\theta)$	Second derivative of d-MUSIC null spectrum, $\ddot{S}(\theta) = \frac{d^2S(\theta)}{d\alpha^2}$
t	Time
$\mathbf{u}, \dot{\mathbf{u}}$	d-MUSIC signal space vectors, see equations (3-19)m and (3-20)
$\mathbf{u}_S, \dot{\mathbf{u}}_S$	Signal components of $\mathbf{u}, \dot{\mathbf{u}}$ (zero noise)
$\mathbf{V}_R(\phi)$	Vector rotation operator, $\mathbf{V}_R(\phi) = \text{diag}\{\mathbf{a}^*(\theta)\}$. The product $\mathbf{V}_R(\phi)\mathbf{a}(\theta)$ rotates the vector $\mathbf{a}(\theta)$ to point in the direction $\eta = \sin^{-1}\{\sin\theta - \sin\phi\}$
$\mathbf{x}(t)$	N×1 array snapshot vector at time t
$\mathbf{W}$	Noise covariance matrix, $\mathbf{W} = E\{\mathbf{n}\,\mathbf{n}^H\}$
$\mathbf{v}$	A signal space vector, $\mathbf{v} = k_1\mathbf{a}(\theta_T) + k_2\,\mathbf{a}(\theta_R)$ where k_1 and k_2 are constants
$\dot{\mathbf{v}}$	$\dot{\mathbf{v}} = \mathbf{D}\,\mathbf{v} = k_1\dot{\mathbf{a}}(\theta_T) + k_2\dot{\mathbf{a}}(\theta_R)$
$\text{var}(\varepsilon_n)_{MU}$	MUSIC error variance
$\text{var}\{\varepsilon_n\}_{d-MU}$	d-MUSIC error variance
$\text{var}(\varepsilon_n)_{CR}$	Asymptotic Cramér-Rao lower bound (CRB) assuming no *a priori* information of signal directions with standard forward-backward averaging of the form $\mathbf{R}_{fb} = (\mathbf{R} + \mathbf{J}\,\mathbf{R}^{*}\mathbf{J})/2$
$\text{var}(\varepsilon)_{CR,\phi=0}$	Asymptotic Cramér-Rao lower bound (CRB) for the case of 2 sources when the cluster center is known

Greek Symbols

α	$\alpha=2\pi d \sin(\theta)/\lambda$, sensor-to-sensor phase shift of a signal arriving along θ
α_T	$\alpha_T = 2\pi d \sin(\theta_T)/\lambda$
α_R	$\alpha_R = 2\pi d \sin(\theta_R)/\lambda$
β	Vertical array tilt angle (from vertical)
$\hat{\beta}$	Estimate for β
γ	$\gamma = (\theta_T - \theta_R)/2$
δ_α	$\delta_\alpha = \alpha_T - \alpha_R$
ε_n	d-MUSIC measurement error for source n
θ_T	Target elevation angle (see Figure 1.1)
θ_R	Multipath depression angle (see Figure 1.1)
λ	Radar wavelength
λ_i	Eigenvalue i of **R**
Λ	Diagonal matrix of eigenvalues (λ_i) for **R**
μ	Phase of N × 1 vector **g** (array calibration error)
π	3.1415926535897....
ρ	Surface reflection coefficient (dependent on grazing angle)
σ^2	Noise variance
τ	Specular multipath time delay
ϕ	Center of a 2 source cluster, i.e., $\phi = (\theta_T + \theta_R)/2$
$\hat{\phi}$	Estimate for ϕ
χ	Phase difference between the direct path and specular multipath signals
ω	Target Doppler shift (rad/sec)

LIST OF ACRONYMS

CRB	Cramér-Rao bound
dB	Decibels
d-MUSIC	Derivative-MUltiple SIgnal Classification
EARS	Experimental Array Radar System
EVD	Eigenvector decomposition
FFT	Fast Fourier Transform
Hz	Hertz
I/Q	In-phase (I) and Quadrature (Q) (i.e., complex data)
IF	Intermediate frequency
kph	Kilometers per hour
MUSIC	MUltiple SIgnal Classification
Pre-amp	Pre-amplifier
PRF	Pulse repetition frequency
RCS	Radar cross section
RMS	Root-mean-square (equivalent to standard deviation)
SCR	Signal-to-clutter ratio
SNR	Signal-to-noise ratio
SVD	Singular value decomposition
T/R	Transmit/receive
2-D	Two dimensional
% BW	Percentage of a Rayleigh beamwidth

ACKNOWLEDGMENTS

It has been my pleasure to have met and worked with many fine people in the course of this work. My thesis supervisor Dr. R. Lynn Kirlin has been a big help of course. His advice has helped me to "keep me on track" and his encouragement gave me much needed confidence boosts at the right times. His patience is especially appreciated as my thesis has been delayed for some time as I fell into the classic trap of writing a thesis while holding down a full-time job.

I would like to extend my special thanks to the people of Raytheon Canada Limited where I have worked for the last 3 years. Through Raytheon I secured a contract with Defence Research Establishment Ottawa (DREO) which provided the data for my thesis. Dr. Tony Ponsford and Mr. Peter Scarlett have always been big boosters of my d-MUSIC work. It helped me get my job at Raytheon so it's paying dividends already.

By giving me access to their data archives, DREO gave me the opportunity to really test my algorithm. I would like to thank Dr. Mylène Toulgoat (now with Nortel) and Mr. Edwin Riseborough of DREO for awarding me with a research contract to test my thesis work. Simulated data only gets you so far in life.

By discussing your work with others you benefit from their comments and their encouragement, and as you struggle to explain your ideas to them it forces you to sharpen your arguments and to dig for that deeper insight. For the many stimulating conversations I have enjoyed I would like to thank Mr. Peter Weber, Dr. Tarun Bhattacharya, Dr. Ambighairajah Yasotharan (Yaso), Dr. Rex Andrews, Mr. Reza Dizaji, Mr. Ken Hickey, Mr. Eugene Guy, Dr. Eric Hung, Mr. Edwin Riseborough and Mr. Peter Scarlett.

DEDICATION

My parents were a big part of my life and much of who I am today was shaped by their love for me and their hope for my happiness. I would like to dedicate this dissertation to the memory of my parents, Lillian Margaret and Alexander Joseph Howell. I know they would be very proud of me.

1 Introduction

1.1 Problem Outline: Low Angle Tracking

A signal processing problem of great interest in sensor array processing is that of estimating the direction-of-arrival (DOA) of a set of closely spaced plane wave signals received by an array of sensors. High resolution beamforming algorithms such as MUSIC [1, 2] can successfully resolve closely spaced signals but its performance rapidly degrades with decreasing signal-to-noise or if the sources within the cluster are coherent.

One of the best known examples in this regard for radar applications is that of estimating the altitude of a low flying aircraft in a multipath environment. Figure 1.1 illustrates the specular multipath low angle tracking problem. The signal model for this case can be represented as

$$\mathbf{x}(t) = s_T(t)\,\mathbf{a}(\theta_T) + \rho\, s_R(t)\,\mathbf{a}(\theta_R) + \mathbf{n}(t) \tag{1-1}$$

where

$\mathbf{x}(t)$	N×1 array snapshot vector at time t
$\mathbf{n}(t)$	N×1 array noise vector at time t
$s_T(t)$	Target signal arriving from direction θ_T
$s_R(t)$	Target signal arriving from direction θ_R
θ_T	Target elevation angle
θ_R	Multipath depression angle
ρ	Surface reflection coefficient (dependent on grazing angle)
$\mathbf{a}(\theta)$	Direction vector (Array phase/amplitude response to a signal arriving along θ)

The signals received by the radar will consist of a target echo arriving via a direct line-of-sight path at elevation angle θ_T, and another target echo arriving via a surface reflected path at a depression angle of θ_R. For low altitude targets the time delay between the two signals will be small resulting in potentially high signal correlation. Low target height will also result in a small difference between θ_T and θ_R, greatly complicating the problem of estimating the true target elevation angle θ_T.

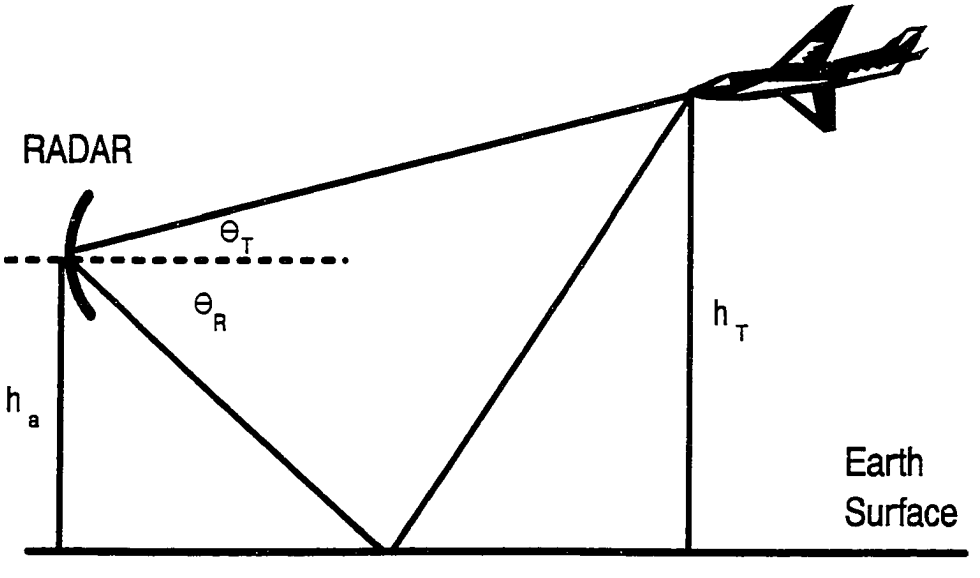

Figure 1.1 Specular multipath geometry

For a discussion of the general multipath problem (both specular and diffuse) in radar applications the reader is referred to [3, chap. 6]. Though it can be applied in other scenarios the application of interest for the d-MUSIC algorithm is the radar low angle tracking problem.

If the sources are closely spaced there will be a wide disparity between the eigenvalues (or signal strength) of the signal space eigenvectors of the data covariance matrix $\mathbf{R}$ [4]. As the noise power for most beamforming problems is equally distributed over all spatial dimensions (typical of Gaussian noise) then there is also a wide disparity between the signal-to-noise ratio (SNR) of each eigenvector. In that event very low noise power and/or very large signal strength is required to ensure that each signal space eigenvector has good SNR. Otherwise, the problem becomes rank deficient as the number of signal space eigenvectors that can be accurately estimated is less than the number of sources.

The covariance matrix can also become rank deficient if the sources within the cluster are correlated. In this event the disparity between the eigenvalues of the signal space vectors increases, exacerbating the requirement for high SNR. In the extreme, if any of the sources are coherent (having a correlation coefficient of ± 1) the rank of the covariance matrix will always be less then the number of sources, even in the noiseless case.

Another complication to the high resolution problem faced by both radar and sonar systems is that typically only a few or possibly one snapshot vector is available to determine the source bearings [5-7]. A limited data collection time is a fact of life in many sensor platforms. Even if the sources are uncorrelated a small number of snapshots may prove insufficient to average the cross correlation terms to zero. The signal directions could be estimated from a single snapshot using a Bayesian technique [6] but at the cost of a computationally intensive non-linear optimization procedure to arrive at a solution. A single snapshot divided into overlapping sub-arrays could be used to build a covariance matrix [7] but at a significant cost in array resolution along with the requirement to use a expensive eigenvector decomposition to estimate the signal and noise spaces.

Even if a large number of time series samples are available there is no guarantee that this set of samples will be at the disposal of the high resolution algorithm to form a covariance matrix. Often, some form of coherent processing (e.g., a FFT to estimate the Doppler spectrum) is required to isolate the target echo from the contending clutter/interference background. This is a fair trade-off as detection must take precedence over parameter estimation. If the target is

constrained to a single Doppler bin then the target Doppler bin for all sensors represents a single array snapshot vector.

Combined, the problems of source correlation and a low number of snapshots will often lead to a rank deficient problem unless additional information is employed. A readily available source of extra information are the spatial derivatives of the known signal space vectors. For closely-spaced sources one source direction vector is related to another source vector and its derivatives via a Taylor series expansion. As such the derivative vectors represent an additional body of information compatible with the signal space span of the set of source vectors.

Derivative information have been employed in other high resolution algorithms. Important insights into the use of derivatives was outlined in the scorefunction technique of [8] . Taking the derivative of the Maximum Likelihood (ML) scorefucntion, a MUSIC-like high resolution algorithm was derived with a superior resolution capability. The MUSIC algorithm seeks to find the bearing(s) θ that minimizes the MUSIC spectrum $\mathbf{a}^{\mathbf{H}}(\theta)\mathbf{V}_N\mathbf{V}_N^{\mathbf{H}}\mathbf{a}(\theta)$ where $\mathbf{a}(\theta)$ is the array response at bearing θ and $\mathbf{V}_N$ is the set of noise space eigenvectors. In [8] the solution points are the set of values of θ that minimizes $\mathbf{a}^{\mathbf{H}}(\theta)\mathbf{V}_N\mathbf{V}_N^{\mathbf{H}}\dot{\mathbf{a}}(\theta)$ where $\dot{\mathbf{a}}(\theta)$ is the derivative of $\mathbf{a}(\theta)$ with respect to the sensor-to-sensor phase shift $\alpha = 2\pi d \sin(\theta)/\lambda$. The algorithm has better resolution than MUSIC but has the drawback of ambiguous nulls. For example, when resolving 2 sources the technique would report 3 peaks, one midway between the 2 sources (not a serious operation issue for just two sources). The algorithm was intended to be more instructive than useful, leading to a better understanding of the minimizing functions in the various subspace high resolution algorithms. In that regard it has certainly been an inspiration here.

In this work, derivative information is employed to construct a second signal space vector using a single array snapshot vector as input. The two vectors are used to construct a rank two signal space projector matrix to replace the projector used in the MUSIC algorithm constructed from the covariance matrix eigenvectors. In recognition of the derivative information it employs the algorithm is named derivative-MUSIC or simply d-MUSIC. Though it can only resolve two source signals it is well suited to the radar low angle tracking problem.

1.2 d-MUSIC Objectives

The design goals of the d-MUSIC algorithm are as follows:

1) The algorithm shall resolve two closely spaced sources for an uniform linear array.

2) The algorithm shall employ only a single array snapshot vector.

3) The algorithm shall be suitable for real-time use. It will not employ a complex matrix factorization technique such as an eigenvector decomposition (EVD) or a singular value decomposition (SVD).

The first restriction of two sources arises from the single snapshot condition. This vector and the second vector constructed from its spatial derivatives will yield a rank two projector. This limits the range of applications for the algorithm but is appealing for the low angle tracking problem where we are assured two source signals for a low flying aircraft. Other applications of interest include resolving two closely spaced aircraft separated in azimuth, resolving the spacing between two stars in a binary system using a radio telescope array and resolving the frequencies of two closely spaced sinusoids for short time sequences.

Generalizing it to the multi-source case may be difficult, but not impossible (multi-dimensional Taylor series expansion is required). An accurate estimate of the number of sources in the cluster is required. The method of [9] can be employed to estimate the number of emitters in a multi-source cluster.

A multi-source problem of practical interest is a cluster of aircraft lying along the same azimuth at different elevation angles, but with an altitude and range much greater than the antenna height. In this case the flat earth multipath model [3, chap. 6] can be applied (the bisector between the target and surface reflected rays is parallel to the surface). As a result each target and multipath image pair all share a common center. An extension to the d-MUSIC algorithm is touched on in Chapter 2 that can be applied to this multi-source problem but it suffers from the drawback of requiring several independent signal space vectors as input. This will likely require a return to the tactic of forming a covariance matrix and performing an eigenvector decomposition.

The d-MUSIC concept is applicable to any array geometry where the sensors have an uniform spacing (necessary for the forward-backward averaging operation of Chapter 2), but the principal interest here is the application of the algorithm to uniform linear arrays. The uniform linear array is the simplest of all array structures and for this reason it serves as a convenient

vehicle to establish the mathematical foundation of the d-MUSIC algorithm. Another more practical reason is that the experiment data available to test the algorithm is from a linear array.

A convenient example to demonstrate the utility of d-MUSIC for other array geometries is the rectangular grid planar array. As it is simply a collection of linear arrays the formulation for its derivatives may be considered to be a simple extension of the linear array case. Appendix A discusses the derivative space for a rectangular planar array and outlines the basic modules of a 2-D d-MUSIC algorithm.

In this work the sources are assumed to have a plane wave structure and to be narrowband. The problem of other wave front structures (e.g., spherical waves) will not be addressed here though it is conceivable that this approach could be generalized to such problems. By the same token the wideband problem will also not be addressed. However, many wideband processors employ an "up-front" spectral decomposition to reduce the problem to a set of N narrowband array snapshots. As such the solution for narrowband sources can be generalized to the wideband case.

Another issue the d-MUSIC algorithm attempts to address is that of software development cost and ease of implementation. A key feature of the algorithm is that it does not employ a complex matrix factorization method like an eigenvector decomposition or a SVD which are difficult to program and generally not suited for real-time use [2, chap. 11]. Algorithm operations are primarily concerned with vector inner products and vector outer products. As such the algorithm is well suited for a simple code development in a real-time implementation.

In the interest of evaluating the algorithm a theoretical estimate for the d-MUSIC error variance is derived and compared to the optimal performance level set by the Cramér-Rao lower bound on the variance. Owing to the complexity of the problem the estimate is derived for the case when the cluster centroid is known (typical of the flat earth approximation case). The performance analysis closely follows the classic work of Stoica and Nehorai [10] to derive both the d-MUSIC error variance and the Cramér-Rao bound (CRB). The CRB for the problem of a known cluster centroid is derived in Appendix B.

The true test of any algorithm is how well it performs in the field. An experiment data set has graciously been made available to this work courtesy of the Surface Radar Section of Defence Research Establishment Ottawa (DREO), Canadian Department of National Defence.

One of the functions of DREO's Experimental Array Radar System (EARS) is to collect radar data over the sea in support of validation studies of signal processing techniques. Operating between 8.9 to 9.4 GHz the EARS radar employs separate transmit and receive antennas with an eight-element vertical array of horn antennas used to measure the elevation angle of targets. Each of the eight channels has its own receiver, providing the equivalent of a "sampled aperture antenna". Such an array represents an ideal test-bed system to study the performance of d-MUSIC.

A subset of the EARS data collected at Osborne Head, Nova Scotia in October 1995 is used to investigate the performance of the algorithm. The data set includes a Sea King helicopter that took up station some 8 km from shore. The helicopter hovered at two different altitudes, resulting in an array response where the direct and multipath signals were separated by 16% and 35% of a beamwidth. The close range of the helicopter resulted in a multipath geometry not suitable to the flat earth approximation. As a result the cluster centroid can not be assumed to be known *a priori*.

1.3 Array Calibration

Though high resolution techniques have much to offer for sensor array processing their use in real systems has been rather limited [11]. One of the reasons often cited for this is their sensitivity to model errors resulting from channel mismatch and system/environment factors. For example, errors in sensor position are common due to wind forces, platform motion, etc. This error may be time-varying, so a highly accurate motion sensor package is required to track it.

Much effort has been directed to study the effects of these errors on various high resolution techniques [12-19]. These studies verify the experimental observations that model errors have a serious detrimental effect on high resolution array processing. In some low angle tracking experiments the accuracy of high resolution processing is not limited by thermal sensor noise, but rather by calibration accuracy [20].

A number of calibration algorithms have been devised to address this problem. One possibility is to treat a naturally occurring phenomenon as a beacon source to calibrate the system [21], but that opportunity rarely presents itself in practice. Other techniques have been developed to calibrate the array assuming that some of the source directions are known [22, 23] or that the statistical distribution of the array errors is known [13, 24].

A number of "blind" techniques have also been developed that require no *a priori* knowledge of the source directions or array errors. One such group includes iterative subspace techniques to perform joint estimation of the signal directions and the array errors [25-27]. These methods, though elegant, involve a substantial amount of computation, making it difficult to apply in a real-time setting. Also the array errors are assumed to be fixed, and not vary with time. Another intriguing development involves the use of cumulants to suppress array errors [28, 29], but these methods require that the source signals be uncorrelated.

In the Osborne Head trials wind gusts exceeded 40 to 60 kph and the calibration/position errors were severe and time-varying. In this setup a mere 2 mm lateral displacement at the top of the array would result in a array tilt of about 10% of a beamwidth whereas the source spacing is only 16% or 35% of a beamwidth. No motion sensor package was utilized in the experiment to measure sensor displacements. Due to a pre-amp failure only the lower 6 channels were available for uniform linear array processing. To successfully apply a high resolution algorithm to this data an adaptive calibration method is required. As it is hoped to develop d-MUSIC along the lines of a computationally simple real-time algorithm, it is desired to make the adaptive calibration scheme real-time as well.

A simple, yet powerful technique that meets this requirement is described in [30]. This method was designed specifically for uniform linear arrays and requires no knowledge of the source directions. It is based on the fact that the covariance matrix $\mathbf{R}$ should be Toeplitz for uncorrelated sources. This is not a problem for low angle tracking as the covariance matrix is nearly Toeplitz for closely spaced sources, even if they are correlated. This will be established in Chapter 4. Significantly adding to the appeal of this method is that the solution for the channel weights is derived as a closed form expression, greatly simplifying its use as a real-time adaptive technique.

The auto-calibration method of [30] is adapted for use in this work. Some modifications were made to better support the Toeplitz approximation for $\mathbf{R}$ and to remove the linear constraint that the mean value of the array phase errors is zero. Combined, the d-MUSIC algorithm and the Toeplitz-based calibration technique forms the foundation of a real-time processor for low angle altitude estimation in a multipath environment. This thesis describes both algorithms and presents test results using data collected at the Osborne Head EARS trials.

1.4 Thesis Organization

The rest of the thesis is organized as follows. Chapter 2 reviews the MUSIC algorithm and describes the full linear array d-MUSIC algorithm for the case of where the cluster centroid is known (flat earth approximation) and for the general case of an unknown centroid. Chapter 2 also outlines the multi-source d-MUSIC algorithm. Appendix A lays the foundation for a 2-D d-MUSIC algorithm by extending the linear array idea to a rectangular grid planar array for the purpose of resolving low angle multipath signals.

Chapter 3 is a performance analysis of the algorithm. The theoretical d-MUSIC error variance for the case of a known cluster centroid is derived and compared to the Cramér-Rao bound (CRB). A number of examples are presented for varying degrees of signal correlation and compared to the MUSIC error variance derived by Stoica and Nehorai [10]. Chapter 3 also presents a number of Monte Carlo simulations to compare the performance of the d-MUSIC algorithm to MUSIC for the case of either a known or unknown cluster centroid.

Chapter 4 outlines the modified version of the Toeplitz calibration technique [30] and presents several simulation examples. The calibration technique and the d-MUSIC algorithm for an unknown cluster centroid are employed in Chapter 5 to analyze the Osborne Head data to estimate the altitude of a low flying helicopter. The results are compared to those obtained using the MUSIC algorithm.

Chapter 6 is a discussion of the main points of the thesis and outlines some future work planned for the algorithm. Of particular interest is the development of a beamspace version of the d-MUSIC algorithm and the extension of the theoretical error analysis to the unknown cluster centroid case.

2 The d-MUSIC Algorithm

2.1 Preamble

This chapter describes the d-MUSIC algorithm. The method developed here is for a uniform linear array receiving two closely spaced narrowband sources. To facilitate this development a review of linear array theory and the MUSIC algorithm [1, 2] is included. Following this review the concept of a direction vector derivative will be defined, leading to the d-MUSIC algorithm.

Though d-MUSIC can be applied to the single source there are inherent dangers in doing so. The issues involved with the single source case are presented along with some suggestions on how to apply the algorithm for the multi-source problem in a multipath environment when the flat earth approximation for specular multipath is valid [3, chap. 6].

2.2 The Linear Array Signal Model

Figure 2-1 illustrates the direction finding problem for an N-element linear array with spacing d between sensors. Due to the different path lengths the incoming plane wave signal will

arrive at each sensor at different times. Assuming that the signal is narrowband in frequency this time delay can be treated as a phase shift. The change in phase of the signal along the array axis is referred to as the *array response* or *direction vector*. For a far-field plane wave source with wavelength λ arriving from direction θ the resulting direction vector is

$$\mathbf{a}(\theta) = e^{j\alpha(N-1)/2}\left[1 \;\; e^{-j\alpha} \; e^{-j2\alpha} \cdots e^{-j(N-1)\alpha}\right]^T \tag{2-1}$$

where $(\cdot)^T$ denotes transpose and

$$\alpha = \frac{2\pi d}{\lambda}\sin\theta \tag{2-2}$$

is the change in phase of the signal from sensor-to-sensor.

Without any loss of generality, the phase reference point for $\mathbf{a}(\theta)$ is chosen to be the center of the array. This has the advantage of making $\mathbf{a}(\theta)$ a centro-Hermitian vector, i.e., $\mathbf{a}(\theta)$ satisfies

$$\mathbf{J}\,\mathbf{a}(\theta) = \mathbf{a}^*(\theta) = \mathbf{a}(-\theta) \tag{2-3}$$

where $(\cdot)^*$ denotes the complex conjugate and $\mathbf{J}$ is a reverse permutation matrix (a matrix with ones running along the anti-diagonal and zero everywhere else). Multiplying a vector by $\mathbf{J}$ reverses the order of the elements of the vector. In this case, reversing all the elements of $\mathbf{a}(\theta)$

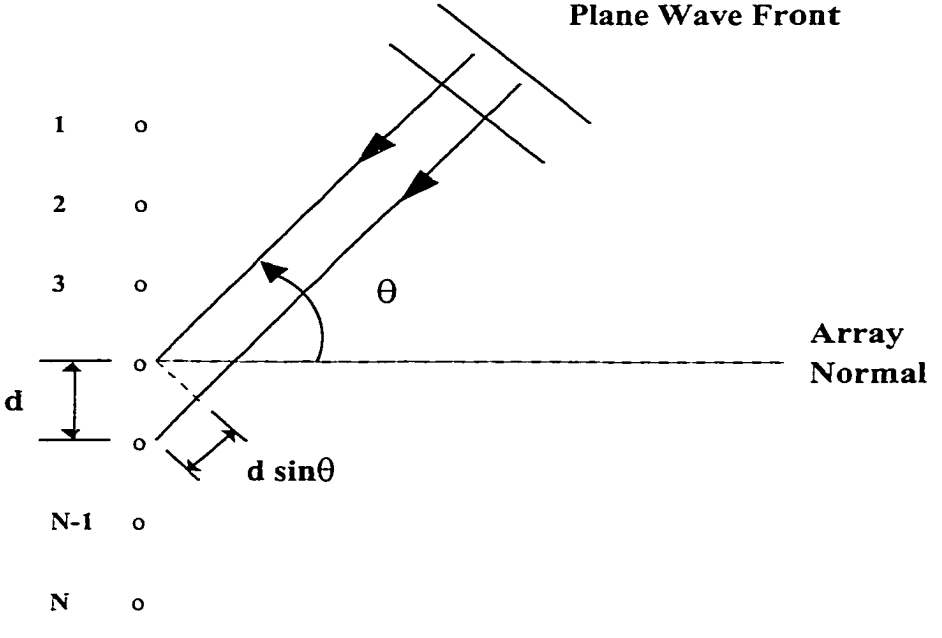

Figure 2-1 Linear array geometry

produces $\mathbf{a}^*(\theta)$. Note that $\mathbf{a}^*(\theta) = \mathbf{a}(-\theta)$ as α depends on $\sin\theta$.

For the case of L narrow-band sources, all having the same wavelength, the output of the N sensors at the kth sample may be arranged in the $N \times 1$ *snapshot* vector

$$\mathbf{x}(k) = \mathbf{A}\,\mathbf{s}(k) + \mathbf{n}(k) \tag{2-4}$$

where $\mathbf{n}(k)$ is the $N \times 1$ noise vector for time sample k, $\mathbf{s}(k) = [s_1(k)\ s_2(k)\ \ldots\ s_L(k)]^T$ is a vector containing the kth sample of the L signal waveforms and $\mathbf{A}$ represents the set of direction vectors for the L directions of arrival:

$$\mathbf{A} = \left[\mathbf{a}(\theta_1)\ \mathbf{a}(\theta_2)\ \ldots\ \mathbf{a}(\theta_L)\right] \tag{2-5}$$

Assuming that the noise is independent of the L signal waveforms and that the signal waveforms are stationary, the covariance matrix of the snapshot vector $\mathbf{x}(k)$ can be written as

$$\mathbf{R} = E\left\{\mathbf{x}(k)\mathbf{x}^H(k)\right\} = \mathbf{A}\mathbf{S}\mathbf{A}^H + \mathbf{W} \tag{2-6}$$

where E denotes the statistical expectation operator and $(\cdot)^H$ denotes the complex conjugate transpose. $\mathbf{W}$ and $\mathbf{S}$ represents the noise and signal covariance matrices, respectively:

$$\mathbf{S} = E\left\{\mathbf{s}(k)\mathbf{s}^H(k)\right\} \tag{2-7}$$

$$\mathbf{W} = E\left\{\mathbf{n}(k)\mathbf{n}^H(k)\right\} \tag{2-8}$$

If the noise is both temporally and spatially white with zero mean and variance σ^2, $\mathbf{W}$ reduces to

$$\mathbf{W} = \sigma^2\,\mathbf{I} \tag{2-9}$$

where $\mathbf{I}$ is the identity matrix.

This is the ideal covariance matrix model. In reality only a finite number of snapshots are available to compute its estimate. For K snapshots of zero mean wide sense stationary data the estimate for the sensor array covariance matrix may be computed as

$$\mathbf{R} = \frac{1}{K}\sum_{k=1}^{K}\mathbf{x}(k)\mathbf{x}^H(k) \tag{2-10}$$

The signal covariance matrix $\mathbf{S}$ plays a critical role in the beamforming problem. The rank

of **S** is equal to the rank of $\mathbf{ASA}^H$ and if this rank is less than the number of signals L, then it is not possible for a signal subspace algorithm such as MUSIC to accurately resolve all the sources. This is equivalent to saying that the available degrees of freedom is less than the number of parameters to be estimated.

The rank of **S** will be less than the number of sources L if some or all of the sources are coherent (e.g., identical signals). If none of the sources are correlated than **S** is a diagonal matrix with rank L. Say if the signals are not coherent, but highly correlated instead, the rank of **S** may be effectively less than L anyway as it will be close to becoming a singular matrix.

2.3 MUSIC

A signal processing problem of considerable interest is the "high resolution" estimation of the parameters of multiple superimposed exponential signals in additive Gaussian noise. The intent of these algorithms is the accurate estimation of the exponential signal parameters even if some or all of the signals are closely spaced in direction for sensor array processing or closely spaced in frequency for time series analysis.

Prominent among the high resolution techniques are the *subspace* algorithms. Included in this set are the MUSIC [1, 2], MINIMUM-NORM [30], and ESPRIT [31] algorithms. For a comprehensive review of these and other high resolution methods the reader is referred to [2, 32, 33].

The MUSIC or MUltiple Signal Classification algorithm is of particular interest to this work. One reason for this is that it is one of the best known and perhaps one of the most popular high resolution methods. It is also commonly used as a basis for assessing the performance of other high resolution algorithms. Another, more important reason stems from the fact that this algorithm is easily modified to include derivative information.

The success of most high resolution algorithms depends upon the special structure of the sensor array covariance matrix when the sensor noise is white. As a means to examine this structure consider the eigenvector decomposition of **R**:

$$\mathbf{R} = \mathbf{Q}\Lambda\mathbf{Q}^H \tag{2-11}$$

where Λ is a diagonal matrix of eigenvalues λ_i and **Q** is an unitary matrix $(\mathbf{QQ}^H = \mathbf{Q}^H\mathbf{Q} = \mathbf{I})$ of

orthogonal eigenvectors:

$$\mathbf{Q} = [\mathbf{q}_1 \ \mathbf{q}_2 \ \cdots \ \mathbf{q}_N] \tag{2-12}$$

Assuming that $\mathbf{W}$ may be well approximated as $\sigma^2\mathbf{I}$, it follows that $\mathbf{ASA}^H = \mathbf{R} - \sigma^2\mathbf{I}$ represents a rank reduced version of $\mathbf{R}$. Let the rank of $\mathbf{R}$ be p where $p \leq N$. Obviously, the last $N-p$ eigenvalues of $\mathbf{R}$ are equal to σ^2 (i.e., $\lambda_i = \sigma^2$, $i = p+1, \ldots, N$). Hence the eigenvector decomposition of $\mathbf{ASA}^H = \mathbf{R} - \sigma^2\mathbf{I}$ is simply

$$\mathbf{ASA}^H = \mathbf{R} - \sigma^2\mathbf{I} = \sum_{i=1}^{p} (\lambda_i - \sigma^2)\mathbf{q}_i\mathbf{q}_i^H \tag{2-13}$$

This result demonstrates the well known fact [1] that the first p eigenvectors of $\mathbf{R}$ belong to the span of the columns of $\mathbf{A}$, i.e.,

$$\text{span}\{\mathbf{q}_1, \mathbf{q}_2, \ldots \mathbf{q}_N\} \subset \text{span}\{\mathbf{a}(\theta_1), \mathbf{a}(\theta_2), \ldots \mathbf{a}(\theta_L)\} \tag{2-14}$$

The span of a set of vectors is the set of all possible linear combinations of these vectors. As such there is a linear relationship between the principal eigenvectors of $\mathbf{R}$ and the source direction vectors. For this reason the principal eigenvectors are often referred to as the *signal subspace* of $\mathbf{R}$. The remaining space of $\mathbf{R}$ is referred to as the *noise subspace*. The span of the principal eigenvectors of $\mathbf{R}$ will equal the span of $\mathbf{A}$ only when the signal covariance matrix $\mathbf{S}$ is full rank (i.e., $p = L$). This condition must be met in order for the MUSIC algorithm to resolve the source directions.

As the signal space eigenvectors are orthogonal to the noise space eigenvectors, it follows that the source direction vectors will also be orthogonal to the noise eigenvectors:

$$\mathbf{q}_i^H \mathbf{a}(\theta_n) = 0, \qquad n = 1, \ldots, L; \quad i = p+1, \ldots, N \tag{2-15}$$

Hence, an estimate for the signal directions may be obtained by finding the values of θ that produce a peak in the MUSIC spectrum estimate

$$S_{\text{MUSIC}}(\theta) = \frac{1}{\mathbf{a}^H(\theta)\mathbf{Q}_W\mathbf{Q}_W^H\mathbf{a}(\theta)} \tag{2-16}$$

where

$$\mathbf{Q}_W = [\mathbf{q}_{p+1} \cdots \mathbf{q}_N] \tag{2-17}$$

This form of MUSIC is known as spectral-MUSIC [2]. To ensure that no peaks are missed a fine grid of θ values are required for the peak search. This can be a computationally expensive procedure, even when using a FFT [2]. Another more efficient approach searches for the denominator zeros of (2-16). This is the approach adopted in the root-MUSIC algorithm [2] for uniform linear arrays.

The MUSIC algorithm is conceptually simple. It involves the decomposition of the sensor array covariance matrix into a signal subspace and an orthogonal noise subspace using an eigenvector decomposition, then estimate the signal bearings based upon their orthogonality to the noise subspace. Of course, this assumes that the signal space span of the covariance matrix fully spans the signal space of **A** and that all signal space eigenvectors have sufficient SNR to permit accurate estimation.

Consider the eigenvector decomposition of two uncorrelated sources with equal power. It is simple to show that the infinite snapshot estimate yields

$$\text{Equi - power uncorrelated sources:} \qquad (2\text{-}18)$$
$$\sqrt{\lambda_1 - \sigma^2}\,\mathbf{q}_1 = \mathbf{a}(\theta_1) + \mathbf{a}(\theta_2)$$
$$\sqrt{\lambda_2 - \sigma^2}\,\mathbf{q}_2 = \mathbf{a}(\theta_1) - \mathbf{a}(\theta_2)$$

Recall that the eigenvectors are normalized such that $\mathbf{q}_i^H \mathbf{q}_i = 1$. For closely spaced sources the norm of $\mathbf{a}(\theta_1)$ - $\mathbf{a}(\theta_2)$ is small, hence λ_2 must also be small. In contrast λ_1 should be much larger.

If an infinite number of data snapshots are available this would present no problem. From a practical standpoint, unless the signal power is high and/or the noise power is low, the ratio λ_2/σ^2 (a SNR measure) for the second eigenvector $\mathbf{q}_2$ may be too low to permit an accurate estimation of this eigenvector. As a result the noise and signal space estimates will overlap resulting in a significant loss of resolution, and possibly a failure to resolve the two sources.

The disparity between the eigenvalues (signal strength of the signal space eigenvectors) will grow if the sources are correlated [4]. Effective methods exist to combat the problem of correlated sources. Included in this set are the methods of spatial smoothing [34-36] and forward-backward averaging [2].

In forward-backward averaging the centro-Hermitian property of (2-3) is used to replace **R** with the matrix

$$\mathbf{R}_{fb} = (\mathbf{R} + \mathbf{J}\mathbf{R}^{*}\mathbf{J})/2 \tag{2-19}$$

Given the fact that a linear array response vector is centro-Hermitian, it is simple to show that $\mathbf{R}_{fb}$ is equivalent to

$$\mathbf{R}_{fb} = \frac{1}{2}\mathbf{A}(\mathbf{S} + \mathbf{S}^{*})\mathbf{A}^{H} + \mathbf{W}_{fb} = \mathbf{A}\,\mathrm{Re}\{\mathbf{S}\}\,\mathbf{A}^{H} + \mathbf{W}_{fb} \tag{2-20}$$

where $\mathrm{Re}\{\bullet\}$ denotes the real component of a complex quantity and $\mathbf{W}_{fb}$ is the forward-backward average of the noise matrix $\mathbf{W}$.

As the main diagonal of $\mathbf{S}$ is real, the main effect of forward-backward averaging is to eliminate the imaginary components of $\mathbf{S}$, and thus reduce the total power of the cross correlation terms. If two sources are correlated but 90° out of phase, the off-diagonal terms of $\mathbf{S}$ will be strictly imaginary and the application of forward-backward averaging will serve to completely decorrelate the two sources.

Another effective technique is spatial smoothing [34-36]. It divides the array into a set of size M overlapping subarrays and averages the correlation matrix for each together. The effect of averaging these matrices is equivalent to sliding a $M \times M$ window along the main diagonal of the $N \times N$ matrix $\mathbf{R}$. Note that this will not effect the autocorrelation terms as they are Toeplitz matrices, but the cross correlation terms are reduced in power as they exhibit a sinusoidal variation along each diagonal.

Note that the methods of forward-backward averaging and spatial smoothing can be combined and often are. Unlike forward-backward averaging, there is a price to pay in using spatial smoothing, and that is the reduction of the dimension of $\mathbf{R}$ from N to M. This can be drawback as the reduced data dimension will surely result in a loss of resolution. Also, if the sources are closely spaced the variation along the diagonal of each cross-correlation term is small and spatial smoothing has only a marginal impact in decorrelating the sources [37].

To resolve two closely spaced sources, the MUSIC algorithm requires two orthogonal signal space vectors. As the estimate for the second, weaker, eigenvector may be subject to large errors due to noise, it is usually this parameter which exerts the greatest influence in determining the success of the bearing estimates obtained by a high resolution algorithm. In many radar applications the algorithm will be expected to work with a small number of data snapshots. In

that event is reasonable to expect that in many circumstances the system may only have sufficient SNR to accurately estimate one signal space vector. For example, the principal eigenvector for covariance based processing or the target peak after Doppler processing.

One signal space vector is not enough for a MUSIC estimate if two sources are present. We have to look to other information to construct a second signal space vector to fill the remaining span for the two source problem. One possible solution is to use derivative information. This will be explored in the next section.

2.4 The Linear Array Direction Vector Derivative

The derivative of $\mathbf{a}(\theta)$ with respect to α is

$$\dot{\mathbf{a}}(\theta) = \frac{d\,\mathbf{a}(\theta)}{d\alpha} = \mathbf{D}\,\mathbf{a}(\theta) \tag{2-21}$$

where

$$\mathbf{D} = \mathrm{j}\,\mathrm{diag}\left\{(N-1)/2 - [0, 1, \cdots N-1]^{\mathrm{T}}\right\} \tag{2-22}$$

$\mathbf{D}$ shall be referred to as the *linear array derivative operator.* The function diag{·} converts a column vector into a diagonal matrix.

Note that (2-21) is an exact expression for the derivative and no knowledge of the signal direction is required. In a similar fashion, the higher-order derivatives of $\mathbf{a}(\theta)$ may be defined by multiplying $\mathbf{a}(\theta)$ by $\mathbf{D}$ an appropriate number of times. For example, the second derivative is

$$\ddot{\mathbf{a}}(\theta) = \frac{d^2\,\mathbf{a}(\theta)}{d\alpha^2} = \mathbf{D}\,\mathbf{D}\,\mathbf{a}(\theta) \tag{2-23}$$

Note that the odd order derivatives are anti-symmetric vectors whereas $\mathbf{a}(\theta)$ and the even order derivatives are symmetric. It follows that the odd order derivatives are orthogonal to $\mathbf{a}(\theta)$ and the even order derivatives. In particular,

$$\mathbf{a}^{\mathrm{H}}(\theta)\dot{\mathbf{a}}(\theta) = \mathbf{0} \tag{2-24}$$

where $\mathbf{0}$ is a vector of zeros and $(\cdot)^{\mathrm{H}}$ denotes the complex conjugate transpose.

If the two sources are closely spaced, we may use the following Taylor series expansions to relate the two direction vectors:

$$\mathbf{a}(\theta_T) = \mathbf{a}(\theta_R) + \delta_\alpha \dot{\mathbf{a}}(\theta_R) + \frac{\delta_\alpha^2}{2}\ddot{\mathbf{a}}(\theta_R) + O\left(|\delta_\alpha|^3\right) \tag{2-25}$$

$$\mathbf{a}(\theta_R) = \mathbf{a}(\theta_T) - \delta_\alpha \dot{\mathbf{a}}(\theta_T) + \frac{\delta_\alpha^2}{2}\ddot{\mathbf{a}}(\theta_T) + O\left(|\delta_\alpha|^3\right) \tag{2-26}$$

where O denotes order with respect to powers of δ_α and

$$\delta_\alpha = \alpha_T - \alpha_R \tag{2-27}$$

The T and R subscripts distinguish the two sources, and in a radar low angle tracking context, they represent the direct and surface reflected rays respectively.

Subtracting the two Taylor series expressions yields

$$\mathbf{a}(\theta_T) - \mathbf{a}(\theta_R) = \frac{\delta_\alpha}{2}\left(\dot{\mathbf{a}}(\theta_T) + \dot{\mathbf{a}}(\theta_R)\right) + \frac{\delta_\alpha^2}{4}\left(\ddot{\mathbf{a}}(\theta_R) - \ddot{\mathbf{a}}(\theta_T)\right) + O\left(|\delta_\alpha|^3\right) \tag{2-28}$$

For closely spaced sources, δ_α is small. In that event terms of order δ_α^2 and higher may be neglected, resulting in the approximation

$$\mathbf{a}(\theta_T) - \mathbf{a}(\theta_R) \approx \frac{\delta_\alpha}{2}\left(\dot{\mathbf{a}}(\theta_T) + \dot{\mathbf{a}}(\theta_R)\right) \quad \text{for small } \delta_\alpha \tag{2-29}$$

The above is a significant result. It provides a means to relate the signal space of two closely spaced sources with that of their derivatives.

As $\mathbf{a}^H(\theta)\dot{\mathbf{a}}(\theta) = \mathbf{0}$ the signal space of $[\mathbf{a}(\theta_T)\ \mathbf{a}(\theta_R)]$ and $[\dot{\mathbf{a}}(\theta_T)\ \dot{\mathbf{a}}(\theta_R)]$ do not overlap. However, if the sources are closely spaced there is an approximate intersection point between the two spaces, specifically $\mathbf{a}(\theta_T) - \mathbf{a}(\theta_R) \approx \delta_\alpha\left(\dot{\mathbf{a}}(\theta_T) + \dot{\mathbf{a}}(\theta_R)\right)/2$. From first inspection this does not seem to add much more information to the problem, but in conjunction with the centro-Hermitian property it leads to a robust high resolution algorithm for the dual-source problem.

To illustrate the utility of derivative information, consider the problem of closely spaced equi-power sources. For uncorrelated signals the ideal covariance matrix will have $\mathbf{a}(\theta_T) + \mathbf{a}(\theta_R)$

and $\mathbf{a}(\theta_T)$ - $\mathbf{a}(\theta_R)$ as its signal space components. For two identical sources, the matrix will be rank deficient with $\mathbf{a}(\theta_T)$ + $\mathbf{a}(\theta_R)$ as its only signal space eigenvector.

Note that the principal eigenvector is the same whether the equi-power signals are uncorrelated or identical. The chief difference is the absence of the eigenvector $\mathbf{a}(\theta_T)$ - $\mathbf{a}(\theta_R)$. But this vector may be well approximated by the derivative of the first eigenvector.

In general, the principal vector of $\mathbf{R}$ will not be $\mathbf{a}(\theta_T)$ + $\mathbf{a}(\theta_R)$ and the derivative of the principal eigenvector will not lie fully in the span of $[\mathbf{a}(\theta_T)\ \mathbf{a}(\theta_R)]$. The d-MUSIC algorithm to be discussed next utilizes the centro-Hermitian property of $\mathbf{a}(\theta)$ to overcome this problem, permitting the creation of a derivative vector independent from the principal vector, but spanning the same signal space.

2.5 d-MUSIC

The principal eigenvector of $\mathbf{R}$ for the noiseless case can be modeled as

$$\mathbf{v} = k_1\mathbf{a}(\theta_T) + k_2\mathbf{a}(\theta_R) \tag{2-30}$$

where k_1 and k_2 are complex constants.

If $k_1 = k_2$ then $\dot{\mathbf{v}} = \mathbf{D}\mathbf{v} \approx 2k_1\big(\mathbf{a}(\theta_T) - \mathbf{a}(\theta_R)\big)/\delta_\alpha$ and both $\mathbf{v}$ and $\dot{\mathbf{v}}$ will span the space of $[\mathbf{a}(\theta_T)\ \mathbf{a}(\theta_R)]$. In general, $k_1 \neq k_2$ and $\dot{\mathbf{v}}$ will not lie fully in the span of the source vectors. To incorporate derivative information into the technique, additional information must be employed. Recall that linear array direction vectors have centro-Hermitian symmetry, i.e.,

$$\mathbf{J}\,\mathbf{a}(\theta) = \mathbf{a}^*(\theta) = \mathbf{a}(-\theta) \tag{2-31}$$

Another useful property of direction vectors is that they can be rotated. Let $\mathbf{a}(\phi)$ be the direction vector for a signal arriving from direction ϕ. The rotation operator is defined as

$$\mathbf{V}_R(\phi) = \mathrm{diag}\left\{\mathbf{a}^*(\phi)\right\} \tag{2-32}$$

The product $\mathbf{V}_R(\phi)\ \mathbf{a}(\theta)$ rotates the vector $\mathbf{a}(\theta)$ to point in the direction

$$\eta = \sin^{-1}\{\sin\theta - \sin\phi\} \tag{2-33}$$

If θ and ϕ are both close to zero (e.g., low altitude aircraft) then η reduces to

$$\eta \approx \theta - \phi \tag{2-34}$$

with the result that the operation $\mathbf{V_R}(\phi)\ \mathbf{a}(\theta)$ effectively rotates the vector $\mathbf{a}(\theta)$ by $-\phi$.

Utilizing the centro-Hermitian and rotation properties together, the following vectors can be defined:

$$\mathbf{u} = (\mathbf{I}+\mathbf{J})\mathbf{S}(\phi)\mathbf{v} = (\mathbf{I}+\mathbf{J})\mathbf{V_R}(\phi)\{k_1\mathbf{a}(\theta_T) + k_2\mathbf{a}(\theta_R)\} \tag{2-35}$$

$$\dot{\mathbf{u}} = \mathbf{D}\mathbf{u} = (\mathbf{I}+\mathbf{J})\mathbf{V_R}(\phi)\{k_1\dot{\mathbf{a}}(\theta_T) + k_2\dot{\mathbf{a}}(\theta_R)\} \tag{2-36}$$

Say that we select ϕ such that $\mathbf{V_R}(\phi)\ \mathbf{a}(\theta_T) = (\mathbf{V_R}(\phi)\ \mathbf{a}(\theta_R))^*$. The rotated vectors will be equivalent to $\mathbf{V_R}(\phi)\ \mathbf{a}(\theta_T) = \mathbf{a}(\gamma)$ and $\mathbf{V_R}(\phi)\ \mathbf{a}(\theta_R) = \mathbf{a}(-\gamma)$ where

$$\gamma = \sin^{-1}\{\sin\theta_T - \sin\phi\} = \sin^{-1}\{\sin\theta_R - \sin\phi\} \tag{2-37}$$

If θ_T and θ_R are both small then $\phi = (\theta_T + \theta_R)/2$ and $\gamma = (\theta_T - \theta_R)/2$ adequately satisfies this condition. $\mathbf{V_R}(\phi)\ \mathbf{v}$ reduces to

$$\text{for } \mathbf{V_R}(\phi)\,\mathbf{a}(\theta) = (\mathbf{V_R}(\phi)\,\mathbf{a}(\theta))^* = \mathbf{a}(\gamma) \tag{2-38}$$

$$\begin{aligned}\mathbf{V_R}(\phi)\mathbf{v} &= \mathbf{V_R}(\phi)\{k_1\,\mathbf{a}(\theta_T) + k_2\,\mathbf{a}(\theta_R)\}\\ &= k_1\,\mathbf{a}(\theta_T - \phi) + k_2\,\mathbf{a}(\theta_R - \phi)\\ &= k_1\,\mathbf{a}(\gamma) + k_2\,\mathbf{a}(-\gamma)\end{aligned}$$

Using the above result for $\mathbf{V_R}(\phi)\ \mathbf{a}(\theta_T) = (\mathbf{V_R}(\phi)\ \mathbf{a}(\theta_R))^* = \mathbf{a}(\gamma)$, $\mathbf{u}$ and $\dot{\mathbf{u}}$ reduces to

$$\begin{aligned}\mathbf{u} &= (\mathbf{I}+\mathbf{J})\mathbf{V_R}(\phi)\,\mathbf{v}\\ &= (\mathbf{I}+\mathbf{J})\{k_1\,\mathbf{a}(\gamma) + k_2\,\mathbf{a}(-\gamma)\}\\ &= k_1\,\mathbf{a}(\gamma) + k_2\,\mathbf{a}(-\gamma) + k_1\,\mathbf{a}(-\gamma) + k_2\,\mathbf{a}(\gamma)\\ &= \{k_1 + k_2\}\{\mathbf{a}(\gamma) + \mathbf{a}(-\gamma)\}\end{aligned} \tag{2-39}$$

$$\begin{aligned}\dot{\mathbf{u}} &= \mathbf{D}\,\mathbf{u}\\ &= \{k_1 + k_2\}\{\dot{\mathbf{a}}(\gamma) + \dot{\mathbf{a}}(-\gamma)\}\\ &\approx \frac{2}{\delta_\alpha}\{k_1 + k_2\}\{\mathbf{a}(\gamma) - \mathbf{a}(-\gamma)\}\end{aligned} \tag{2-40}$$

Clearly $[\mathbf{u}\ \dot{\mathbf{u}}]$ spans the space of $[\mathbf{a}(\gamma/2)\ \mathbf{a}(-\gamma/2)]$. Reversing the vector rotation produces

$$[\mathbf{p}\ \dot{\mathbf{p}}] = \mathbf{V}_R(-\phi)[\mathbf{u}\ \dot{\mathbf{u}}] \tag{2-41}$$

and $[\mathbf{p}\ \dot{\mathbf{p}}]$ spans the space of $[\mathbf{a}(\theta_T)\ \mathbf{a}(\theta_R)]$. As $\mathbf{p}$ and $\dot{\mathbf{p}}$ are symmetric and anti-symmetric vectors, respectively, it follows that $\mathbf{p}^H\dot{\mathbf{p}} = \mathbf{0}$. With two orthogonal vectors spanning the same rank two signal space we may construct the idempotent signal space projector

$$\mathbf{P}_s = \frac{\mathbf{p}\mathbf{p}^H}{\mathbf{p}^H\mathbf{p}} + \frac{\dot{\mathbf{p}}\dot{\mathbf{p}}^H}{\dot{\mathbf{p}}^H\dot{\mathbf{p}}} \tag{2-42}$$

The MUSIC algorithm attempts to construct this signal space projector using a matrix decomposition technique. By direct analogy to the MUSIC algorithm we can employ this signal space projector to estimate θ_T and θ_R. For computational simplicity $\mathbf{P}_s$ can be employed in a root-MUSIC [2] algorithm to estimate the signal directions. Root-MUSIC forms a polynomial from $\mathbf{P}_s$ to locate its roots. The two roots closest to the unit circle are selected as the solution for this problem.

This is a profound result. Using only a single signal space vector as input the d-MUSIC algorithm constructs a second vector using derivative information and the centro-Hermitian property to directly build a rank 2 signal space projector without resorting to the use of an expensive matrix factorization technique.

The drawback to this method is that the cluster centroid sin ϕ midway between the direction cosines sin θ_T and sin θ_R resulting in $\mathbf{V}_R(\phi)\ \mathbf{a}(\theta_T) = (\mathbf{V}_R(\phi)\ \mathbf{a}(\theta_R))^* = \mathbf{a}(\gamma)$ must be known *a priori*. Often this value is known in advanced, especially for air traffic control problems.

The specular multipath diagram of Figure 1.1 depicts the general low angle multipath problem. Employing a standard 4/3 effective earth radius model to account for atmospheric refraction the target angles θ_T and θ_R can be expressed in terms of the antenna height h_A, target altitude h_T and target range R_T [3, chap. 6]. When the aircraft altitude and range are much larger than the antenna height the direct and reflected ray paths are nearly parallel with the result that $\theta_R = -\theta_T$ and $\phi = 0$ (the flat earth approximation). This is still a low angle tracking problem however, as θ_T and θ_R may be small, especially for distant aircraft.

This description of the problem applies to the majority of commercial air traffic up until the

point the aircraft is about to land. At that point the target elevation angle θ_T is large and the multipath problem is no longer an issue as the depression angle θ_R will be a large negative number, placing it in the blind region of most antennas, especially if the array is tilted [39, chap. 22]. Standard beamforming can be applied to estimate θ_T during the final approach.

If an aircraft is flying low (treetop/sea skimming level) there is no simple relationship between the source angles θ_T and θ_R [3, 39-41]. The solution adopted here is to search over a grid of ϕ values and locate the value of ϕ which best fits the input data **v**.

The criteria for locating the d-MUSIC solution for unknown ϕ is straightforward. Let θ_1 and θ_2 be the solution for a given ϕ. The projector orthogonal to the space of $[\mathbf{a}(\theta_1)\ \mathbf{a}(\theta_2)]$ is

$$\mathbf{P}_N = \mathbf{I} - \frac{\mathbf{p}_1 \mathbf{p}_1^H}{\mathbf{p}_1^H \mathbf{p}_1} - \frac{\mathbf{p}_2 \mathbf{p}_2^H}{\mathbf{p}_2^H \mathbf{p}_2} \tag{2-43}$$

where

$$\mathbf{p}_1 = \mathbf{a}(\theta_1) + \mathbf{a}(\theta_2) \tag{2-44}$$

$$\mathbf{p}_2 = \mathbf{a}(\theta_1) - \mathbf{a}(\theta_2) \tag{2-45}$$

We require that $\mathbf{P}_N \mathbf{v}$ be a minimum. The objective is to find ϕ such that the scalar function

$$E(\phi) = \mathbf{P}_N \mathbf{v} \mathbf{v}^H \mathbf{P}_N \tag{2-46}$$

is minimized. By employing a discrete grid of ϕ values clustered around 0, a search can be performed to find the value of ϕ that minimizes $E(\phi)$.

Though the amount of computation required to implement this version of d-MUSIC for unknown ϕ is substantially greater than for known ϕ, both algorithms are very simple to implement, requiring only vector inner products and vector outer products. As all operations associated with the d-MUSIC algorithms are highly vectorized it can be readily implemented in real-time utilizing parallel processors if desired.

This is distinctive from the vast majority of high resolution algorithms. Most subspace algorithms require either an eigenvector decomposition (EVD) or a singular value decomposition (SVD) to estimate the signal space. Such matrix factorization techniques are generally not suited

for real-time implementation [2]. Many maximum likelihood methods [33, 34] perform a nonlinear optimization, which is not only computationally expensive, but difficult to implement in real-time.

Another interesting feature of the d-MUSIC algorithm is that it is highly insensitive to the problem of signal correlation. As d-MUSIC employs a single vector as input it is largely irrelevant if the two signals are correlated. As a matter of fact it is preferable if the signals were coherent with a correlation coefficient of +1 (identical signals) in order to maximize the SNR of the input vector **v**. This premise will be borne out in the performance analysis of chapter 3.

Though d-MUSIC is relatively insensitive to signal correlation, it fails in one noteworthy case. Specifically $\mathbf{v} = \mathbf{a}(\theta_T) - \mathbf{a}(\theta_R)$. d-MUSIC attempts to construct the vector $\mathbf{a}(\theta_T) - \mathbf{a}(\theta_R)$ using **v**. If **v** is already $\mathbf{a}(\theta_T) - \mathbf{a}(\theta_R)$ then d-MUSIC cannot produce a second signal space vector. This is a moot point however. If $\mathbf{v} = \mathbf{a}(\theta_T) - \mathbf{a}(\theta_R)$ then the SNR of the target echo will be a minimum and the probability of detection is low.

In comparison to the standard MUSIC algorithm, d-MUSIC should exhibit better SNR performance. As noted earlier, the second signal space eigenvector may have poor SNR even if the principal eigenvector SNR (and indeed the detection SNR) is good. In order for all signal components to have sufficient SNR the detection SNR must be very high. d-MUSIC circumvents this problem by only using the principal eigenvector or a strong signal space vector.

In summary, the steps required to implement the d-MUSIC algorithm are listed in Table 2-1:

Table 2-1 d-MUSIC Algorithm

1) Extract the array vector **v** from the data.

v may be either a single data snapshot, or the target peak after Doppler processing , or the principal eigenvector of **R**, or a projection of **R** onto a beam, etc.

2) If ϕ is known then

$$\mathbf{V}_R(\phi) = \mathrm{diag}\{\mathbf{a}^*(\phi)\}$$
$$\mathbf{u} = (\mathbf{I}+\mathbf{J})\mathbf{V}_R(\phi)\mathbf{v}$$
$$\dot{\mathbf{u}} = \mathbf{D}\mathbf{u}$$
$$[\mathbf{p}\ \dot{\mathbf{p}}] = \mathbf{V}_R(-\phi)[\mathbf{u}\ \dot{\mathbf{u}}]$$
$$\mathbf{P}_s = \frac{\mathbf{p}\mathbf{p}^H}{\mathbf{p}^H\mathbf{p}} + \frac{\dot{\mathbf{p}}\dot{\mathbf{p}}^H}{\dot{\mathbf{p}}^H\dot{\mathbf{p}}}$$

Use the signal space projector $\mathbf{P}_s$ in a root-MUSIC procedure [2] to extract θ_1 and θ_2, the roots closest to the unit circle. θ_1 and θ_2 is the d-MUSIC solution.

3) If ϕ is not known then for a length M grid of ϕ values perform the following loop

for $k = 1$ to M,

$$\mathbf{V}_R(\phi(k)) = \mathrm{diag}\{\mathbf{a}^*(\phi(k))\}$$
$$\mathbf{u} = (\mathbf{I}+\mathbf{J})\mathbf{V}_R(\phi(k))\mathbf{v}$$
$$\dot{\mathbf{u}} = \mathbf{D}\mathbf{u}$$
$$[\mathbf{p}\ \dot{\mathbf{p}}] = \mathbf{V}_R(-\phi(k))[\mathbf{u}\ \dot{\mathbf{u}}]$$
$$\mathbf{P}_s = \frac{\mathbf{p}\mathbf{p}^H}{\mathbf{p}^H\mathbf{p}} + \frac{\dot{\mathbf{p}}\dot{\mathbf{p}}^H}{\dot{\mathbf{p}}^H\dot{\mathbf{p}}}$$

Use the signal space projector $\mathbf{P}_s$ in a root-MUSIC procedure [2] to extract the bearing estimates $\theta_1(k)$ and $\theta_2(k)$.

If the root-MUSIC solution point is too far displaced from the unit circle subject to a user defined criteria, set $E(k) = \infty$ and skip to the next value of k.

Otherwise,

$$\mathbf{p}_1 = \mathbf{a}(\theta_1(k)) + \mathbf{a}(\theta_2(k))$$
$$\mathbf{p}_2 = \mathbf{a}(\theta_1(k)) - \mathbf{a}(\theta_2(k))$$
$$\mathbf{P}_N = \mathbf{I} - \frac{\mathbf{p}_1\mathbf{p}_1^H}{\mathbf{p}_1^H\mathbf{p}_1} - \frac{\mathbf{p}_2\mathbf{p}_2^H}{\mathbf{p}_2^H\mathbf{p}_2}$$
$$E(k) = \mathbf{P}_N\mathbf{v}\mathbf{v}^H\mathbf{P}_N$$

end of loop

Find index k_s at which $|E|$ is a minimum. The d-MUSIC solution is $\theta_1(k_s)$ and $\theta_2(k_s)$

2.6 Application to the Multi-Source Multipath Problem

The d-MUSIC idea can be readily applied to the multi-source problem in a multipath environment if the target altitude and range is sufficiently large compared to the antenna height so that ϕ is known (the flat earth approximation, [3, chap. 6]). If the array is perfectly vertical we have $\phi = 0$ and $\theta_R = -\theta_T$. Without any loss of generality, assume $\phi = 0$.

Consider the vertical linear array response to two sources at an elevation of θ_{T1} and θ_{T2}:

$$\mathbf{v} = k_1\,\mathbf{a}(\theta_{T1}) + k_2\,\mathbf{a}(-\theta_{T1}) + k_3\,\mathbf{a}(\theta_{T2}) + k_4\,\mathbf{a}(-\theta_{T2}) \tag{2-47}$$

where k_1, k_2, k_3, and k_4 are complex constants. Using the same approach as before we can construct the vectors

$$\begin{aligned}\mathbf{u} &= (\mathbf{I} + \mathbf{J})\mathbf{v} \\ &= \{k_1 + k_2\}\{\mathbf{a}(\theta_{T1}) + \mathbf{a}(-\theta_{T1})\} + \{k_3 + k_4\}\{\mathbf{a}(\theta_{T2}) + \mathbf{a}(-\theta_{T2})\}\end{aligned} \tag{2-48}$$

$$\begin{aligned}\dot{\mathbf{u}} &= \mathbf{D}\,\mathbf{u} \\ &\approx \frac{2}{\delta_{\alpha 1}}\{k_1 + k_2\}\{\mathbf{a}(\theta_{T1}) - \mathbf{a}(-\theta_{T1})\} + \frac{2}{\delta_{\alpha 2}}\{k_3 + k_4\}\{\mathbf{a}(\theta_{T2}) - \mathbf{a}(-\theta_{T2})\}\end{aligned} \tag{2-49}$$

Say that a number of snapshots are available. Each vector can be modeled along the lines of equation (2-47) if we assume that k_1, k_2, k_3, and k_4 can vary with time. Even for fast moving targets the direct and multipath component of each signal pair ($k_1(t)$, $k_2(t)$) and ($k_3(t)$, $k_4(t)$) differs primarily by a constant phase/amplitude difference for a short time interval (i.e., $k_1/k_2 \approx$ constant and $k_3/k_4 \approx$ constant). For two uncorrelated targets, the rank of the sequence of snapshots will lie between 2 to 4. As the ratio $(k_1 + k_2)/(k_3 + k_4)$ is likely to be different for each snapshot (or covariance matrix eigenvector), the vector set $[\mathbf{u}\ \dot{\mathbf{u}}]$ may be unique for each input vector as well.

Applying this operation to $\mathbf{V} = [v_1, v_2, \ldots v_m]$, the set of m snapshots (or eigenvectors) we can create the companion set of signal space vectors $\mathbf{U} = [\mathbf{u}_1, \dot{\mathbf{u}}_1, \mathbf{u}_2, \dot{\mathbf{u}}_2, \ldots \mathbf{u}_m, \dot{\mathbf{u}}_m]$. Though not guaranteed, it may be possible that the matrix [U V] is full rank. A SVD can be applied to the data matrix [U V] to create an orthogonal basis used to construct a full rank projector for a MUSIC-like algorithm.

The use of a matrix factorization technique is an expensive proposition, but one that can lead to a robust estimator for the multi-source multipath problem. However, we are back to the

old problem of requiring several snapshots. If only one snapshot is available we can divide the snapshot into overlapping subarrays to compute the covariance matrix much in the same manner as [7], at the cost of reduced array resolution.

For 3 or more sources, all in a tight cluster, the same idea can be applied to all snapshots or eigenvectors, hopefully leading to a full rank projector. Though not guaranteed to produce a full rank projector, it is likely to increase the dimension of the span we know.

2.7 Notes on the Single Source Problem

Technically, the d-MUSIC algorithm can be applied to the single source problem but it is strongly recommended to avoid this case owing to the very real danger that the algorithm may predict the presence of two distinct sources where there is only one. When one source is present with bearing θ the algorithm is likely to arrive at $\phi = \theta$ for the solution point with the result that the predicted target angles are $\theta_1 = \theta_2 = \theta$ and one may draw the conclusion that only one source is present. However the effects of noise may result in a small difference between θ_1 and θ_2 resulting in the erroneous conclusion that there are two very closely spaced sources present.

From an operational standpoint this need not be a critical concern. The favored application of the d-MUSIC algorithm is the radar low angle tracking where we are guaranteed both a direct path and multipath ray for each target. Ideally, the user should first apply an algorithm such as [9] to predict the number of sources present in the cluster. If only one source is suspected then standard beamforming is sufficient to isolate the source.

3 Performance Analysis

3.1 Preamble

The d-MUSIC algorithm is attractive for the low angle direction finding problem in a multipath environment, especially for aircraft tracking scenarios where the center of the cluster is known (typical of flat earth case for distant aircraft). As it employs a single array snapshot as input it should be relatively insensitive to the problem of signal correlation and can be easily integrated into the signal processing chain of most applications employing some form of time series analysis to aid detection (e.g., Doppler processing using a FFT). From an implementation viewpoint it has much to offer as it requires no complex matrix factorization techniques such as a EVD or a SVD and all remaining operations are highly vectorized, making it a suitable candidate for real time implementation.

Though implementation issues are critical to the success of a high resolution algorithm, the most important issue is accuracy. This chapter performs an error analysis of the d-MUSIC algorithm and derives a theoretical expression for the mean and variance of the error. The error

estimate is compared to the theoretical estimate for the MUSIC algorithm, and both are compared to the Cramér-Rao lower bound (CRB) on the variance. The CRB characterizes the optimum performance of the error variance for any unbiased algorithm [33]. As it is not specific to any algorithm, but rather a measure of the best performance that can be obtained, it is a widely accepted standard for comparing algorithms and provides useful insights on performance limitations.

The error analysis described here follows the classic approach developed by Stoica and Nehorai [10] who developed an expression for the error statistics of the MUSIC algorithm and developed a general expression for the Cramér-Rao lower bound for the multi-source beamforming problem in Gaussian noise.

When the cluster centre is known the problem of resolving two sources reduces to estimating one parameter, the spacing between the sources. This is in sharp contrast to a general technique such as MUSIC that does not try to exploit any *a priori* knowledge of the source locations.

Obviously the Cramér-Rao lower bound for a single parameter is much lower than that for a second parameter. Based on the general framework developed by Stoica and Nehorai a CRB is derived in Appendix B for the problem of estimating the spacing between two sources when the centre of the cluster is known. This CRB is appropriate as the chief focus of the chapter is the case when the aircraft/emitter altitude and range is much larger than the antenna height (flat earth approximation) so that the cluster centre is known. This case is the most common low angle tracking problem and is the best application for the d-MUSIC algorithm.

In support of the theoretical analysis Monte Carlo simulations are performed to test the performance of d-MUSIC relative to that of root-MUSIC employing forward-backward averaging. The results are both a function of SNR and signal correlation. The simulation tests also examine the performance of the alternate version of d-MUSIC where the cluster centre is unknown and must be located using a grid search.

Much of the theoretical error analysis will focus on the errors due to Gaussian sensor noise, however it is a relatively simple matter to include the effects of other error sources that are fixed in value. Specifically, the errors that result when the error for the estimate of ϕ and the array errors are constants. For example, an error for ϕ may result when the tilt angle of the array is not

known exactly. In normal operation the tilt angle of the array may change slowly due to temperature effects or pedestal wear/settling, thus introducing a bias for ϕ.

The issues of random ϕ and array errors are difficult to address. To derive a theoretical estimate for its effects one must assume a statistical distribution for the error. This is rather difficult to do as the errors, especially position errors, may not be strictly a random effect but rather a complicated, possibly deterministic, mechanism that may include periodic components. In any event for some applications, especially air traffic control, the system designer can take steps to control the variability of such errors. An air traffic control sensor will likely be attached to a fixed mount and not subject to the much larger errors common to a mobile platform. Also, it could be housed inside a protective enclosure to protect it from the elements (e.g., a radome). In that case the array errors may be relatively steady.

As a starting point for the discussion a proof is presented to verify that d-MUSIC provides an unique and unbiased estimate for two source locations for the case of zero noise and no array and ϕ errors. This provides some insight into the algorithm and its relation to MUSIC. Following this proof a statistical model for the d-MUSIC signal space estimate is presented (noise is spatially correlated).

3.2 Performance in the Noiseless Case

The following is a proof that the d-MUSIC algorithm produces an unbiased and unique solution for the two-source problem assuming the centre of the source cluster is known exactly.

Proof:

The idealized d-MUSIC signal space projector for the noiseless case with no array errors is

$$\mathbf{P}_s = \frac{\left[\mathbf{a}(\theta_1)+\mathbf{a}(\theta_2)\right]\left[\mathbf{a}(\theta_1)+\mathbf{a}(\theta_2)\right]^H}{\left[\mathbf{a}(\theta_1)+\mathbf{a}(\theta_2)\right]^H\left[\mathbf{a}(\theta_1)+\mathbf{a}(\theta_2)\right]} + \frac{\left[\dot{\mathbf{a}}(\theta_1)+\dot{\mathbf{a}}(\theta_2)\right]\left[\dot{\mathbf{a}}(\theta_1)+\dot{\mathbf{a}}(\theta_2)\right]^H}{\left[\dot{\mathbf{a}}(\theta_1)+\dot{\mathbf{a}}(\theta_2)\right]^H\left[\dot{\mathbf{a}}(\theta_1)+\dot{\mathbf{a}}(\theta_2)\right]} \tag{3-1}$$

The d-MUSIC algorithm seeks values of θ which minimize the d-MUSIC null spectrum

$$S(\theta) = \mathbf{a}^H(\theta)(\mathbf{I}-\mathbf{P}_s)\mathbf{a}(\theta) \tag{3-2}$$

The derivative of the null spectrum with respect to $\alpha = 2\pi d\sin(\theta)/\lambda$ is

$$\frac{dS(\theta)}{d\alpha} = -\mathbf{a}^{H}(\theta)\left\{\mathbf{D}^{H}\mathbf{P}_{s} + \mathbf{P}_{s}\mathbf{D}\right\}\mathbf{a}(\theta) \tag{3-3}$$

The values of θ which minimize $S(\theta)$ can be obtained by setting $dS(\theta)/d\alpha$ to zero. This yields

$$\mathbf{a}^{H}(\theta)\left\{\begin{array}{l}\dfrac{\left[\dot{\mathbf{a}}(\theta_1)+\dot{\mathbf{a}}(\theta_2)\right]\left[\mathbf{a}(\theta_1)+\mathbf{a}(\theta_2)\right]^{H}}{\left[\mathbf{a}(\theta_1)+\mathbf{a}(\theta_2)\right]^{H}\left[\mathbf{a}(\theta_1)+\mathbf{a}(\theta_2)\right]} + \dfrac{\left[\ddot{\mathbf{a}}(\theta_1)+\ddot{\mathbf{a}}(\theta_2)\right]\left[\dot{\mathbf{a}}(\theta_1)+\dot{\mathbf{a}}(\theta_2)\right]^{H}}{\left[\dot{\mathbf{a}}(\theta_1)+\dot{\mathbf{a}}(\theta_2)\right]^{H}\left[\dot{\mathbf{a}}(\theta_1)+\dot{\mathbf{a}}(\theta_2)\right]} \\ + \dfrac{\left[\mathbf{a}(\theta_1)+\mathbf{a}(\theta_2)\right]\left[\dot{\mathbf{a}}(\theta_1)+\dot{\mathbf{a}}(\theta_2)\right]^{H}}{\left[\mathbf{a}(\theta_1)+\mathbf{a}(\theta_2)\right]^{H}\left[\mathbf{a}(\theta_1)+\mathbf{a}(\theta_2)\right]} + \dfrac{\left[\dot{\mathbf{a}}(\theta_1)+\dot{\mathbf{a}}(\theta_2)\right]\left[\ddot{\mathbf{a}}(\theta_1)+\ddot{\mathbf{a}}(\theta_2)\right]^{H}}{\left[\dot{\mathbf{a}}(\theta_1)+\dot{\mathbf{a}}(\theta_2)\right]^{H}\left[\dot{\mathbf{a}}(\theta_1)+\dot{\mathbf{a}}(\theta_2)\right]}\end{array}\right\}\mathbf{a}(\theta) = 0 \tag{3-4}$$

As a linear array steering vector is centro-Hermitian it follows that $\mathbf{p}^{H}\mathbf{q} = \mathbf{q}^{H}\mathbf{p}$ where $\mathbf{p}$ and $\mathbf{q}$ are steering vectors or a derivative of a steering vector. The above equation can be reduced to the equality

$$\frac{\mathbf{a}^{H}(\theta)\left(\dot{\mathbf{a}}(\theta_1)+\dot{\mathbf{a}}(\theta_2)\right)\left(\mathbf{a}(\theta_1)+\mathbf{a}(\theta_2)\right)^{H}\mathbf{a}(\theta)}{\left[\mathbf{a}(\theta_1)+\mathbf{a}(\theta_2)\right]^{H}\left[\mathbf{a}(\theta_1)+\mathbf{a}(\theta_2)\right]} = \frac{-\mathbf{a}^{H}(\theta)\left(\ddot{\mathbf{a}}(\theta_1)+\ddot{\mathbf{a}}(\theta_2)\right)\left(\dot{\mathbf{a}}(\theta_1)+\dot{\mathbf{a}}(\theta_2)\right)^{H}\mathbf{a}(\theta)}{\left[\dot{\mathbf{a}}(\theta_1)+\dot{\mathbf{a}}(\theta_2)\right]^{H}\left[\dot{\mathbf{a}}(\theta_1)+\dot{\mathbf{a}}(\theta_2)\right]} \tag{3-5}$$

Noting that

$$\begin{aligned}&\mathbf{a}^{H}(\theta)\ddot{\mathbf{a}}(\theta_1) = -\dot{\mathbf{a}}^{H}(\theta)\dot{\mathbf{a}}(\theta_1),\ \mathbf{a}^{H}(\theta)\ddot{\mathbf{a}}(\theta_2) = -\dot{\mathbf{a}}^{H}(\theta)\dot{\mathbf{a}}(\theta_2)\\ &(\dot{\mathbf{a}}(\theta_1)+\dot{\mathbf{a}}(\theta_2))^{H}(\dot{\mathbf{a}}(\theta_1)+\dot{\mathbf{a}}(\theta_2)) = 2\dot{\mathbf{a}}^{H}(\theta_1)(\dot{\mathbf{a}}(\theta_1)+\dot{\mathbf{a}}(\theta_2))\\ &(\mathbf{a}(\theta_1)+\mathbf{a}(\theta_2))^{H}(\mathbf{a}(\theta_1)+\mathbf{a}(\theta_2)) = 2\mathbf{a}^{H}(\theta_1)(\mathbf{a}(\theta_1)+\mathbf{a}(\theta_2))\end{aligned} \tag{3-6}$$

the above equality reduces to

$$\frac{\left\{\mathbf{a}(\theta_1)+\mathbf{a}(\theta_2)\right\}^{H}\left[\mathbf{a}(\theta)\dot{\mathbf{a}}^{H}(\theta_1)\right]\left\{\dot{\mathbf{a}}(\theta_1)+\dot{\mathbf{a}}(\theta_2)\right\}}{\left\{\mathbf{a}(\theta_1)+\mathbf{a}(\theta_2)\right\}^{H}\left[\mathbf{a}(\theta_1)\dot{\mathbf{a}}^{H}(\theta)\right]\left\{\dot{\mathbf{a}}(\theta_1)+\dot{\mathbf{a}}(\theta_2)\right\}} = 1 \tag{3-7}$$

For centro-Hermitian vectors we have $(\mathbf{a}(\theta_1)+\mathbf{a}(\theta_2))^{H}\mathbf{a}(\theta_1) = (\mathbf{a}(\theta_1)+\mathbf{a}(\theta_2))^{H}\mathbf{a}(\theta_2)$ and $\dot{\mathbf{a}}^{H}(\theta_1)(\dot{\mathbf{a}}(\theta_1)+\dot{\mathbf{a}}(\theta_2)) = \dot{\mathbf{a}}^{H}(\theta_2)(\dot{\mathbf{a}}(\theta_1)+\dot{\mathbf{a}}(\theta_2))$. As such, the above could also be written as

$$\frac{\left\{\mathbf{a}(\theta_1)+\mathbf{a}(\theta_2)\right\}^{H}\left[\mathbf{a}(\theta)\dot{\mathbf{a}}^{H}(\theta_2)\right]\left\{\dot{\mathbf{a}}(\theta_1)+\dot{\mathbf{a}}(\theta_2)\right\}}{\left\{\mathbf{a}(\theta_1)+\mathbf{a}(\theta_2)\right\}^{H}\left[\mathbf{a}(\theta_2)\dot{\mathbf{a}}^{H}(\theta)\right]\left\{\dot{\mathbf{a}}(\theta_1)+\dot{\mathbf{a}}(\theta_2)\right\}} = 1 \tag{3-8}$$

The only difference in the numerator and denominator of (3-7) and (3-8) is the inner matrix.

In order for these equalities to hold we require that either $\mathbf{a}(\theta) = \mathbf{a}(\theta_1)$ or $\mathbf{a}(\theta) = \mathbf{a}(\theta_2)$. Hence, for the case of zero noise the d-MUSIC algorithm will provide an unbiased and unique solution for the two source directions.

This completes the proof.

Owing to its close similarity, the d-MUSIC null spectrum $S(\theta)$ produces a response similar to the MUSIC null spectrum, $S_M(\theta)$. There are several important differences however.

For the noiseless case the MUSIC null spectrum will produce true nulls at the source bearings, i.e., $\mathbf{a}^H(\theta_1)\, S_M(\theta)\, \mathbf{a}(\theta_1) = \mathbf{a}^H(\theta_2)\, S_M(\theta)\, \mathbf{a}(\theta_2) = 0$. In contrast, d-MUSIC will have a minimum at these values, but not a true zero, i.e., $\mathbf{a}^H(\theta_1)\, S(\theta)\, \mathbf{a}(\theta_1) = \mathbf{a}^H(\theta_2)\, S(\theta)\, \mathbf{a}(\theta_2) =$ a small positive number. This must be as $\dot{\mathbf{a}}(\theta_1) + \dot{\mathbf{a}}(\theta_2)$ does not lie fully in the signal subspace.

One may interpret this result as the d-MUSIC response having a flatter null near the solution point. As the source spread increases the first order Taylor series approximation weakens, with the result that the residual value increases and the null will appear flatter. In many respects d-MUSIC behaves as a spatial lowpass filtered version of MUSIC. The inspiration for this analogy stems from the errors associated with the first-order Taylor series approximation.

The Taylor series approximation of equation (2-29) may be characterized as

$$\dot{\mathbf{a}}(\theta_1) + \dot{\mathbf{a}}(\theta_2) = \frac{2}{\delta}\left\{\mathbf{a}(\theta_1) - \mathbf{a}(\theta_2)\right\} + \mathbf{e} \tag{3-9}$$

where $\delta = \alpha_1 - \alpha_2 = 2\pi d \sin(\theta_1)/\lambda - 2\pi d \sin(\theta_2)/\lambda$ and $\mathbf{e}$ is the approximation error.

The structure of $\mathbf{e}$ provides useful insights on how d-MUSIC works. The nth element of the above equation is

$$\dot{\mathbf{a}}(\theta_1, n) + \dot{\mathbf{a}}(\theta_2, n) = \frac{2}{\delta}\left\{\mathbf{a}(\theta_1, n) - \mathbf{a}(\theta_2, n)\right\} + \mathbf{e}(n) \tag{3-10}$$

or

$$\left(n-\frac{N-1}{2}\right)e^{j\left(\frac{\alpha_1+\alpha_2}{2}\right)\left(n-\frac{N-1}{2}\right)}\cos\left(\frac{\delta}{2}\left(n-\frac{N-1}{2}\right)\right)= \tag{3-11}$$
$$\frac{\mathbf{e}(n)}{2j}+\frac{2}{\delta}e^{j\left(\frac{\alpha_1+\alpha_2}{2}\right)\left(n-\frac{N-1}{2}\right)}\sin\left(\frac{\delta}{2}\left(n-\frac{N-1}{2}\right)\right)$$

The error is thus

$$\mathbf{e}(n)=2je^{j\left(\frac{\alpha_1+\alpha_2}{2}\right)\left(n-\frac{N-1}{2}\right)}\left\{\begin{array}{l}\left(n-\frac{N-1}{2}\right)\cos\left(\frac{\delta}{2}\left(n-\frac{N-1}{2}\right)\right)\\ -\frac{2}{\delta}\sin\left(\frac{\delta}{2}\left(n-\frac{N-1}{2}\right)\right)\end{array}\right\} \tag{3-12}$$

Note that each element of $\dot{\mathbf{a}}(\theta_1)+\dot{\mathbf{a}}(\theta_2)$, $\mathbf{a}(\theta_1)+\mathbf{a}(\theta_2)$ and $\mathbf{e}$ all have the same phase. Hence, The Taylor series approximation does not introduce a phase error, only an amplitude error.

Thus an equivalent model for the first order Taylor series approximation is

$$\dot{\mathbf{a}}(\theta_1)+\dot{\mathbf{a}}(\theta_2)=\mathbf{C}\{\mathbf{a}(\theta_1)-\mathbf{a}(\theta_2)\} \tag{3-13}$$

where the nth element of the diagonal matrix $\mathbf{C}$ is defined as

$$\mathbf{C}(n,n)=\left(n-\frac{N-1}{2}\right)\frac{\cos\left(\frac{\delta}{2}\left(n-\frac{N-1}{2}\right)\right)}{\sin\left(\frac{\delta}{2}\left(n-\frac{N-1}{2}\right)\right)}=\left(n-\frac{N-1}{2}\right)\cot\left(\frac{\delta}{2}\left(n-\frac{N-1}{2}\right)\right) \tag{3-14}$$

Figure 3-1 is a plot of the amplitude weights for a 10 element linear array with $\lambda/2$ spacing and a source spacing of 2 and 3° (distance from peak to first null of the broadside beam is 11.5°, 3 dB beamwidth is 10.2°). The weights are normalized with respect to a centre element. Clearly, the amplitude weights act as a spatially lowpass window function. The window tapering increases as the source spacing increases.

Though it only applies to one of the signal space vectors the analogy of d-MUSIC acting as a spatial lowpass filtered version of MUSIC becomes clear. Like normal beamforming, the application of an even symmetric window function does not change the phase information content of the data or introduce a bias in the direction estimate, but it will act to broaden the main lobe of the beam response. In this context we can interpret this behavior as a broadening or

flattening of the d-MUSIC nulls.

To solidify this point, Figure 3-2 depicts the d-MUSIC and MUSIC null spectra for a $d = \lambda/2$ spaced 10 element linear array for a source spacing of 2° with zero noise. The sources are uncorrelated. The curves are plotted as $-10 \log_{10} S(\theta)$ in order for a null to appear as a peak.

Double precession arithmetic was employed so the MUSIC spectrum estimate reached a peak of 140 dB (near machine precision). Due to the amplitude errors associated with the Taylor series approximation the d-MUSIC estimate, though unbiased, represents a "blunted" version of the MUSIC response. The peak value of 50 dB matches the residual value for this case

From first inspection it would appear that MUSIC has a distinct advantage over d-MUSIC in terms of resolution. When one considers other issues such as the fact that d-MUSIC exploits *a priori* information and also weigh the problems associated with noise, signal correlation and that of extracting an accurate estimate for all signal space eigenvectors for a finite number of samples, this "gap" will tend to close. The remainder of this chapter studies the performance of the d-MUSIC algorithm in the presence of Gaussian sensor noise and compares its performance to that of MUSIC.

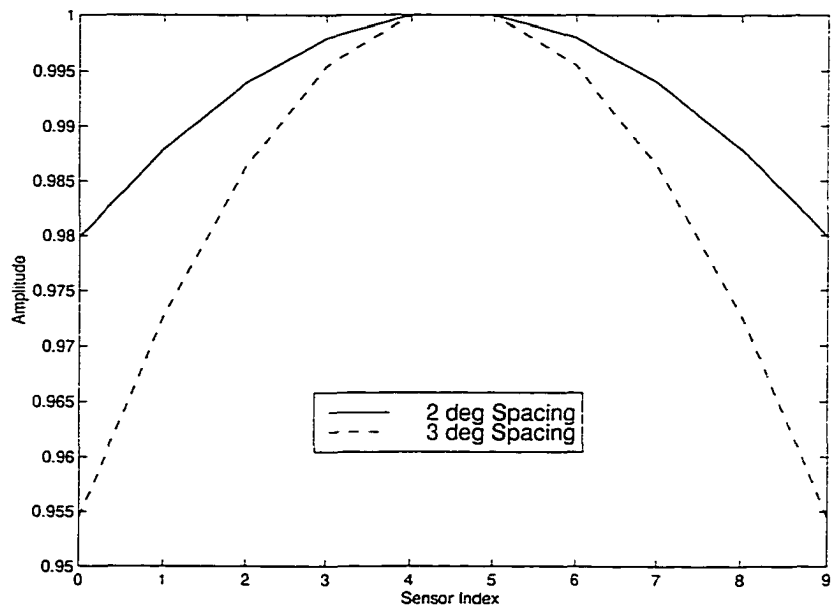

Figure 3.1 Taylor series amplitude distortion for a 10 sensor array with array spacing $d = \lambda/2$.

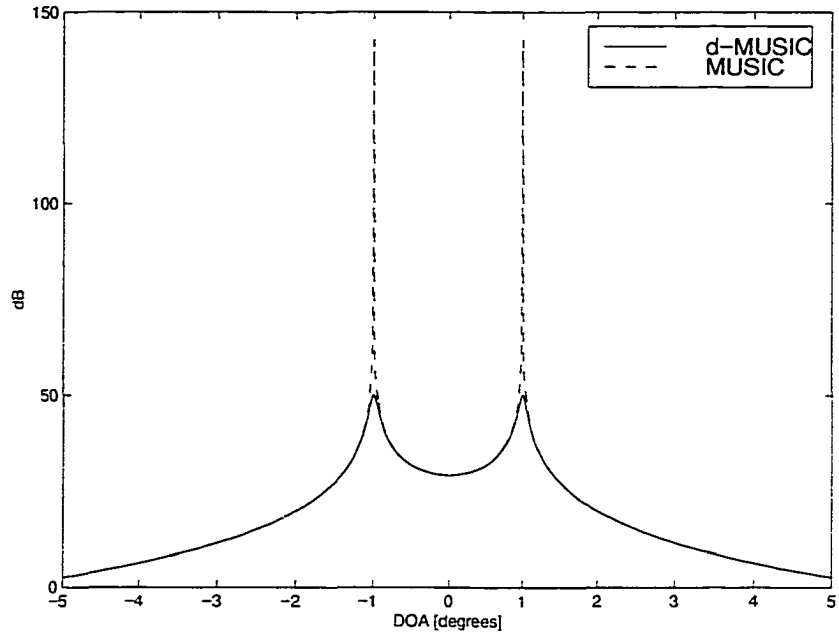

Figure 3.2 MUSIC and d-MUSIC spectra for a 10 sensor array, d = λ/2, and a 2° source spacing.

3.3 Signal Model

Assuming a set of fixed array and ϕ errors, the signal model for a single array snapshot generated from the coherent addition of K snapshots (e.g., Doppler processing using a FFT) is

$$\mathbf{x} = \mathbf{V}_R(-\beta)\mathbf{G}\{k_1\mathbf{a}(\theta_T) + k_2\mathbf{a}(\theta_R)\} + \mathbf{n} \tag{3-15}$$

where $\mathbf{G}$ is a diagonal matrix of array error weights, $\mathbf{V}_R(-\beta)$ is a rotation operator (a diagonal matrix) representing the array tilt angle β (see equation 2-32). The elevation angles θ_T and θ_R are with respect to a reference line parallel to the surface extending from the center of the array (see Figure 1-1). The signal is assumed to be deterministic (typical of radar problems).

The temporally and spatially white Gaussian noise vector $\mathbf{n}$ has statistics

$$\begin{aligned} E\{\mathbf{n}\} &= 0 \\ E\{\mathbf{n}\mathbf{n}^H\} &= \mathbf{I}\sigma^2 / K \end{aligned} \tag{3-16}$$

where $E\{\bullet\}$ denotes the statistical expectation operator. Note that the noise variance is normalized by the number of snapshots K to reflect the fact that some form of coherent processing is employed.

Further note that the sensor noise vector is not multiplied by the array errors **G**. **G** is assumed to result from gain and phase differences between receivers and between antennas. As the noise term is assumed to be the result of receiver thermal noise, which is assumed to the same for all receivers, the calibration errors **G** should only effect the signal term.

Say that an estimate $\hat{\phi}$ for the cluster centroid $\phi = (\theta_T + \theta_R)/2$ is available and the array tilt angle is estimated as $\hat{\beta}$. The array snapshot vector can be adjusted as

$$\begin{aligned} \mathbf{x}_P &= \mathbf{V}_R(\hat{\phi})\mathbf{V}_R(\hat{\beta})\mathbf{x} \\ &= \mathbf{V}_R(\hat{\phi})\mathbf{V}_R(\hat{\beta})\mathbf{V}_R(-\beta)\mathbf{G}\{k_1\mathbf{a}(\theta_T) + k_2\mathbf{a}(\theta_R)\} + \mathbf{n} \\ &= \mathbf{V}_R(\hat{\phi})\mathbf{V}_R(\hat{\beta})\mathbf{V}_R(-\beta)\mathbf{V}_R(-\phi)\mathbf{G}\{k_1\mathbf{a}(\gamma) + k_2\mathbf{a}(-\gamma)\} + \mathbf{n} \\ &= \mathbf{V}_R(\eta_\phi)\mathbf{V}_R(\eta_\beta)\mathbf{G}\{k_1\mathbf{a}(\gamma) + k_2\mathbf{a}(-\gamma)\} + \mathbf{n} \end{aligned} \tag{3-17}$$

where

$$\begin{aligned} \gamma &= (\theta_T - \theta_R)/2 \\ \eta_\phi &= \sin^{-1}\{\sin\hat{\phi} - \sin\phi\} \\ \eta_\beta &= \sin^{-1}\{\sin\hat{\beta} - \sin\beta\} \end{aligned} \tag{3-18}$$

Note that the phase weights $\mathbf{V}_R(\hat{\phi})\mathbf{V}_R(\hat{\beta})$ do not affect the noise vector **n**. The application of phase weights to each of the independent noise channels does not affect its statistics.

The d-MUSIC signal space vectors are

$$\mathbf{u} = (\mathbf{I}+\mathbf{J})\mathbf{x}_P = \mathbf{u}_s + \mathbf{n}_d \tag{3-19}$$

$$\dot{\mathbf{u}} = \mathbf{D}\mathbf{u} = \dot{\mathbf{u}}_s + \mathbf{D}\mathbf{n}_d \tag{3-20}$$

where

$$\mathbf{u}_S = (\mathbf{I}+\mathbf{J})\mathbf{V}_R(\eta_\phi)\mathbf{V}_R(\eta_\beta)\mathbf{G}\{k_1\mathbf{a}(\gamma) + k_2\mathbf{a}(-\gamma)\} \tag{3-21}$$

$$\mathbf{n}_d = (\mathbf{I}+\mathbf{J})\mathbf{n} \tag{3-22}$$

The above model includes the effects of Gaussian sensor noise, fixed array errors and a fixed tilt bias. Say that $\eta_\phi = \eta_\beta = 0$ and $\mathbf{G} = \mathbf{I}$, then $\mathbf{u}_S = \{k_1 + k_2\}\{\mathbf{a}(\gamma) + \mathbf{a}(-\gamma)\}$ and we have the

desired result. In the error analysis no assumptions will be made regarding the structure of $\mathbf{u}_S$ other than the fact that $\mathbf{J}\,\mathbf{u}_S = \mathbf{u}_S$ which is obvious given equation (3-21).

The d-MUSIC noise vector $\mathbf{n}_d$ has several important properties. Due to the forward-backward averaging operation $\mathbf{I} + \mathbf{J}$ the noise is now spatially correlated with statistics

$$\begin{aligned} E\{\mathbf{n}_d\} &= \mathbf{0} \\ E\{\mathbf{n}_d \mathbf{n}_d^H\} &= (\mathbf{I}+\mathbf{J})\sigma^2 / K \end{aligned} \tag{3-23}$$

The cost of removing the need to estimate k_1 and k_2 via the $\mathbf{I} + \mathbf{J}$ operation is to convert spatially white noise into spatially correlated noise. In this case the noise covariance matrix has the same power along the main diagonal and the anti-diagonal. The effect of this spatially correlated noise is to increase the variance of the d-MUSIC estimate.

3.4 The Statistics of the d-MUSIC Null Spectrum

To set the stage for the theoretical error analysis we need to evaluate both the mean and variance of several d-MUSIC projection terms related to the null spectrum. Based on the signal model of the last section the estimate for the d-MUSIC signal space projector is

$$\hat{\mathbf{P}}_S = \frac{\mathbf{u}\,\mathbf{u}^H}{\mathbf{u}^H\mathbf{u}} + \frac{\dot{\mathbf{u}}\,\dot{\mathbf{u}}^H}{\dot{\mathbf{u}}^H\dot{\mathbf{u}}} \tag{3-24}$$

As the denominator terms also contain noise it will be convenient to define the estimate for the d-MUSIC null spectrum as

$$S(\theta) = \mathbf{a}^H(\theta)\hat{\mathbf{P}}_N\,\mathbf{a}(\theta) \tag{3-25}$$

where the estimate for the noise space projector is defined as

$$\hat{\mathbf{P}}_N = c\,\mathbf{I} - c\,\hat{\mathbf{P}}_S \tag{3-26}$$

and

$$c = (\mathbf{u}^H\mathbf{u})(\dot{\mathbf{u}}^H\dot{\mathbf{u}}) \tag{3-27}$$

Note that $\hat{\mathbf{P}}_N$ will not match the true noise space projector even for zero array errors and no noise due to the model error associated with the Taylor series approximation. Retaining terms to

the second moment, the expected value of $\hat{\mathbf{P}}_N$ is

$$
\begin{aligned}
E\left\{\hat{\mathbf{P}}_N\right\} = {} & (\mathbf{u}_S^H\mathbf{u}_S)(\dot{\mathbf{u}}_S^H\dot{\mathbf{u}}_S)\mathbf{I} - (\dot{\mathbf{u}}_S^H\dot{\mathbf{u}}_S)\mathbf{u}_S\mathbf{u}_S^H - (\mathbf{u}_S^H\mathbf{u}_S)\dot{\mathbf{u}}_S\dot{\mathbf{u}}_S^H \\
& + \frac{\sigma^2}{K}\left\{2\,\mathrm{tr}(\mathbf{D}^H\mathbf{D})\mathbf{u}_S^H\mathbf{u}_S + 2N\dot{\mathbf{u}}_S^H\dot{\mathbf{u}}_S - 4\mathbf{u}_S^H\ddot{\mathbf{u}}_S - 4\ddot{\mathbf{u}}_S^H\mathbf{u}_S\right\}\mathbf{I} \\
& - \frac{\sigma^2}{K}\left\{2(\dot{\mathbf{u}}_S^H\dot{\mathbf{u}}_S)(\mathbf{I}+\mathbf{J}) + 2(\mathbf{u}_S^H\mathbf{u}_S)\mathbf{D}(\mathbf{I}+\mathbf{J})\mathbf{D}^H\right\} \\
& - \frac{\sigma^2}{K}\left\{2\,\mathrm{tr}(\mathbf{D}^H\mathbf{D})\mathbf{u}_S\mathbf{u}_S^H + (2N+8)\dot{\mathbf{u}}_S\dot{\mathbf{u}}_S^H - 4\mathbf{u}_S\ddot{\mathbf{u}}_S^H - 4\ddot{\mathbf{u}}_S\mathbf{u}_S^H\right\}
\end{aligned}
\tag{3-28}
$$

where $\mathrm{tr}\{\bullet\}$ denotes the matrix trace operation (sum of main diagonal).

Another useful statistic is the mean of $c\hat{\mathbf{P}}_S$. Retaining terms to the second moment the expected value is

$$
\begin{aligned}
E\left\{c\hat{\mathbf{P}}_S\right\} = {} & (\dot{\mathbf{u}}_S^H\dot{\mathbf{u}}_S)\mathbf{u}_S\mathbf{u}_S^H + (\mathbf{u}_S^H\mathbf{u}_S)\dot{\mathbf{u}}_S\dot{\mathbf{u}}_S^H \\
& + \frac{\sigma^2}{K}\left\{2(\dot{\mathbf{u}}_S^H\dot{\mathbf{u}}_S)(\mathbf{I}+\mathbf{J}) + 2(\mathbf{u}_S^H\mathbf{u}_S)\mathbf{D}(\mathbf{I}+\mathbf{J})\mathbf{D}^H\right\} \\
& + \frac{\sigma^2}{K}\left\{2\,\mathrm{tr}(\mathbf{D}^H\mathbf{D})\mathbf{u}_S\mathbf{u}_S^H + (2N+8)\dot{\mathbf{u}}_S\dot{\mathbf{u}}_S^H - 4\mathbf{u}_S\ddot{\mathbf{u}}_S^H - 4\ddot{\mathbf{u}}_S\mathbf{u}_S^H\right\}
\end{aligned}
\tag{3-29}
$$

A statistic of particular interest in the error analysis is $E\left\{(\mathbf{p}^H c\hat{\mathbf{P}}_S\mathbf{q})(\mathbf{r}^H c\hat{\mathbf{P}}_S\mathbf{s})\right\}$ where $\mathbf{p}$, $\mathbf{q}$, $\mathbf{r}$, and $\mathbf{s}$ are steering vectors or a steering vector derivative. Its value to second order is

$$
\begin{aligned}
E\left\{(\mathbf{p}^H c\hat{\mathbf{P}}_S\mathbf{q})(\mathbf{r}^H c\hat{\mathbf{P}}_S\mathbf{s})\right\} = {} & C_1C_2 + \frac{\sigma^2}{K}\mathbf{b}_1^T\mathbf{B}_1^H\mathbf{B}_4\mathbf{b}_4 + \sigma_C^2\,\mathbf{b}_3^T\mathbf{B}_3^H\mathbf{B}_2\mathbf{b}_2 \\
& + \frac{\sigma^2}{K}\left\{\sum_{n=1}^{6} C_2\mathbf{b}_5(n)\mathbf{B}_5^H(:,n)\mathbf{B}_6(:,n) + C_1\mathbf{b}_6(n)\mathbf{B}_7^H(:,n)\mathbf{B}_8(:,n)\right\} \\
& + \frac{\sigma^2}{K}C_2\left\{2\,\mathrm{tr}(\mathbf{D}^H\mathbf{D})\mathbf{p}^H\mathbf{u}_S\mathbf{u}_S^H\mathbf{q} + 2N\mathbf{p}^H\dot{\mathbf{u}}_S\dot{\mathbf{u}}_S^H\mathbf{q}\right\} \\
& + \frac{\sigma^2}{K}C_1\left\{2\,\mathrm{tr}(\mathbf{D}^H\mathbf{D})\mathbf{r}^H\mathbf{u}_S\mathbf{u}_S^H\mathbf{s} + 2N\mathbf{r}^H\dot{\mathbf{u}}_S\dot{\mathbf{u}}_S^H\mathbf{s}\right\}
\end{aligned}
\tag{3-30}
$$

where the (:,n) notation denotes the nth column of a matrix and

$$C_1 = (\dot{\mathbf{u}}_S^H \dot{\mathbf{u}}_S)(\mathbf{p}^H \mathbf{u}_S)(\mathbf{u}_S^H \mathbf{q}) + (\mathbf{u}_S^H \mathbf{u}_S)(\mathbf{p}^H \dot{\mathbf{u}}_S)(\dot{\mathbf{u}}_S^H \mathbf{q}) \tag{3-31}$$

$$C_2 = (\dot{\mathbf{u}}_S^H \dot{\mathbf{u}}_S)(\mathbf{r}^H \mathbf{u}_S)(\mathbf{u}_S^H \mathbf{s}) + (\mathbf{u}_S^H \mathbf{u}_S)(\mathbf{r}^H \dot{\mathbf{u}}_S)(\dot{\mathbf{u}}_S^H \mathbf{s}) \tag{3-32}$$

$$\mathbf{b}_1 = \left[-2(\mathbf{p}^H \mathbf{u}_S)(\mathbf{u}_S^H \mathbf{q}), (\dot{\mathbf{u}}_S^H \dot{\mathbf{u}}_S)(\mathbf{u}_S^H \mathbf{q}), 2(\mathbf{p}^H \dot{\mathbf{u}}_S)(\dot{\mathbf{u}}_S^H \mathbf{q}), -(\mathbf{u}_S^H \mathbf{u}_S)(\dot{\mathbf{u}}_S^H \mathbf{q})\right]^T \tag{3-33}$$

$$\mathbf{b}_2 = \left[-2(\mathbf{p}^H \mathbf{u}_S)(\mathbf{u}_S^H \mathbf{q}), (\dot{\mathbf{u}}_S^H \dot{\mathbf{u}}_S)(\mathbf{p}^H \mathbf{u}_S), 2(\mathbf{p}^H \dot{\mathbf{u}}_S)(\dot{\mathbf{u}}_S^H \mathbf{q}), -(\mathbf{u}_S^H \mathbf{u}_S)(\mathbf{p}^H \dot{\mathbf{u}}_S)\right]^T \tag{3-34}$$

$$\mathbf{b}_3 = \left[-2(\mathbf{r}^H \mathbf{u}_S)(\mathbf{u}_S^H \mathbf{s}), (\dot{\mathbf{u}}_S^H \dot{\mathbf{u}}_S)(\mathbf{u}_S^H \mathbf{s}), 2(\mathbf{r}^H \dot{\mathbf{u}}_S)(\dot{\mathbf{u}}_S^H \mathbf{s}), -(\mathbf{u}_S^H \mathbf{u}_S)(\dot{\mathbf{u}}_S^H \mathbf{s})\right]^T \tag{3-35}$$

$$\mathbf{b}_4 = \left[-2(\mathbf{r}^H \mathbf{u}_S)(\mathbf{u}_S^H \mathbf{s}), (\dot{\mathbf{u}}_S^H \dot{\mathbf{u}}_S)(\mathbf{r}^H \mathbf{u}_S), 2(\mathbf{r}^H \dot{\mathbf{u}}_S)(\dot{\mathbf{u}}_S^H \mathbf{s}), -(\mathbf{u}_S^H \mathbf{u}_S)(\mathbf{r}^H \dot{\mathbf{u}}_S)\right]^T \tag{3-36}$$

$$\mathbf{b}_5 = \left[-2\mathbf{p}^H \mathbf{u}_S, -2\mathbf{u}_S^H \mathbf{q}, \dot{\mathbf{u}}_S^H \dot{\mathbf{u}}_S, -2\mathbf{p}^H \dot{\mathbf{u}}_S, -2\dot{\mathbf{u}}_S^H \mathbf{q}, \mathbf{u}_S^H \mathbf{u}_S\right]^T \tag{3-37}$$

$$\mathbf{b}_6 = \left[-2\mathbf{r}^H \mathbf{u}_S, -2\mathbf{u}_S^H \mathbf{s}, \dot{\mathbf{u}}_S^H \dot{\mathbf{u}}_S, -2\mathbf{r}^H \dot{\mathbf{u}}_S, -2\dot{\mathbf{u}}_S^H \mathbf{s}, \mathbf{u}_S^H \mathbf{u}_S\right]^T \tag{3-38}$$

$$\mathbf{B}_1 = \left[\ddot{\mathbf{u}}_S, \mathbf{p} + \mathbf{p}^*, \mathbf{u}_S, \dot{\mathbf{p}} + (\dot{\mathbf{p}})^*\right] \tag{3-39}$$

$$\mathbf{B}_2 = \left[\ddot{\mathbf{u}}_S, \mathbf{q} + \mathbf{q}^*, \mathbf{u}_S, \dot{\mathbf{q}} + (\dot{\mathbf{q}})^*\right] \tag{3-40}$$

$$\mathbf{B}_3 = \left[\ddot{\mathbf{u}}_S, \mathbf{r} + \mathbf{r}^*, \mathbf{u}_S, \dot{\mathbf{r}} + (\dot{\mathbf{r}})^*\right] \tag{3-41}$$

$$\mathbf{B}_4 = \left[\ddot{\mathbf{u}}_S, \mathbf{s} + \mathbf{s}^*, \mathbf{u}_S, \dot{\mathbf{s}} + (\dot{\mathbf{s}})^*\right] \tag{3-42}$$

$$\mathbf{B}_5 = \left[\ddot{\mathbf{u}}_S, \mathbf{p} + \mathbf{p}^*, \mathbf{p} + \mathbf{p}^*, \mathbf{u}_S, \dot{\mathbf{p}} + (\dot{\mathbf{p}})^*, \dot{\mathbf{p}} + (\dot{\mathbf{p}})^*\right] \tag{3-43}$$

$$\mathbf{B}_6 = \left[\mathbf{q} + \mathbf{q}^*, \ddot{\mathbf{u}}_S, \mathbf{q} + \mathbf{q}^*, \dot{\mathbf{q}} + (\dot{\mathbf{q}})^*, \mathbf{u}_S, \dot{\mathbf{q}} + (\dot{\mathbf{q}})^*\right] \tag{3-44}$$

$$\mathbf{B}_7 = \left[\ddot{\mathbf{u}}_S, \mathbf{r} + \mathbf{r}^*, \mathbf{r} + \mathbf{r}^*, \mathbf{u}_S, \dot{\mathbf{r}} + (\dot{\mathbf{r}})^*, \dot{\mathbf{r}} + (\dot{\mathbf{r}})^*\right] \tag{3-45}$$

$$\mathbf{B}_8 = \left[\mathbf{s} + \mathbf{s}^*, \ddot{\mathbf{u}}_S, \mathbf{s} + \mathbf{s}^*, \dot{\mathbf{s}} + (\dot{\mathbf{s}})^*, \mathbf{u}_S, \dot{\mathbf{s}} + (\dot{\mathbf{s}})^*\right] \tag{3-46}$$

The large numbers of terms appearing in (3-30) reflects the fact that the noise is spatially correlated and that the noise of $\mathbf{u}$ and $\dot{\mathbf{u}}$ is correlated. If ϕ were treated as an additional random variable the number of terms would dramatically increase, making the problem of deriving the

error variance for the case of unknown ϕ very difficult.

3.5 Error Statistics

Let θ_n denote the d-MUSIC estimate for a source bearing with true value γ_n. In this context $\gamma_1 = \gamma$ and $\gamma_2 = -\gamma$. The d-MUSIC measurement error will be

$$\varepsilon_n = \frac{2\pi d}{\lambda}\{\sin\theta_n - \sin\gamma_n\} \tag{3-47}$$

Owing to the non-linearity of the problem an exact expression for the error is difficult to derive. Following the approach of [10] an approximate expression for the error will be obtained via a first order Taylor series expansion of the first derivative of $S(\theta)$. At the solution point the first derivative of $S(\theta)$ is zero. Assuming that the errors are small we may write

$$0 = \dot{S}(\theta_n) \approx \dot{S}(\gamma_n) + \varepsilon_n \ddot{S}(\gamma_n) \tag{3-48}$$

The first and second derivatives of the null spectrum $S(\theta)$ with respect to $\alpha = 2\pi d \sin(\theta)/\lambda$ is

$$\begin{aligned}\dot{S}(\theta) = \frac{dS(\theta)}{d\alpha} &= \mathbf{a}^H(\theta)\left\{\mathbf{D}^H c\hat{\mathbf{P}}_S + c\hat{\mathbf{P}}_S \mathbf{D}\right\}\mathbf{a}(\theta) \\ &= \dot{\mathbf{a}}^H(\theta) c\hat{\mathbf{P}}_S \mathbf{a}(\theta) + \mathbf{a}^H(\theta) c\hat{\mathbf{P}}_S \dot{\mathbf{a}}(\theta)\end{aligned} \tag{3-49}$$

$$\begin{aligned}\ddot{S}(\theta) = \frac{d^2 S(\theta)}{d\alpha^2} &= \mathbf{a}^H(\theta)\left\{\mathbf{D}^H\mathbf{D}^H c\hat{\mathbf{P}}_S + 2\mathbf{D}^H c\hat{\mathbf{P}}_S \mathbf{D} + c\hat{\mathbf{P}}_S \mathbf{D}\,\mathbf{D}\right\}\mathbf{a}(\theta) \\ &= \ddot{\mathbf{a}}^H(\theta) c\hat{\mathbf{P}}_S \mathbf{a}(\theta) + 2\dot{\mathbf{a}}^H(\theta) c\hat{\mathbf{P}}_S \dot{\mathbf{a}}(\theta) + \mathbf{a}^H(\theta) c\hat{\mathbf{P}}_S \ddot{\mathbf{a}}(\theta)\end{aligned} \tag{3-50}$$

The estimate for the error is thus

$$\varepsilon_n \approx \frac{-\dot{S}(\gamma_n)}{\ddot{S}(\gamma_n)} \tag{3-51}$$

In the Stoica and Nehorai analysis the second derivative was replaced by its expected value. This is a good approximation for the d-MUSIC problem as well. Near the solution point the signal term of $\dot{S}(\gamma_n)$ is small while the signal term of $\ddot{S}(\gamma_n)$ is large. Figure 3-3 is a plot of the first and second derivative of $S(\theta)$ for a 10 element array with $d = \lambda/2$ and a source spacing of 2°.

Using the results of the last section we can compare the statistics of the numerator and

denominator of (3-51) for the case of no array and ϕ errors. Continuing with the 10 element linear array example with d = $\lambda/2$ and a source spacing of 2°, we will assume K = 100 snapshots and σ^2 equal to either 0.1 or 1 (roughly a 40 and 30 dB SNR, respectively for a broadside beam). The mean and standard deviation of $\dot{S}(\gamma_n)$ and $\ddot{S}(\gamma_n)$ for this case is listed in Table 3-1.

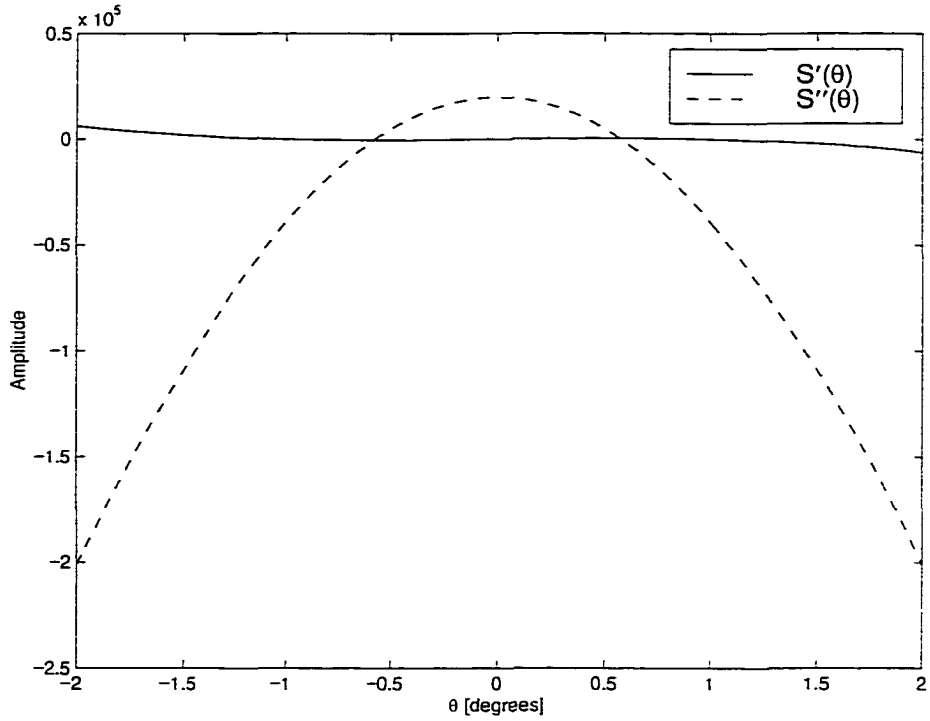

Figure 3.3 First and second derivative of S(θ) for a 10 sensor array (d=$\lambda/2$) and a 2° source spacing

Table 3-1

Mean and Standard Deviation of $\dot{S}(\gamma_n)$ and $\ddot{S}(\gamma_n)$ for K = 100 snapshots of a 10 element array with d = $\lambda/2$, source spacing of 2°, signal weights $k_1 = k_2 = 1$ and no array or ϕ errors

σ^2	$E\{\dot{S}(\gamma_n)\}$	std$\{\dot{S}(\gamma_n)\}$	$E\{\ddot{S}(\gamma_n)\}$	std$\{\ddot{S}(\gamma_n)\}$
0.1	4.37	5.53×10^3	-6.25×10^5	1.24×10^5
1.0	43.71	1.75×10^4	-6.27×10^5	3.93×10^5

The notation std{x} represents the standard deviation of random variable x.

Though the standard deviation of $\ddot{S}(\gamma_n)$ is nearly the same magnitude as its mean value the standard deviation of $\dot{S}(\gamma_n)$ clearly dominates over its mean value. Hence, the randomness of ε_n is largely determined by its numerator term $\dot{S}(\gamma_n)$ and as a first order approximation we can replace $\ddot{S}(\gamma_n)$ with its expected value.

This has the effect of reducing the overall mean and variance of the error ε_n but is a reasonable approximation in order to realize a tractable result. Otherwise we would need to compute the statistics of the ratio of two random variables, each of which contain terms up to fourth order in products of Gaussian random variables. Not an appealing prospect.

The same approximation is used by Stoica and Nehorai. Their argument was that the asymptotic (large K) distribution for the error should not be affected by the statistics of $\ddot{S}(\gamma_n)$. Like their problem, the effect of the variance of $\ddot{S}(\gamma_n)$ diminishes as σ^2/K decreases, so the asymptotic distribution of the d-MUSIC errors should not be affected by the statistics of $\ddot{S}(\gamma_n)$.

Replacing the second derivative term with its expected value the expression for the error reduces to

$$\varepsilon_n \approx \frac{-\dot{S}(\gamma_n)}{E\left\{\ddot{S}(\gamma_n)\right\}} \tag{3-52}$$

The mean of the first and second derivative of $S(\gamma_n)$ is

$$E\left\{\dot{S}(\gamma_n)\right\} = \dot{\mathbf{a}}^{\mathrm{H}}(\gamma_n) E\left\{c\hat{\mathbf{P}}_{\mathrm{S}}\right\} \mathbf{a}(\gamma_n) + \mathbf{a}^{\mathrm{H}}(\gamma_n) E\left\{c\hat{\mathbf{P}}_{\mathrm{S}}\right\} \dot{\mathbf{a}}(\gamma_n) \tag{3-53}$$

$$E\left\{\ddot{S}(\gamma_n)\right\} = \ddot{\mathbf{a}}^{\mathrm{H}}(\gamma_n) E\left\{c\hat{\mathbf{P}}_{\mathrm{S}}\right\} \mathbf{a}(\gamma_n) + 2\,\dot{\mathbf{a}}^{\mathrm{H}}(\gamma_n) E\left\{c\hat{\mathbf{P}}_{\mathrm{S}}\right\} \dot{\mathbf{a}}(\gamma_n) + \mathbf{a}^{\mathrm{H}}(\gamma_n) E\left\{c\hat{\mathbf{P}}_{\mathrm{S}}\right\} \ddot{\mathbf{a}}(\gamma_n) \tag{3-54}$$

where $E\left\{c\hat{\mathbf{P}}_{\mathrm{S}}\right\}$ is defined in equation (3-29).

The mean of the d-MUSIC error (bias) is

$$E\left\{\varepsilon_n\right\}_{\text{d-MU}} = -E\left\{\dot{S}(\gamma_n)\right\} / E\left\{\ddot{S}(\gamma_n)\right\} \tag{3-55}$$

and its variance is

$$\mathrm{var}\{\varepsilon_n\}_{\text{d-MU}} = E\left\{\left(\mathbf{p}^{\mathrm{H}} c\hat{\mathbf{P}}_{\mathrm{S}}\,\mathbf{q}\right)\left(\mathbf{r}^{\mathrm{H}} c\hat{\mathbf{P}}_{\mathrm{S}}\,\mathbf{s}\right)\right\}_{\substack{p=r=\hat{a}(\theta)\\ q=s=a(\theta)}} + E\left\{\left(\mathbf{p}^{\mathrm{H}} c\hat{\mathbf{P}}_{\mathrm{S}}\,\mathbf{q}\right)\left(\mathbf{r}^{\mathrm{H}} c\hat{\mathbf{P}}_{\mathrm{S}}\,\mathbf{s}\right)\right\}_{\substack{q=s=\hat{a}(\theta)\\ p=r=a(\theta)}} \tag{3-56}$$
$$+ 2E\left\{\left(\mathbf{p}^{\mathrm{H}} c\hat{\mathbf{P}}_{\mathrm{S}}\,\mathbf{q}\right)\left(\mathbf{r}^{\mathrm{H}} c\hat{\mathbf{P}}_{\mathrm{S}}\,\mathbf{s}\right)\right\}_{\substack{p=s=\hat{a}(\theta)\\ q=r=a(\theta)}} - \left|E\{\varepsilon_n\}\right|^2$$

where $\mathrm{var}\{\bullet\}$ denotes variance and $E\left\{(\mathbf{p}^{\mathrm{H}} c\hat{\mathbf{P}}_{\mathrm{S}}\mathbf{q})(\mathbf{r}^{\mathrm{H}} c\hat{\mathbf{P}}_{\mathrm{S}}\mathbf{s})\right\}$ is defined in equation (3-30). Owing to the symmetry of the problem the statistics of ε_1 are identical to those of ε_2, for the case of no array or ϕ errors.

A key point of this analysis is that the deterministic signal undergoes some form of coherent processing involving K snapshots. This assumes that the signal terms can be coherently added so that the signal energy grows relative to noise as K increases. As the number of snapshots increases, σ^2/K decreases, with the result that the mean value of the d-MUSIC error in (3-55) will go to zero in the limit as K approaches infinity. Hence, the asymptotic (large K) distribution of the d-MUSIC error can be treated as zero-mean for non-random signals (typical of target echoes for many radar applications). As such we can compare the asymptotic d-MUSIC error variance to the Cramér-Rao Bound.

3.6 The Cramér-Rao Bound (CRB) and MUSIC Errors

As forward-backward averaging of the form $\mathbf{R}_{\text{fb}} = (\mathbf{R} + \mathbf{J}\,\mathbf{R}^{*}\mathbf{J})/2$ is a relatively inexpensive operation to implement for the MUSIC algorithm, it shall be assumed throughout that the signal covariance matrix $\mathbf{S}$ for the MUSIC problem is in fact $\mathbf{S}_{\text{fb}} = (\mathbf{S} + \mathbf{J}\,\mathbf{S}^{*}\mathbf{J})/2$.

As the autocorrelation terms (main diagonal) of $\mathbf{S}$ are real, forward-backward averaging will remove the imaginary component of the cross correlation terms and thus reduce the total cross-correlation power. If the two signals are separated in phase by 90°, forward-backward averaging will serve to completely decorrelate the two signals.

From Stoica and Nehorai's analysis, the MUSIC errors were shown to be asymptotically zero mean. With forward-backward averaging, the asymptotic (large K) expression for the MUSIC error variance for two symmetrically placed sources is derived in [10] as

$$\mathrm{var}(\varepsilon_n)_{\text{MU}} = \left(\frac{\sigma^2}{2\mathrm{K}}\right)\left\{\left[\mathbf{S}_{\text{fb}}^{-1}\right]_{n,n} + \sigma^2\left[\mathbf{S}_{\text{fb}}^{-1}(\mathbf{A}^{\mathrm{H}}\mathbf{A})^{-1}\mathbf{S}_{\text{fb}}^{-1}\right]_{n,n}\right\} / h(\gamma_n) \tag{3-57}$$

where the notation $[\bullet]_{n,n}$ represents element (n,n) of a matrix and

$$h(\gamma_n) = \dot{\mathbf{a}}^H(\gamma_n)\left[\mathbf{I} - \mathbf{A}(\mathbf{A}^H\mathbf{A})^{-1}\mathbf{A}^H\right]\dot{\mathbf{a}}(\gamma_n) \tag{3-58}$$

$$\mathbf{A} = \left[\mathbf{a}(\gamma_1)\ \mathbf{a}(\gamma_2)\right] = \left[\mathbf{a}(\gamma)\ \mathbf{a}(-\gamma)\right] \tag{3-59}$$

A general expression for the asymptotic Cramér-Rao lower bound (CRB) assuming no *a priori* information is derived in [10]. With forward-backward averaging this expression becomes

$$\mathrm{var}(\varepsilon_n)_{CR} = \left(\frac{\sigma^2}{2K}\right)\left[\left(\left\{\dot{\mathbf{A}}^H\left[\mathbf{I} - \mathbf{A}(\mathbf{A}^H\mathbf{A})^{-1}\mathbf{A}^H\right]\dot{\mathbf{A}}\right\} \bullet \mathbf{S}_{fb}^T\right)^{-1}\right]_{n,n} \tag{3-60}$$

where $\mathbf{A} \bullet \mathbf{B}$ denotes the Hadamard (element-by-element) product of matrices **A** and **B**. For two sources symmetrically placed about the broadside direction we have

$$\dot{\mathbf{A}} = \left[\dot{\mathbf{a}}(\gamma_1)\ \dot{\mathbf{a}}(\gamma_2)\right] = \left[\dot{\mathbf{a}}(\gamma)\ \dot{\mathbf{a}}(-\gamma)\right] \tag{3-61}$$

Assuming that the geometric center of the source cluster is known it follows that $\gamma_1 = -\gamma_2 = \gamma$. In that case Stoica and Nehorai's derivation for the CRB can be easily adapted to provide a lower bound on the variance of the estimate for γ, half the source spacing. The CRB for this case is derived in Appendix B. From equation (B-13) of Appendix B, we have

$$\mathrm{var}(\varepsilon)_{CR,\,\phi=0} = \left(\frac{\sigma^2}{2K}\right) / \mathrm{Re}\left[\begin{bmatrix}1 & 1\end{bmatrix}\left\{\mathbf{H} \bullet \mathbf{S}^T\right\}\begin{bmatrix}1\\1\end{bmatrix}\right] \tag{3-62}$$

where ε is the error for the estimate of $2\pi d \sin(\gamma)/\lambda$ and

$$\mathbf{H} = \mathbf{D}_\gamma^*\left[\mathbf{I} - \mathbf{A}(\mathbf{A}^*\mathbf{A})^{-1}\mathbf{A}^*\right]\mathbf{D}_\gamma \tag{3-63}$$

$$\mathbf{D}_\gamma = \frac{\partial \mathbf{A}}{\partial \gamma} = \left[\mathbf{D}\mathbf{a}(\gamma)\,(\mathbf{D}\mathbf{a}(\gamma))^*\right] = \left[\dot{\mathbf{a}}(\gamma)\,(\dot{\mathbf{a}}(\gamma))^*\right] \tag{3-64}$$

The notation $\phi = 0$ identifies the CRB expression as having known ϕ.

3.7 Error Analysis: Comparison to MUSIC and the CRB

To explore the characteristics of the d-MUSIC algorithm we shall compare the asymptotic variance of equation (3-56) to the Cramér-Rao bound of equation (3-62) (ϕ is known). It will

also be instructive to compare these results to the asymptotic MUSIC variance of (3-57) and the general Cramér-Rao bound of equation (3-60) when the cluster center ϕ is not known.

The particulars of the array structure used in this study are listed below in Table 3-2.

Table 3-2 Linear array structure for the theoretical error analysis

Number of Sensors	10
Sensor Spacing (d)	$\lambda/2$
Rayleigh Resolution Beamwidth	11.53°

In the examples to follow the source spacing is referenced to the *Rayleigh resolution beamwidth* defined as the distance between the peak of the broadside beam to the first null for unity array weights. The Rayleigh resolution criterion has long been established as a bound for the resolving power of Fourier-based estimation techniques. High resolution techniques such as MUSIC seek to overcome this well known limit of standard (low resolution) beamforming. If one prefers to reference source spacing to the 3 dB beamwidth of the array, the spacing between 3 dB points of the broadside beam is 10.2° for this case. However, all results will be referenced with respect to the Rayleigh beamwidth in this work.

For convenience, the number of snapshots K will be set at 100. The two sources will also have equal power with signal covariance matrix

$$\mathbf{S} = \begin{bmatrix} 1 & e^{j\chi} \\ e^{-j\chi} & 1 \end{bmatrix} \tag{3-65}$$

In effect we have $k_1 = 1$ and $k_2 = e^{j\chi}$. If $\chi = 0°$ then the sources are coherent with a correlation coefficient of +1 and the target SNR is a maximum. If $\chi = 90°$ then the sources can be considered uncorrelated after forward-backward averaging. As χ nears 180° the SNR reaches a minimum and the probability of detection is reduced considerably.

This structure for **S** has an interesting interpretation for the radar low angle tracking problem. The target echo is often a Doppler shifted version of the narrowband transmit pulse and the short time delay between the direct and surface reflected rays can be modeled as a simple phase shift. As the target moves the path length difference between the two rays will change and so will the relative phase between signals. A problem of keen concern in low angle tracking are

the periods of low signal level known as *multipath nulls* [39-41] where the phase difference χ between signals is close to 180°. A radar will often cycle through a number of transmit frequencies to avoid such nulls.

After forward-backward averaging **S** reduces to

$$\mathbf{S}_{fb} = (\mathbf{S} + \mathbf{J}\mathbf{S}^*\mathbf{J})/2 = \begin{bmatrix} 1 & \cos\chi \\ \cos\chi & 1 \end{bmatrix} \tag{3-66}$$

S will be full rank for all values of χ except $\chi = 0°$ (coherent signal case). However, $\chi = 0°$ is the case when the combined signal attains its maximum SNR for the low angle tracking problem, but is precisely the case where the MUSIC algorithm breaks down.

The first 3 examples assume no array or ϕ errors. As the sources have the same power and the problem is symmetric about the array axis the variance of ε_1 and ε_2 is equal for either the MUSIC and d-MUSIC algorithms. In that event we need only show one set of results for each case. Note that the variance of ε_1 and ε_2 are equal for the d-MUSIC algorithm for no array or ϕ errors even if the sources have different powers. This is due to the d-MUSIC **I** + **J** forward-backward operation after which each steering vector is weighted by the same value, i.e., $k_1 + k_2$.

The first example uses $\sigma^2 = 0.1$. For 100 snapshots and a 10 sensor array the SNR of the detection will be a little over 40 dB if the sources cohere. The d-MUSIC variance versus the known ϕ CRB, $\text{var}(\varepsilon)_{CR,\phi=0}$ is plotted in Figure 3-4 while the MUSIC variance versus the two parameter CRB, $\text{var}(\varepsilon)_{CR}$ is plotted in Figure 3-5.

For the high SNR case of Figure 3-4 the d-MUSIC attains a much lower error variance than the MUSIC algorithm and in fact, nearly attains the Cramér-Rao bound $\text{var}(\varepsilon)_{CR,\phi=0}$. As the source spacing increases the d-MUSIC variance diverges from the CRB at about a beamwidth spacing. This is due to the degradation of the first order Taylor series approximation for a wide source spacing in creating the second signal space vector (d-MUSIC model error).

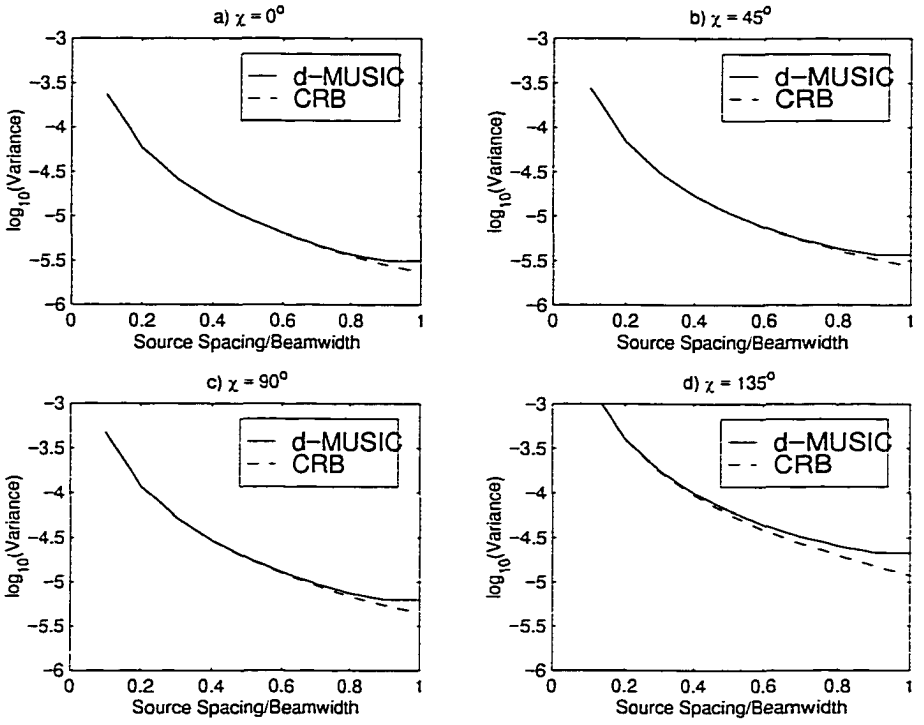

Figure 3.4 d-MUSIC variance and $\text{var}(\varepsilon)_{CR,\phi=0}$ for $\sigma^2 = 0.1$

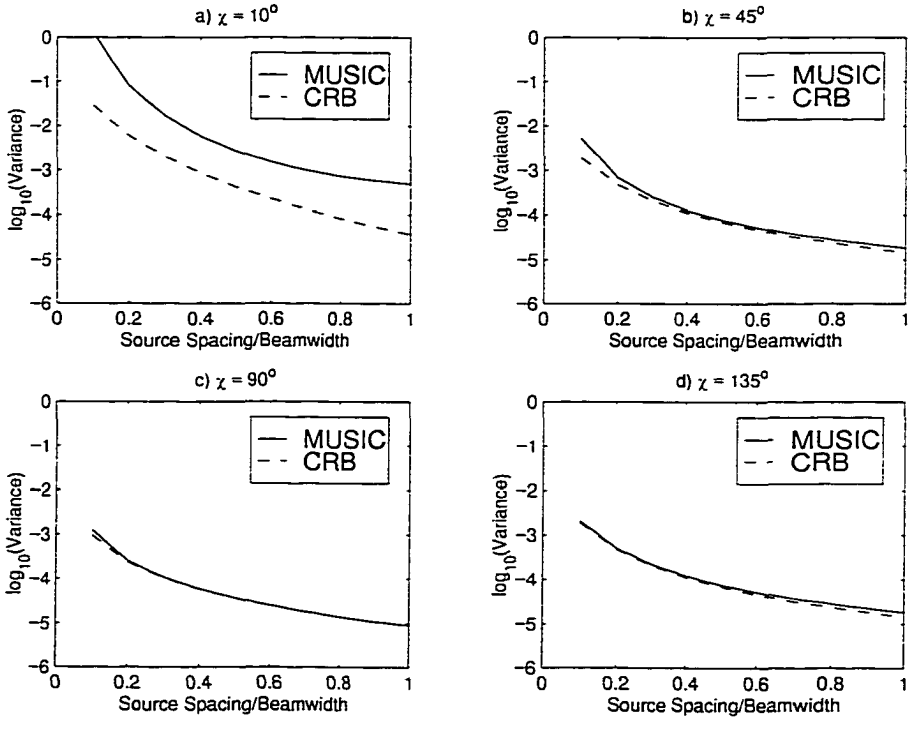

Figure 3.5 MUSIC variance and $\text{var}(\varepsilon)_{CR}$ for $\sigma^2 = 0.1$

The important thing to note from Figure 3-4 is that the performance of the d-MUSIC algorithm displays only a weak dependence on signal correlation, thus confirming the prediction of Chapter 2. As MUSIC will fail to resolve the sources for $\chi = 0°$ a value of $\chi = 10°$ is used in its place in order to compare it to the $\chi = 0°$ case for d-MUSIC. The best results for d-MUSIC are obtained when the sources cohere at $\chi = 0°$ (maximum SNR) and the results degrade as χ approaches 180° (minimum SNR).

This is in agreement with the Cramér-Rao bound $\text{var}(\varepsilon)_{CR,\,\phi=0}$ which displays a similar dependence on signal correlation as d-MUSIC. What the CRB has to teach us in this instance is that the problem of signal correlation is greatly diminished if the geometric center of the target cluster is known. This result confirms that the d-MUSIC solution of employing the $\mathbf{I} + \mathbf{J}$ forward-backward operation plus derivative information is indeed an effective strategy for defeating the correlated source problem when the cluster center is known.

In comparison, the MUSIC results of Figure 3-5 is affected by signal correlation and really only attains the CRB if the sources are uncorrelated ($\chi = 90°$). Note that the single parameter Cramér-Rao bound $\text{var}(\varepsilon)_{CR,\,\phi=0}$ is less than the two parameter bound $\text{var}(\varepsilon)_{CR}$, as expected.

The next case is for $\sigma^2 = 1$. If the sources cohere the SNR at detection using a broadside beam will be about 30 dB. The d-MUSIC results are plotted in Figure 3-6 while the MUSIC results are plotted in Figure 3-7. As expected, the variance of all estimates increase with the 10 dB drop in SNR, but d-MUSIC still achieves a lower variance than MUSIC. The attributes of the response as a function of χ (signal correlation/phase difference) is essentially the same.

One important difference for this case is that the MUSIC variance undergoes a greater displacement from the CRB than d-MUSIC. This indicates that d-MUSIC may have a better noise performance than MUSIC, and possibly a lower resolution threshold.

The next case is for $\sigma^2 = 10$ and the SNR at detection is roughly 20 dB for coherent signals. The results are plotted in Figures 3-8 and 3-9. The additional 10 dB increase in noise raises the variance of the d-MUSIC estimate yet it remains in close proximity to the CRB. In contrast, the MUSIC variance is now well separated from the CRB. This lends credence to the supposition that d-MUSIC may have a better noise performance than MUSIC for the case of known ϕ.

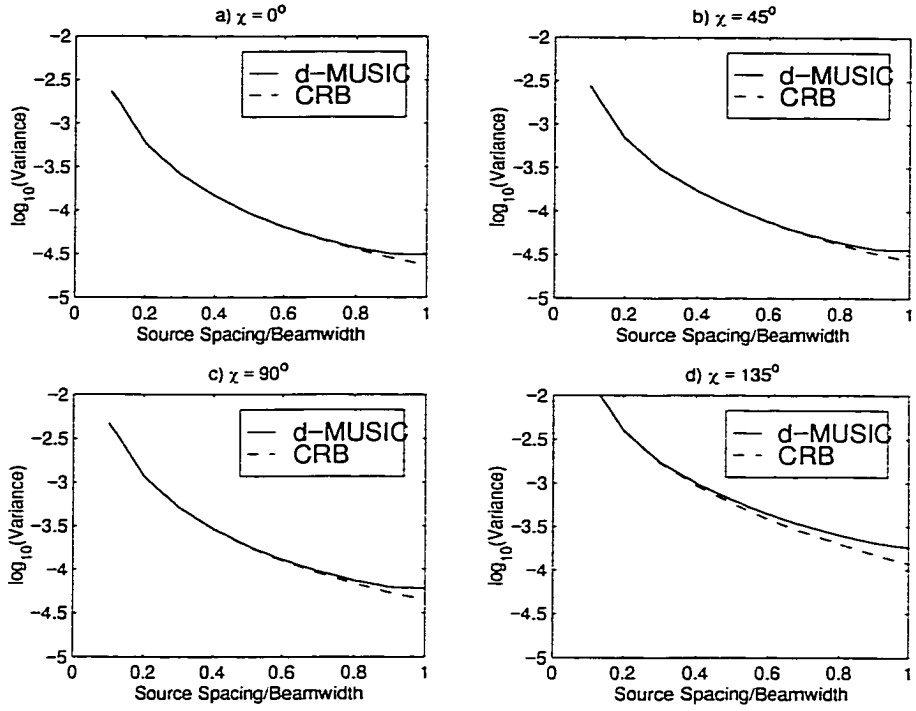

Figure 3.6 d-MUSIC variance and $\text{var}(\varepsilon)_{CR,\,\phi=0}$ for $\sigma^2 = 1$

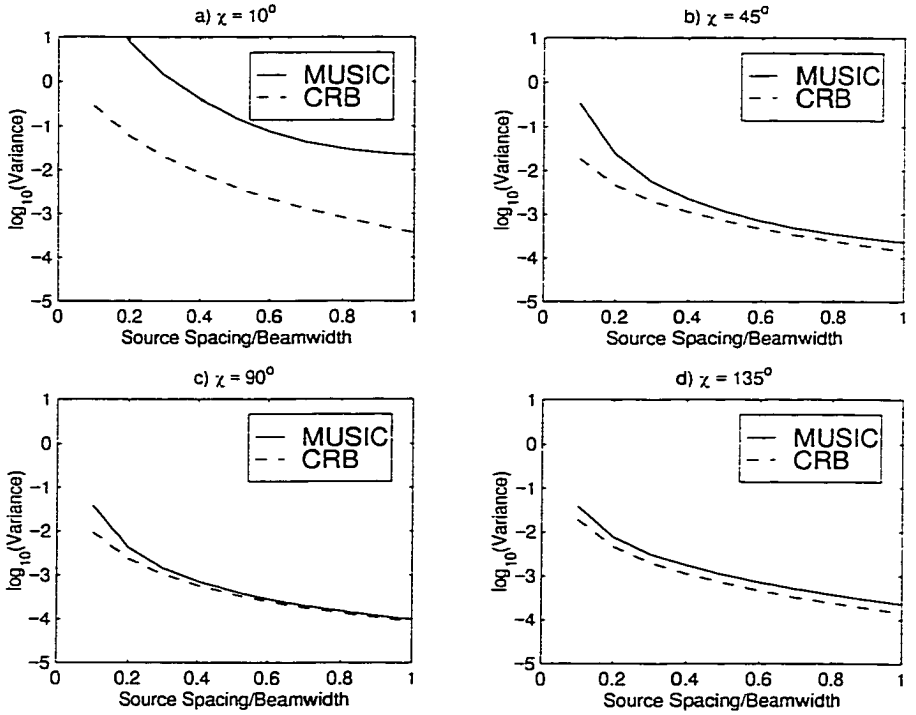

Figure 3.7 MUSIC variance and $\text{var}(\varepsilon)_{CR}$ for $\sigma^2 = 1$

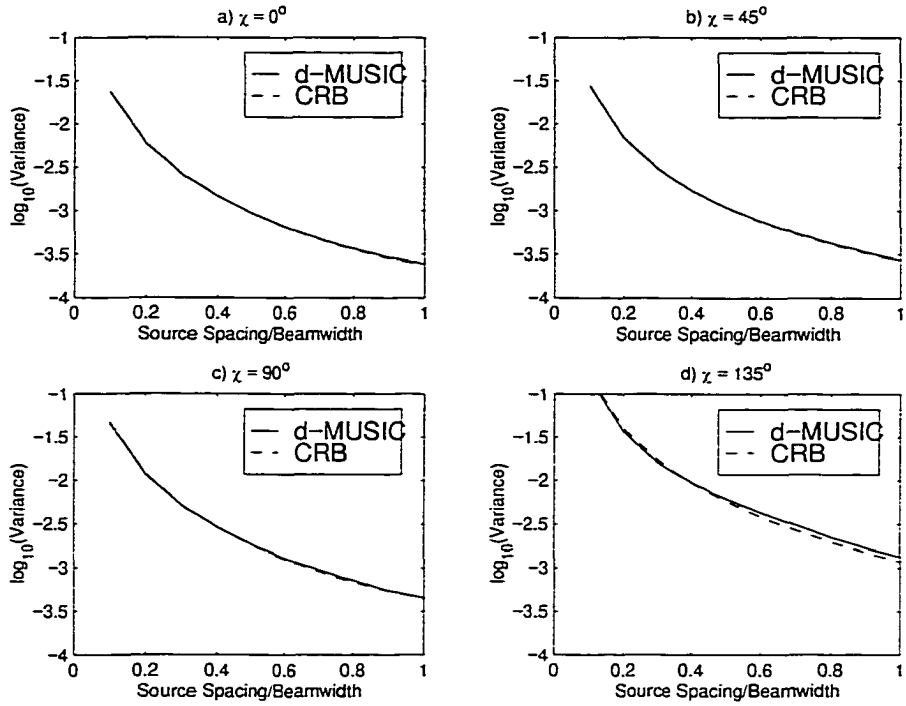

Figure 3.8 d-MUSIC variance and $\text{var}(\varepsilon)_{CR,\phi=0}$ for $\sigma^2 = 10$

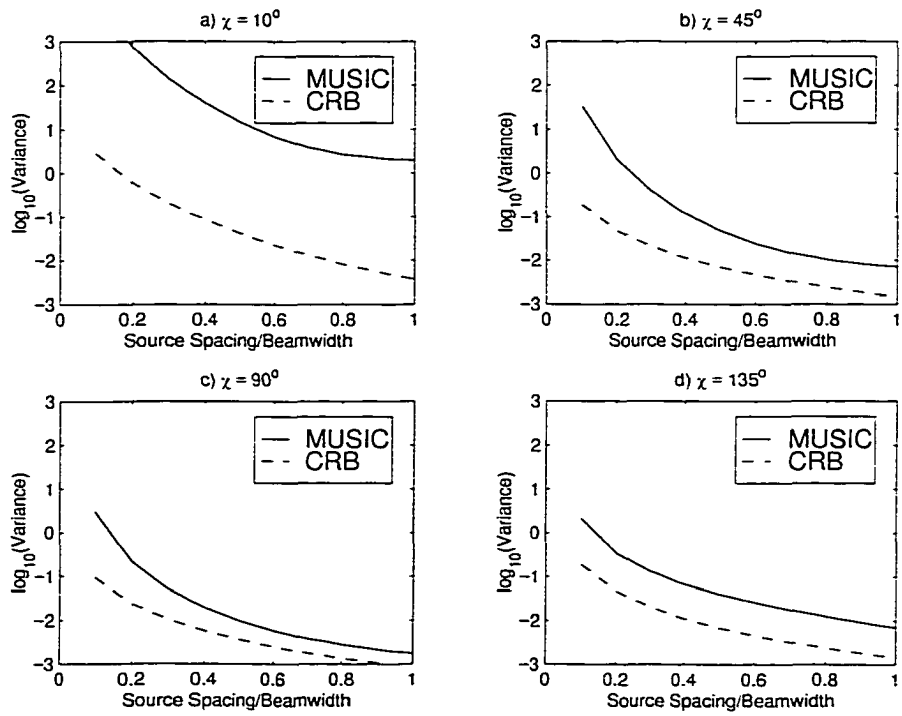

Figure 3.9 MUSIC variance and $\text{var}(\varepsilon)_{CR}$ for $\sigma^2 = 10$

This improved SNR performance is logical when one considers the fact that d-MUSIC utilizes *a priori* information and that it uses only one signal space vector. The SNR of this vector is roughly equivalent to that of the principal eigenvector of the covariance matrix. As the second eigenvector has a much lower SNR than the principal vector for closely spaced sources [4], the second vector will likely be overwhelmed by noise unless the SNR is very high.

Note that the d-MUSIC divergence from the CRB near a spacing of a beamwidth is less pronounced in Figure 3.8 (20 dB SNR) compared to Figures 3-4 and 3-6. This is likely due to the fact that the errors due to noise are greater than the d-MUSIC model error at this point.

The low sensitivity of d-MUSIC to signal correlation/phase difference is a necessary property for robust low angle tracking. A problem of great frustration in low angle tracking is the fact that the combined signal attains its maximum SNR when the signals are in-phase, and this is where MUSIC tends to break down. d-MUSIC overcomes this problem and now the accuracy of the estimate really only depends on target SNR, with the best results being obtained when the signals constructively add as confirmed by the single parameter CRB $\text{var}(\varepsilon)_{CR,\,\phi=0}$.

An important case where d-MUSIC will fail is if the two signals have equal power and are 180° out of phase. The input signal vector is identical to the second vector d-MUSIC attempts to create so the d-MUSIC problem is no longer full rank. This is a moot point as the probability of detection is low at this point. In terms of target tracking the phase relationship between the direct and multipath signals will cycle through a full 360° many times as the aircraft travels through the radar coverage zone. Given this reality the system must accurately estimate the aircraft altitude at those instances when the SNR is high enough to permit detection.

In the interest of greater utility, we would like to obtain an accurate estimate of the aircraft altitude for a large range of χ values. Figure 3-10 is the d-MUSIC and MUSIC variance for the case of $\sigma^2 = 0.1$ and $\chi = 160°$. Though d-MUSIC is technically a little better than MUSIC the results are roughly comparable. Hence, MUSIC does not offer a better alternative to d-MUSIC for this case where the two signals are nearly 180° out of phase.

The d-MUSIC error analysis also includes the effects of fixed array and ϕ errors, so long as the increase in error is small enough so that the first order Taylor series approximation of (3-47) is still good. In the interest of demonstrating the threat posed by array errors on high resolution analysis, consider the case where there is no error for ϕ and the array errors only include an

amplitude component. The magnitude of the array errors are

$$|\mathbf{g}| = [0.967, 0.916, 1.050, 1.149, 0.945, 0.915, 0.975, 1.066, 0.915, 0.880]^T \qquad (3\text{-}67)$$

and the array error matrix is $\mathbf{G} = \text{diag}\{\mathbf{g}\}$. The amplitude errors have a RMS value of 8.5%.

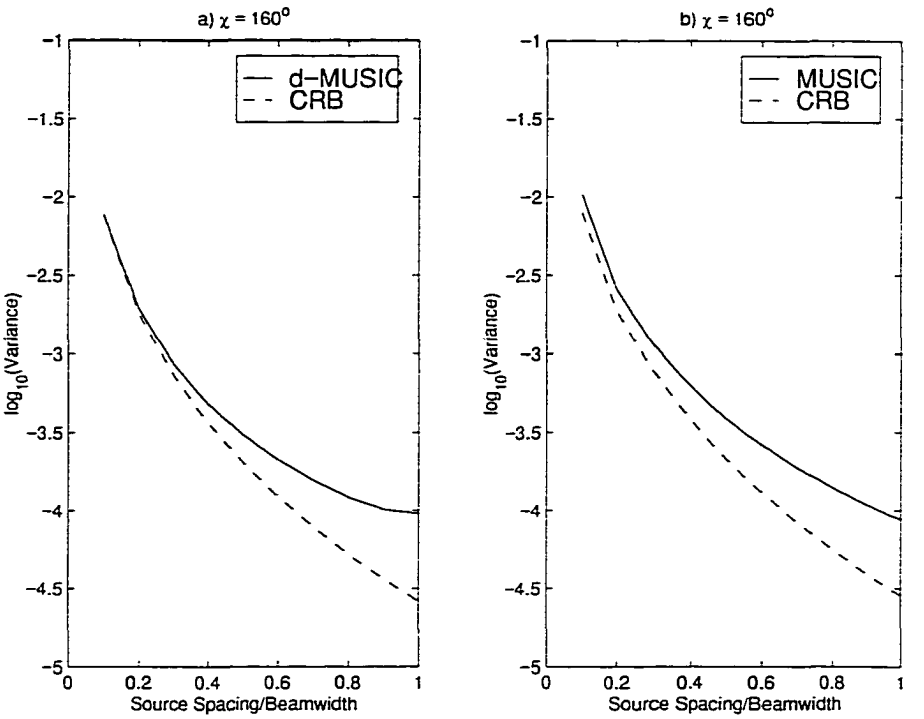

Figure 3.10 d-MUSIC and MUSIC variance for $\sigma^2 = 0.1$ and $\chi = 160°$ (signals nearly subtract)

Figure 3-11 is a plot of the d-MUSIC variance for $\sigma^2 = 0.1$ and $\chi = 0°$. The CRB variance assumes no array errors. Compare the $\sigma^2 = 0.1$ and $\chi = 0°$ plot of Figure 3-4(a). There is a dramatic increase in error variance due to the array errors with the greatest effect for close source spacing. Bear in mind that this is a rather "mild" example as no phase errors were included. However, it does underscore the danger represented by array errors. This subject will be dealt with in more detail in the next two chapters.

As an independent confirmation of some of the results derived in the theoretical error analysis we will now explore the behavior of both the MUSIC and d-MUSIC algorithms via a series of simulation tests.

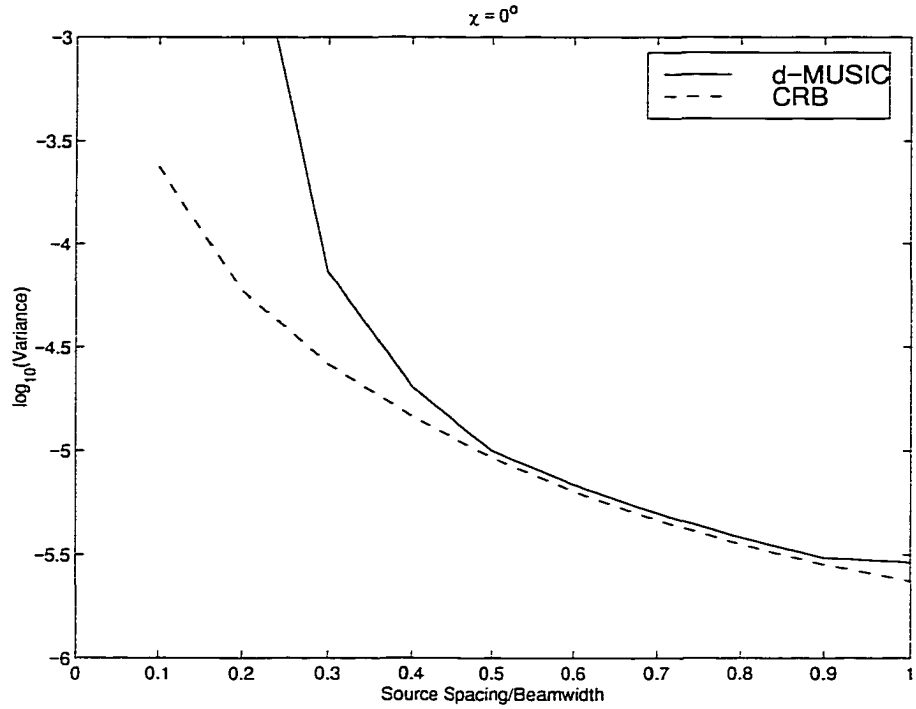

Figure 3.11 d-MUSIC variance with array errors for $\sigma^2 = 0.1$ and $\chi = 0°$

3.8 Simulation Tests

3.8.1 Setup

In order to prepare the way for the analysis of the Osborne Head data, the array structure selected for the simulation matches that of the EARS radar for 6 channels. The particulars of the simulation model are listed in Table 3-3. Note that the signal model employed in Table 3-3 corresponds to a Doppler shifted target echo with frequency ω. As before, the phase difference between the two signals is χ.

Note the 3.7917 wavelength spacing between sensors for the EARS array at an operating frequency of 9.1 GHz. The large spacing is easily justified as the first grating lobe for the broadside beam appears at an elevation of 15°. As most aircraft will not reach this elevation unless very close to the radar (e.g., an aircraft at a line-of-sight range of 50 km flying at 35,000 feet), the increased aperture obtained by a near 4 wavelength spacing easily outweighs any concerns regarding grating lobes.

To investigate some of the general properties of the d-MUSIC algorithm a number of Monte Carlo tests are performed to determine how its performance compares to that of root-MUSIC

with forward-backward averaging as a function of SNR for equi-power sources. 100 snapshots were processed for each run. 100 runs in all were analyzed for each example.

The spatial separation between the equi-power direct and surface reflected signals was set at 0.5° or 20% of a Rayleigh resolution beamwidth. The signal correlation is adjusted to produce a correlation coefficient of either 0 ($\chi = \pi/2$, uncorrelated sources) or 1 ($\chi = 0$, coherent sources).

Table 3-3 Simulation Model

Linear Array Parameters:

Radar Frequency	9.1 GHz
Number of Channels	6
Sensor Spacing (d)	0.125 m (3.7917 λ)
Array Height	27.8 m
Rayleigh Resolution Beamwidth	2.51°
3 dB Beamwidth	2.26°

Data Acquisition:

Sampling Period	$T = 10^{-3}$ seconds
# Snapshots per dwell	100

Baseband Signal Model:

Signal frequency	$\omega = \pi/2T$ (one-half of the Nyquist limit)
Signal 1	$s_1(n) = e^{j\omega nT}$
Signal 2	$s_2(n) = e^{j\chi}e^{j\omega nT}$

Noise Model:

Zero mean Gaussian, temporally and spatially white with variance σ^2.

The results presented here only show the estimate for the source spacing. In estimating the altitude of a low flying aircraft with known range this is the quantity of interest [3, chap. 6]. A summary of the test results is listed in Table 3-4.

Table 3-4 Summary of Simulation Results

			d-MUSIC			root-MUSIC		
σ^2	χ	ϕ	Figure	Bias	rms Error	Figure	Bias	Rms Error
0.1	90°	known	3-12	0.03°	0.12°	3-13	-0.02°	0.14°
0.1	0°	known	3-14	0.01°	0.09°			
0.5	90°	known	3-15	0.11°	0.17°	3-16	0.07°	0.57°
0.5	0°	known	3-17	0.07°	0.14°			
1.0	0°	known	3-18	0.11°	0.17°			
4.0	0°	known	3-19	0.24°	0.22°			
0.5	90°	unknown	3-20	0.14°	0.19°			
0.5	0°	unknown	3-21	0.18°	0.13°			
1.0	90°	unknown	3-22	0.18°	0.24°			
1.0	0°	unknown	3-23	0.22°	0.19°			

3.8.2 Known Cluster Centroid

The first case is for $\sigma^2 = 0.1$ and ϕ is treated as known. For 6 sensors and 100 snapshots the SNR of an array beam will be roughly 40 dB if the two signals constructively add. Figures 3-12 and 3-13 are the d-MUSIC and MUSIC results for 100 runs with uncorrelated sources ($\chi = 90°$) and Figure 3-14 is the d-MUSIC result for 100 runs with coherent sources ($\chi = 0°$).

For this high SNR d-MUSIC slightly outperforms MUSIC when the signals are uncorrelated (compare Figure 3-12 to 3-13, $\chi = 90°$). Note that the d-MUSIC result for the coherent signal case (Figure 3-14, $\chi = 0°$) is slightly better than that of the uncorrelated signal ($\chi = 90°$) examples.

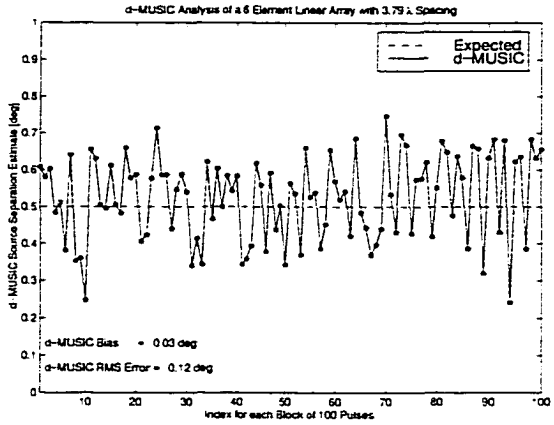

Figure 3.12 d-MUSIC analysis of simulated EARS data for $\chi = 90°$ and $\sigma^2 = 0.1$

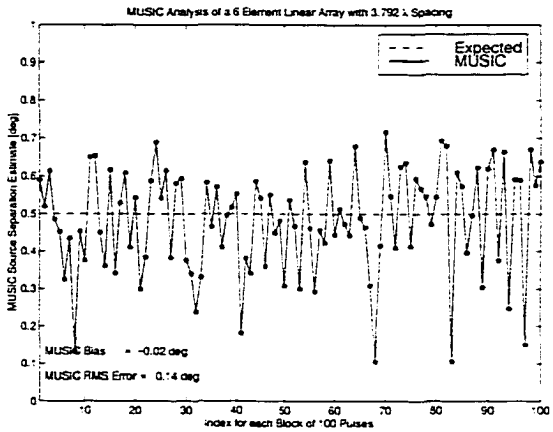

Figure 3.13 MUSIC analysis of simulated EARS data for $\chi = 90°$ and $\sigma^2 = 0.1$

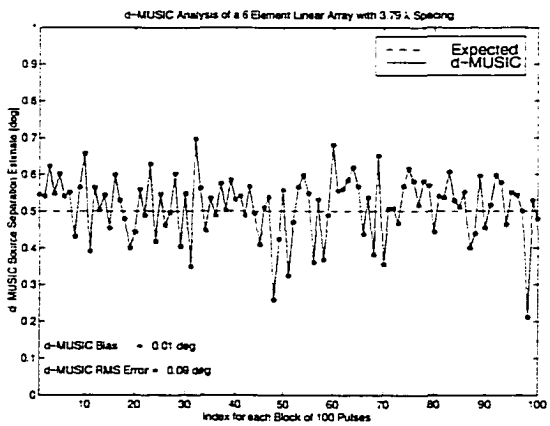

Figure 3.14 d-MUSIC analysis of simulated EARS data for $\chi = 0°$ and $\sigma^2 = 0.1$

The next 3 plots are for $\sigma^2 = 0.5$ and the array SNR is roughly 33 dB (ϕ is treated as known by d-MUSIC). Figures 3-15 and 3-16 are the d-MUSIC and MUSIC results for 100 runs using uncorrelated signals and Figure 3-17 is the d-MUSIC result for coherent sources. The d-MUSIC results experienced only a slight degradation in performance relative to that of the 40 dB examples, but the MUSIC result for uncorrelated sources (its best case) is widely scattered (rms error has jumped from 0.14° to 0.57° for a 7 dB drop in SNR).

For $\sigma^2 = 1$ the MUSIC rms error is a little over 2°. We can conclude then that $\sigma^2 = 0.5$ is close to the threshold point for the MUSIC algorithm for this experiment setup.

The next 2 cases are for d-MUSIC alone with coherent sources and $\sigma^2 = 1$ and 4 (30 and 24 dB array SNR, respectively). The results are plotted in Figures 3-18 and 3-19. As the SNR decreases the d-MUSIC result degrades but continues to resolve the two sources. The RMS bias of 0.24° and RMS error of 0.22° for $\sigma^2 = 4$ indicates that d-MUSIC is nearing its threshold point.

These simulation tests support the findings of the last section that for the case of known ϕ d-MUSIC should obtain a lower error variance than MUSIC with the best results being obtained when the sources cohere and that d-MUSIC has a lower noise threshold than MUSIC.

3.8.3 Unknown Cluster Centroid

The theoretical error analysis did not include the second version of d-MUSIC where a grid search is performed to locate ϕ. As the helicopter in the Osborne Head trials was hovering at an extremely low altitude at close range we can not assume that ϕ is known for this data set. To gain some confidence that this alternate version of d-MUSIC may be suitable to analyze the Osborne Head data, we show in Figures 3-20 to 3-23 a number of simulation results using this other version of d-MUSIC. In these examples the search grid was limited to a 0.5° sector centered around the array axis and $\phi = 0$.

Figures 3-20 and 3-21 are the d-MUSIC results for unknown ϕ with $\sigma^2 = 0.5$ and $\chi = 90°$ and 0°, respectively. As the algorithm must estimate two independent parameters instead of one, the results display a marked decrease in performance compared to Figures 3-15 and 3-17 which are the corresponding d-MUSIC results for known ϕ. However, these results are better than the MUSIC result of Figure 3-16 for the same SNR, though the bias is higher.

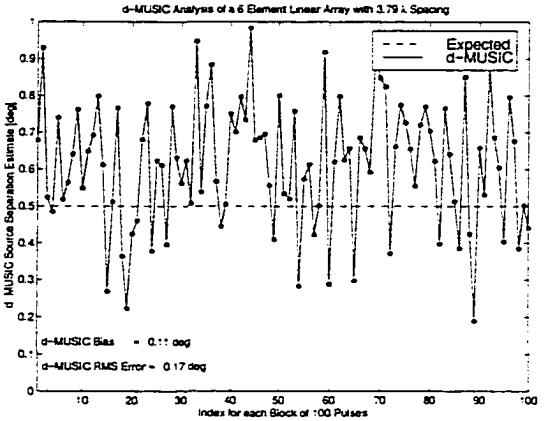

Figure 3.15 d-MUSIC analysis of simulated EARS data for $\chi = 90°$ and $\sigma^2 = 0.5$

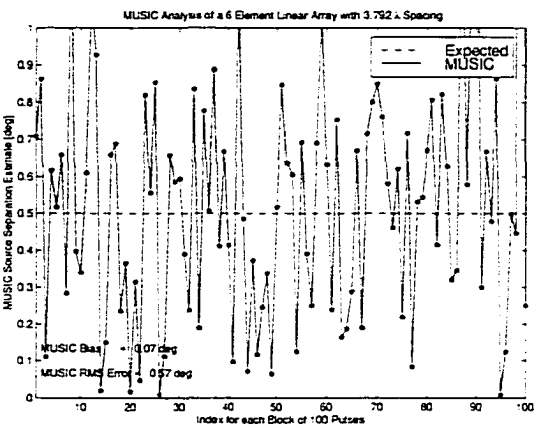

Figure 3.16 MUSIC analysis of simulated EARS data for $\chi = 90°$ and $\sigma^2 = 0.5$

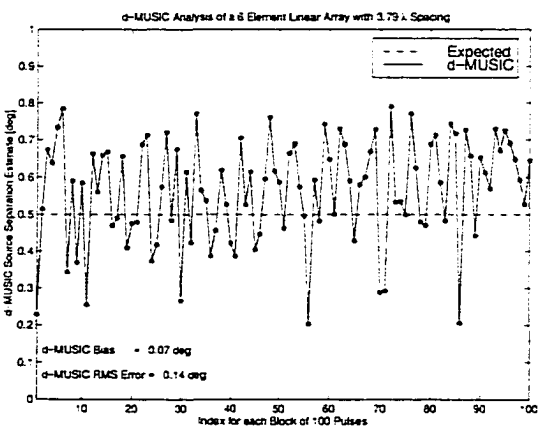

Figure 3.17 d-MUSIC analysis of simulated EARS data for $\chi = 0°$ and $\sigma^2 = 0.5$

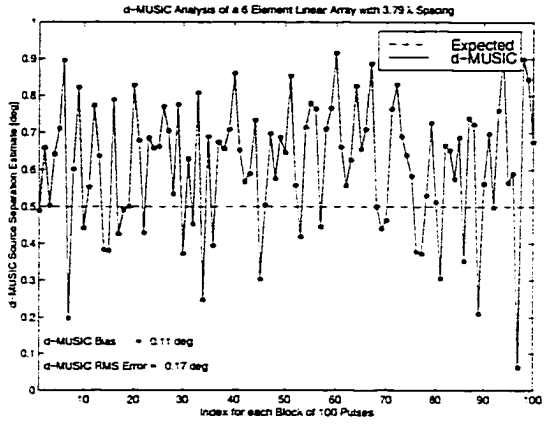

Figure 3.18 d-MUSIC analysis of simulated EARS data for $\chi = 0°$ and $\sigma^2 = 1$

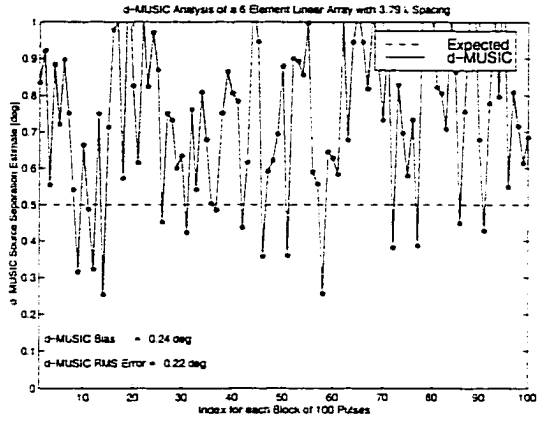

Figure 3.19 d-MUSIC analysis of simulated EARS data for $\chi = 90°$ and $\sigma^2 = 4$

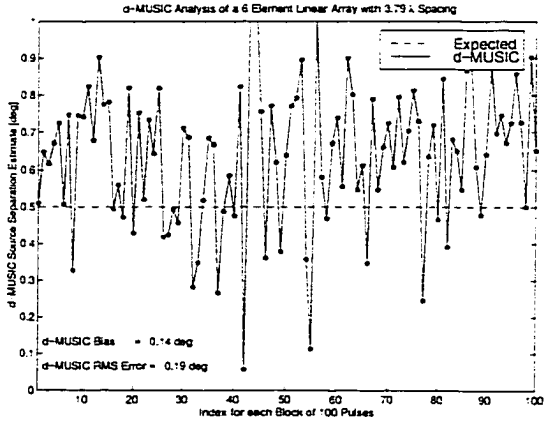

Figure 3.20 d-MUSIC analysis with unknown ϕ for simulated EARS data with $\chi = 90°$ and $\sigma^2 = 0.5$

Increasing the noise to $\sigma^2 = 1.0$, Figures 3-22 and 3-23 are the d-MUSIC results for unknown ϕ with $\chi = 90°$ and $0°$, respectively. Figure 3-18 is the d-MUSIC result for known ϕ with $\chi = 0°$. As expected, the d-MUSIC results degrade when ϕ is unknown. However, the algorithm continues to produce reasonable results beyond the point where MUSIC fails, and like the known ϕ version of d-MUSIC, demonstrates a high degree of insensitivity to the problem of correlated signals. The fact that the algorithm employs the same basic $\mathbf{I} + \mathbf{J}$ forward backward operation as the known ϕ version of d-MUSIC may explain its relative insensitivity to the problem of correlated signals.

Though like MUSIC, this version of d-MUSIC must estimate two independent parameters, it does employ more information than MUSIC however. Specifically, the approximation $\mathbf{D}(\mathbf{a}(\gamma) + \mathbf{a}(-\gamma)) \approx 2((\mathbf{a}(\gamma) - \mathbf{a}(-\gamma))/\delta$ is used. Also the algorithm only uses one signal space vector, allowing it to escape the classic MUSIC problem of extracting an accurate estimate for all signal space eigenvectors, one of which may have very low SNR, even though the array SNR may be high.

Though a rigorous error analysis was only performed for the known ϕ d-MUSIC algorithm, the results of these simulation tests gives us strong reason to believe that the grid search version of d-MUSIC to locate ϕ shares many of the same basic characteristics as the known ϕ algorithm, but with degraded performance. It also seems to operate beyond the noise threshold point for the MUSIC algorithm

The SNR of the Osborne Head data is often in excess of 30 dB. With this relatively high SNR it is within the scope of both the grid search version of d-MUSIC and the MUSIC algorithm to predict the helicopter altitude. However, we must first employ a technique to calibrate the EARS array prior to analyzing this data set. This is the subject of the next chapter.

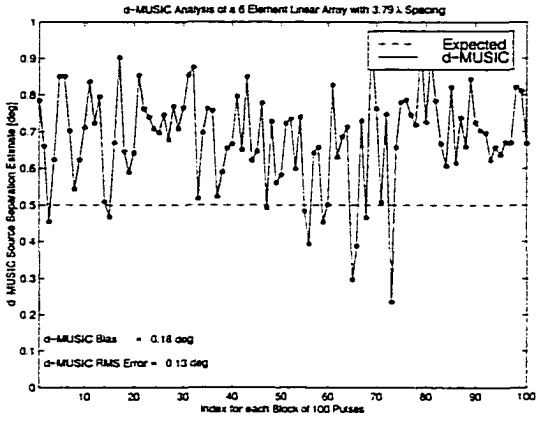

Figure 3.21 d-MUSIC analysis with unknown ϕ for simulated EARS data with $\chi = 0°$ and $\sigma^2 = 0.5$

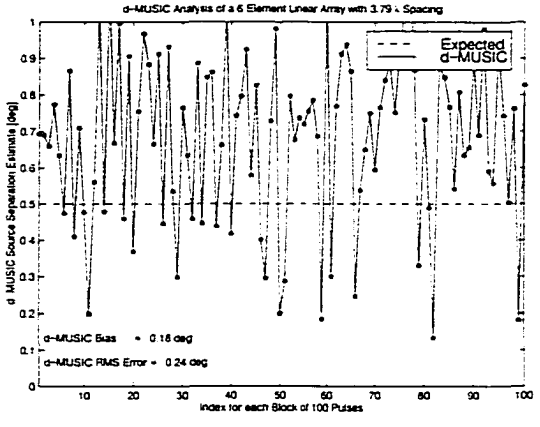

Figure 3.22 d-MUSIC analysis with unknown ϕ for simulated EARS data with $\chi = 90°$ and $\sigma^2 = 1$

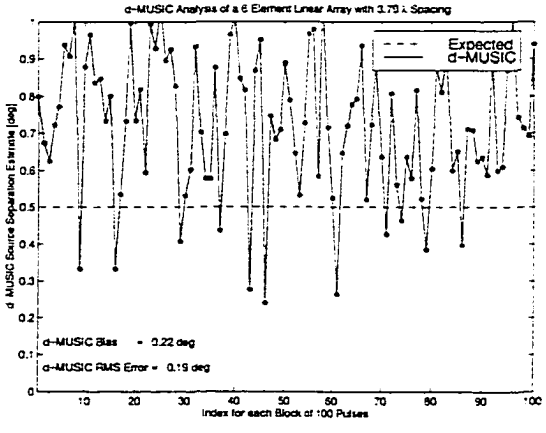

Figure 3.23 d-MUSIC analysis with unknown ϕ for simulated EARS data with $\chi = 0°$ and $\sigma^2 = 1$

4 Array Calibration

4.1 Preamble: Sources of Array Errors

In resolving closely spaced sources we require a precise model for the phase/amplitude response of the array over all space. This model is commonly referred to as the *array manifold.* Thus far it has been assumed that the exponential vector representation for $\mathbf{a}(\theta)$ of equation (2-1) represents the manifold for a linear array. In reality this vector is corrupted by a set of complex channel errors which may be dependent on θ. A general model for the linear array manifold is

$$\text{Array Manifold:} \quad \mathbf{a}_M(\theta) = \mathbf{G}(\theta)\mathbf{a}(\theta) \tag{4-1}$$

where $\mathbf{G}(\theta)$ is a diagonal matrix of complex weights representing the array phase/amplitude error at bearing θ. Note that the error $\mathbf{G}(\theta)$ is not dependent on time. It will be assumed that the errors are constant over a short time interval and a calibration vector will be calculated for each short data block.

Array model errors can be due to a number of sources. Chief among this set are [39-41]

- Gain and phase mismatch due to receiver/RF equipment
- Array position errors
- Anomalous propagation
- Diffuse reflection
- Environmental factors

Equipment mismatches are due to gain and phase differences between antennas, cables, waveguides and receiver electronics. Such errors are usually steady and, in theory, easy to correct. However, regular updates are required as the response of the equipment may change with component aging and temperature effects. Antennas and other RF equipment may also experience mutual electromagnetic coupling.

It is difficult to calibrate a set of antennas in practice. A transmit source is required to broadcast a signal which is then compared on a channel-to-channel basis. This presents several problems, not the least of which is uncontrolled reflections (multipath) which distorts the wavefront. That in itself is not an obstacle so long as the wavefront structure is known. But given the uncertainty in predicting the surface reflection coefficient, the path length difference between the direct and multipath components, the diffuse reflection component, and the azimuth spread of the multipath, it is difficult to estimate the wavefront in advance.

Array position errors are due to the physical movement of the array elements. In typical deployments position errors can be a grave concern [12-20]. In the EARS data set to be studied here the antenna height is 27.8 m and a lateral deflection of less than a millimeter (mm) can produce large phase errors. For example, if the EARS array were to lean back with the top of the array moving a mere 2 mm, the elevation angle of a signal will change by 0.26°, more than 10% of a beamwidth. Given the fact that the targets in this experiment have a direct path and multipath separation from 0.42° to 0.85°, such errors can be catastrophic. On the day of the Osborne Head trials, conditions were stormy with winds gusting from 40 to 60 kph. Given the fact that the large reflector antenna feeding the vertical linear array of horns resembles a sail, the array may have experienced a significant amount of "wobbling" under such conditions.

Position errors are difficult to monitor as the array may not simply tilt, but flex with a distinct curvature, dependent on the mechanical design of the array. Array flexure may arise from wind stress or due to thermal expansion/contraction. Even in calm conditions large position errors are common due to mechanical vibrations/forces imparted on the array by the ship, aircraft or vehicle which carries it. Usually, the array is mounted on a mechanically stabilized pedestal, but can never truly be immune to platform motion on bumpy terrain, a heaving sea or turbulent air.

In order to correct for position errors precise monitoring is required. In the Osborne Head data no additional sensors were installed to monitor array motion. Indeed, such sensor networks are uncommon in modern radar systems as these systems are typically designed to form a set of narrow beams.

Anomalous propagation effects can be important (e.g., ducting) but are usually overlooked. Dependent on the array placement relative to its surroundings, diffraction sources may be created. Say that the array is placed near a cliff edge as was the case in the Osborne Head trials. The cliff edge can potentially act as a "knife-edge" diffraction source causing the wavefront at low elevation angles to be distorted. Such propagation mechanisms are difficult to model in practice, and are usually studied via experimentation.

Diffuse reflection refers to non-specular reflection from the surface. As a surface may be rough the multipath signal can arrive from more than one direction. Typically, the specular reflection component is dominant resulting in a narrow spread for the multipath depression angle [3].

The phase errors of the EARS data are estimated to have a RMS value on the order of 31° (Chapter 5). Such large errors present a serious obstacle to any high resolution algorithm attempting to separate signals with a spacing of less than a beamwidth. It is clear that some form of array calibration is needed. In view of the fact that the errors may be time-varying, the calibration algorithm may need to be applied "on-the-fly". With a view to practical field use, the calibration algorithm should have a real-time capability and not require any knowledge of the signal directions.

This is a tall order, but the algorithm presented here attempts to fulfill this requirement. The foundation for this approach is that even though the direct and multipath signals are correlated,

the close spacing of the signals produces a covariance matrix **R** that is nearly Toeplitz. Recall that a Toeplitz matrix [2, chap. 2] is a matrix having the same value for all elements along a diagonal. Calibration errors will distort the Toeplitz structure of **R**. The problem then is to find a calibration vector $\mathbf{c}_A$ such that the Toeplitz structure of **R** is restored. Mathematically, this objective can be stated as

$$\begin{aligned} &\text{Find } \mathbf{c}_A \text{ such that} \\ &\mathbf{R}_C = \mathbf{C}_A \mathbf{R} \mathbf{C}_A^H \quad \text{is Toeplitz} \end{aligned} \tag{4-1}$$

where

$$\mathbf{C}_A = \text{diag}\{\mathbf{c}_A\} \tag{4-2}$$

In the above model it is assumed that that the calibration error is the same for $\mathbf{a}(\theta_T)$ and $\mathbf{a}(\theta_R)$. This assumption need not be true in real life but will be assumed here for the sake of making the problem tractable, and to make it independent of the signal directions. As θ_T and θ_R are close in value this can be considered to be a reasonable premise.

In developing the calibration technique the following array snapshot model will be assumed

$$\mathbf{x}(t) = \mathbf{G}\{s_T(t)\mathbf{a}(\theta_T) + \rho s_R(t)\mathbf{a}(\theta_R)\} + \mathbf{n}(t) \tag{4-3}$$

Note that the above equation is the same as equation (2-1), except that the signal data is multiplied by the calibration error **G**. Ideally, we want to estimate $\mathbf{C}_A = \mathbf{G}^{-1}$ as the calibration matrix. Note that the noise term **n**(t) is not multiplied by **G**. In most systems the noise term is primarily due to receiver noise. As it is a relatively simple matter to calibrate a set of receivers via a common loopback signal to ensure that the receivers have no gain discrepancies, we can assume that the noise on each channel has the same power. Phase discrepancies between channels are irrelevant for white Gaussian noise assumed to exist here.

The covariance matrix **R** is modeled as

$$\begin{aligned} \mathbf{R} &= E\{\mathbf{x}\mathbf{x}^H\} \\ &= \mathbf{G}\mathbf{A}\mathbf{S}\mathbf{A}^H\mathbf{G}^H + \sigma^2\mathbf{I} \end{aligned} \tag{4-4}$$

where $E\{\cdot\}$ denotes the statistical expectation operator, σ^2 is the noise power (same for all

channels) and

$$\mathbf{A} = [\mathbf{a}(\theta_T)\ \mathbf{a}(\theta_R)] \tag{4-5}$$

$$\mathbf{S} = \begin{bmatrix} s_{11} & s_{12} \\ s_{21} & s_{22} \end{bmatrix} = \begin{bmatrix} E\{s_T s_T^*\} & \rho^* E\{s_T s_R^*\} \\ \rho E\{s_R s_T^*\} & |\rho|^2 E\{s_R s_R^*\} \end{bmatrix} \tag{4-6}$$

Note that $s_{21} = s_{12}^*$.

The method adapted for use here to restore the Toeplitz structure of **R** is that developed in [30]. The method assumes that the set of signals are uncorrelated resulting in a Toeplitz **R.** It seeks to correct for the phase difference across channels by subtracting the phase of the first element of a diagonal of **R** from the phase of all other elements along the same diagonal. This has the effect of removing the signal phase term, leaving only the array error phase. The result is a linear system of equations for the phase of $\mathbf{c}_A$. An alternate approach is to subtract the phase of adjacent elements along a diagonal. This is the approach adopted here as it tends to minimize the error resulting from the non-Toeplitz terms of **R**.

To make the system of equations full rank, an additional constraint was adopted in [30] to force the sum of the array phase errors to be zero. This restraint will be removed to produce a rank deficient-by-one system of equations. The resulting solution is not guaranteed to be unique, but simulation tests demonstrate that it provides a least squares solution with an acceptable level of accuracy. Before introducing the algorithm we need first justify the Toeplitz approximation for **R** for closely spaced correlated sources.

4.2 Toeplitz Approximation

The signal matrix $\mathbf{A}\,\mathbf{S}\,\mathbf{A}^H$ from equation (4-4) may be expanded as

$$\begin{aligned} \mathbf{A}\mathbf{S}\mathbf{A}^H = {} & s_{11}\mathbf{a}(\theta_T)\mathbf{a}^H(\theta_T) + s_{12}\mathbf{a}(\theta_T)\mathbf{a}^H(\theta_R) \\ & + s_{21}\mathbf{a}(\theta_R)\mathbf{a}^H(\theta_T) + s_{22}\mathbf{a}(\theta_R)\mathbf{a}^H(\theta_R) \end{aligned} \tag{4-7}$$

The individual terms of $\mathbf{A}\,\mathbf{S}\,\mathbf{A}^H$ may be categorized as either "stationary" (Toeplitz) or "non-stationary" (non-Toeplitz). Non-Toeplitz terms result from signal correlation. The Toeplitz terms are $\mathbf{a}(\theta_T)\,\mathbf{a}^H(\theta_T)$ and $\mathbf{a}(\theta_R)\,\mathbf{a}^H(\theta_R)$. The non-Toeplitz terms are $\mathbf{a}(\theta_T)\,\mathbf{a}^H(\theta_R)$ and $\mathbf{a}(\theta_R)\,\mathbf{a}^H(\theta_T)$. For these matrices the entries along each diagonal exhibit a sinusoidal variation.

Though spatial smoothing [2, 35-37] can be highly effective in reducing the cross correlation terms, it produces only a marginal improvement when decorrelating closely spaced sources. When the sources are closely spaced, the variation along the diagonal of each non-Toeplitz term is small and averaging has little impact.

To illustrate the point, let k denote the kth diagonal of a matrix. k varies from -(N-1) to N-1, where a positive, zero and negative value represents a super, main and sub-diagonal, respectively. Denoting the row index as m, the elements of $\mathbf{a}(\theta_T)\,\mathbf{a}^H(\theta_R)$ and $\mathbf{a}(\theta_R)\,\mathbf{a}^H(\theta_T)$ are

$$\begin{aligned} &\mathbf{a}(\theta_T)\mathbf{a}^H(\theta_R)\text{: element } m \text{ of diagonal } k = e^{-jm(\alpha_T-\alpha_R)}e^{jk\alpha_R} \\ &\mathbf{a}(\theta_R)\mathbf{a}^H(\theta_T)\text{: element } m \text{ of diagonal } k = e^{jm(\alpha_T-\alpha_R)}e^{jk\alpha_T} \end{aligned} \tag{4-8}$$

where $\alpha_T = 2\,\pi\,d\,\sin(\theta_T)/\lambda$ and $\alpha_R = 2\,\pi\,d\,\sin(\theta_R)/\lambda$. The variation along each non-Toeplitz matrix diagonal is sinusoidal with a frequency of $\pm(\alpha_T - \alpha_R)$. For closely spaced sources $\alpha_T - \alpha_R$ is small with the result that $\mathbf{a}(\theta_T)\,\mathbf{a}^H(\theta_R)$ and $\mathbf{a}(\theta_R)\,\mathbf{a}^H(\theta_T)$ are nearly Toeplitz. If the concern is only to compare adjacent elements along a diagonal, this approximation is even stronger.

The preceding serves as justification for the assumption that $\mathbf{A\,S\,A}^H$ can be approximated as Toeplitz for two closely spaced sources. With this knowledge in hand, a real-time algorithm can be developed to calibrate the covariance matrix without knowledge of the signal directions, signal correlation, or the surface reflection coefficient.

4.3 Blind Calibration via the Toeplitz Property

The covariance matrix $\mathbf{R_C} = \mathbf{C_A R C_A^H}$, where $\mathbf{C_A} = \text{diag}\{\mathbf{c_A}\}$ is considered "calibrated" in the sense that it is nearly Toeplitz. For this reason, a "blind" calibration technique can be developed to calibrate the array data without knowledge of the signal directions and other propagation conditions. For convenience, the array error $\mathbf{g}$ where g(i) = G(i,i) is normalized with respect to a specific channel. Here, it will be assumed that $\mathbf{g}(1) = 1$ and $\mathbf{c_A}(1) = 1$.

Correcting for gain errors is straightforward if $\alpha_T - \alpha_R \approx 0$. The main diagonal of $\mathbf{R}$ represents the average power of each channel, which should be the same. For high SNR the calibration magnitude can be estimated as

$$\left|\mathbf{c}_A(n)\right| = \sqrt{\frac{\mathbf{R}(1,1)}{\mathbf{R}(n,n)}}, \quad n = 1 \text{ to } N \tag{4-9}$$

The phase error problem will require the solution to a system of equations. Let $\angle\,\mathbf{R}(m,n)$ denote the phase angle of $\mathbf{R}(m,n)$ and $\mu(n)$ denote the phase angle of g(n) with $\mu(1) = 0$. As elements along a diagonal should have the same value, the difference between them will primarily be due to array errors. Neglecting noise and signal cross-correlation, the phase difference between elements m_1 and m_2 of diagonal k is

$$\angle\mathbf{R}(m_1, m_1+k) - \angle\mathbf{R}(m_2, m_2+k) \;=\; \mu(m_1) - \mu(m_1+k) - \{\mu(m_2) - \mu(m_2+k)\} \tag{4-10}$$

In [30] a system of equations for multiple sources is built using (4-10). In that work each element of a diagonal is compared to the first element only. There really is no reason why all possible pair combinations for each diagonal could be used, however it will not add to the rank of the problem.

In this application we will only compare adjacent elements along a diagonal. In the last section it was established that each diagonal of the non-Toeplitz terms have a sinusoidal variation with a frequency of $\pm(\alpha_T - \alpha_R)$. As $\alpha_T - \alpha_R$ is small the variation of the non-Toeplitz terms over the length of a diagonal will be small, but the smallest difference will likely occur for adjacent terms. By comparing adjacent terms along each diagonal we will tend to reduce the error resulting from the non-Toeplitz cross-correlation terms.

By applying this result for all adjacent pairs along the same diagonal, the following system of equations can be developed

$$\mathbf{T}\,\mu(2{:}N) = \mathbf{b} \tag{4-11}$$

where T is a (N-1)(N-2)/2 × (N-1) matrix of constants defined as

$$\mathbf{T}(\mathrm{m}+\{\mathrm{k}-1\}\{\mathrm{N}-1-\mathrm{k}/2\},\mathrm{p}) = \begin{cases} 1, & \text{if } p = m-1 \\ 1, & \text{if } p = m+k \\ -2, & \text{if } p = m+k,\ \mathrm{k}=1 \\ -1, & \text{if } p = m,\ \mathrm{k}>1 \\ -1, & \text{if } p = m+k-1,\ \mathrm{k}>1 \\ 0, & \text{otherwise} \end{cases} \tag{4-12}$$

for $k = 1, \ldots, N-2,\ m = 1, \ldots, N-k-1$ and $p = 1, \ldots, N-1$

and the (N-1)(N-2)/2 × 1 vector b has elements

$$\mathbf{b}(\mathrm{m}+\{\mathrm{k}-1\}\{\mathrm{N}-1-\mathrm{k}/2\}) = \angle\mathbf{R}(m, m+k) - \angle\mathbf{R}(m+1, m+k+1) \tag{4-13}$$

for $k = 1, \ldots, N-2$ and $m = 1, \ldots, N-k-1$

Note that the above system of equations do not include information from either the main diagonal or any of the subdiagonals. The subdiagonals represent a redundant set of information due to the Hermitian symmetry of **R**. As the main diagonal is strictly real, it carries no phase information. Errors due to noise are not modeled here. As the noise is concentrated on the main diagonal this helps to reduce the error, but only if a sufficient number of snapshots are used to estimate **R**

The estimate for μ(2:N) is

$$\hat{\mu}(2:N) = \mathbf{T}^{-1}\mathbf{b} \tag{4-14}$$

As only N-2 diagonals are employed the rank of **T** will be N-2, one less than the required rank of N-1 to solve for μ(2:N). Hence the solution derived here is not unique. In [30] an additional equation was used to make the problem full rank, specifically $\sum \mu(2{:}N) = 0$. This constraint does not necessarily reflect reality and will not be used here. Though equation (4-14) does not provide an unique solution, it does represents a serviceable calibration method. An optimal technique is not really the goal here. What is important is to employ a blind adaptive scheme to track the array errors for the Osborne Head data, in the absence of any other information. It appeared to do just that and good results have been obtained. In another application it may not work, especially for lower SNR or signal-to-clutter (SNC). However its performance here has been satisfactory.

An attractive feature of this straightforward technique is that the matrix **T** does not depend on the data. For a given array geometry **T** is a fixed quantity. As a consequence, the inverse of **T** can be stored in advance and used for each block of data. This is where the real-time capability of the calibration algorithm emerges. To compute the calibration error phase all one need do is multiply a known matrix with a column vector of covariance matrix terms.

In this work, a calibration vector is calculated for individual, non-overlapping data blocks. An update period of at least 0.1 seconds is typically employed. The calibration algorithm is only applied to those range bins where a detection is made. The covariance matrix at the target range is then "corrected" using the calibration scheme.

4.4 Simulation Examples

Inspired by the EARS system, the array model of Table 4-1 will be used for all examples

Table 4-1: Array Model for Array Calibration Tests

Radar Frequency	8.9 GHz
Number of Channels	6
Sensor Spacing (d)	0.125 m
Array Height	27.8 m
PRF	1000 Hz
Number of Snapshots	25

The calibration errors are as follows

$$|\mathbf{c}_A| = [1\ 0.8\ 1.4\ 0.6\ 1.2\ 0.7]^T \qquad (4\text{-}15)$$
$$\angle\mathbf{c}_A = [8\ -19\ 28\ -23\ -6\ 12]^T \quad \text{(degrees)}$$

The simulation test has a moving target with an altitude of 30.5 m , a range of 8 km and a Doppler shift of 250 Hz. Assuming specular reflection and a reflection coefficient magnitude of 0.6, the following parameters were derived based on a 4/3 effective earth radius refraction model for the lower atmosphere [3, chap 6]

$$\theta_T = 0 \qquad (4\text{-}16)$$
$$\theta_R = -0.43^\circ$$
$$\tau = 6.65 \times 10^{-10} \text{ seconds} \qquad \text{(multipath delay)}$$
$$\rho = -0.6 e^{j 2\pi C \tau / \lambda}$$

where λ is the radar wavelength and C is the velocity of light.

In this example the path length difference due to the multipath delay τ is exactly an integer multiple of the wavelength. The two signals are thus in phase (coherent). Gaussian noise is added to the channel data. Using 25 snapshots the signal power was selected to produce a target SNR of 20 dB. This is the SNR at detection using a beam pointed at the horizon. The calibration error of this example has a RMS magnitude error of 2.8 dB while the RMS phase error is 19.6°. This level of calibration error can be considered severe.

Plots of the phase and magnitude estimates versus actual values for one 25 snapshot run are shown in Figures 4-1 and 4-2. The phase error was plotted with a phase offset equal to the average difference between the actual and estimated values. This helps to "balance" the plot over channel. The residual calibration error for this estimate has a RMS value of 0.26 dB for magnitude and 3.81° for phase.

The experiment was repeated 100 times and the results are presented in Figures 4-3 and 4-4. The average RMS errors are 0.36 dB and 4.42°. In the noiseless case the RMS phase error is 3.95°. The similarity of the phase RMS error can be attributed to the weakness of noise terms off the main diagonal.

The Toeplitz-based calibration technique has dramatically improved the quality of the data. The calibration errors are reduced to a level that can be considered tolerable for low angle tracking. In any event it appears to have a beneficial effect if the array errors are large to begin with, which is the case for the Osborne Head data. In view of its real-time capability, the Toeplitz-based calibration technique is a serious contender for operational use. As no other calibration data is available this algorithm is applied to calibrate the EARS data for the d-MUSIC algorithm tests in chapter 5.

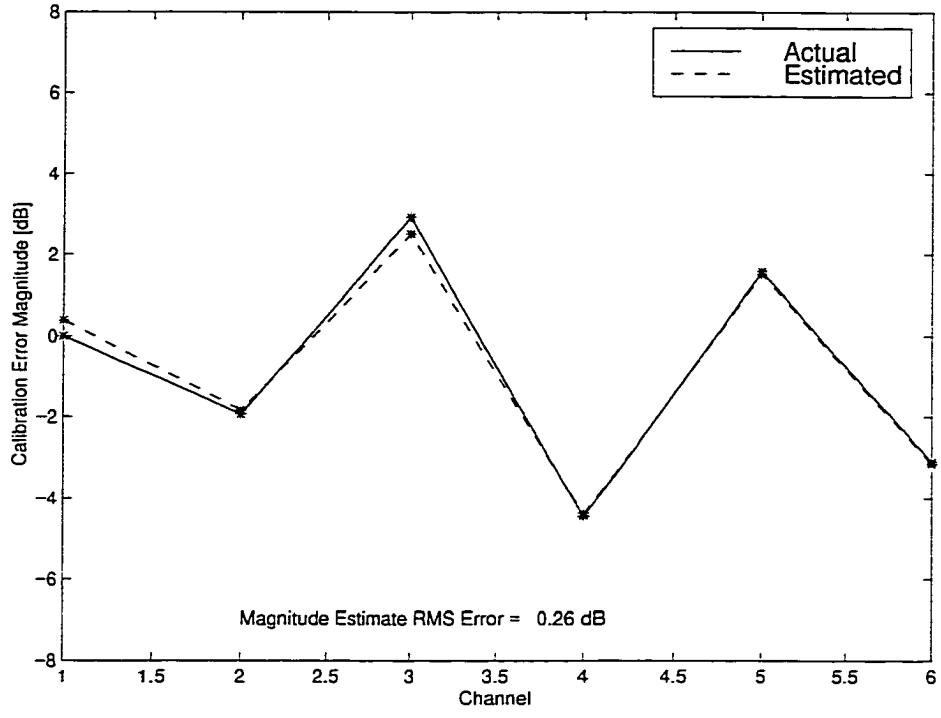

Figure 4.1 Calibration magnitude estimate for one run with 20 dB SNR

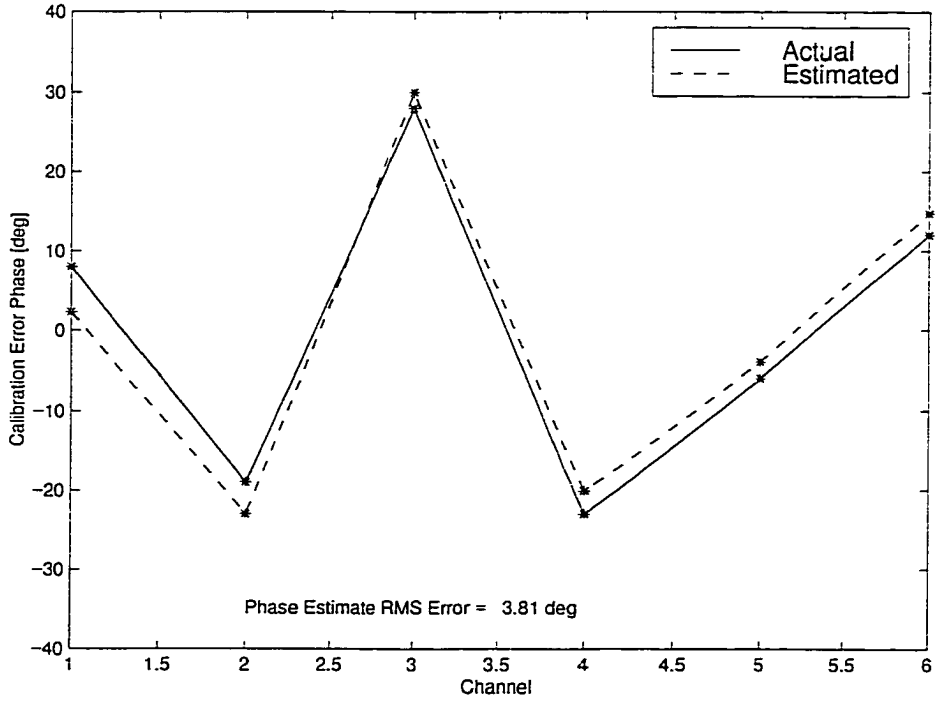

Figure 4.2 Calibration phase estimate for one run with 20 dB SNR

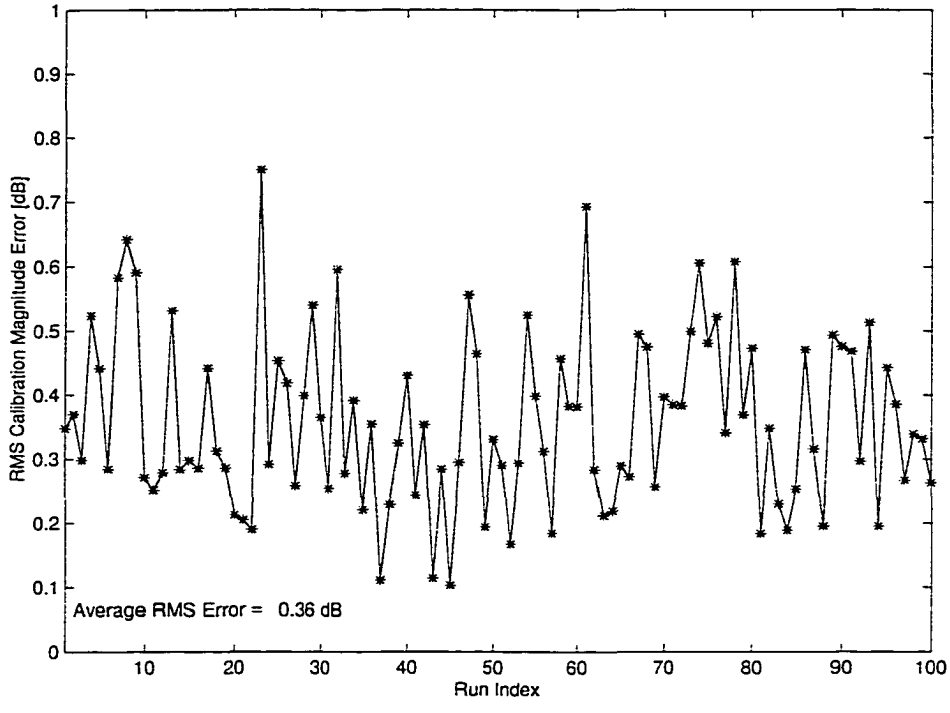

Figure 4.3 RMS error of magnitude estimate for 100 runs at 20 dB SNR

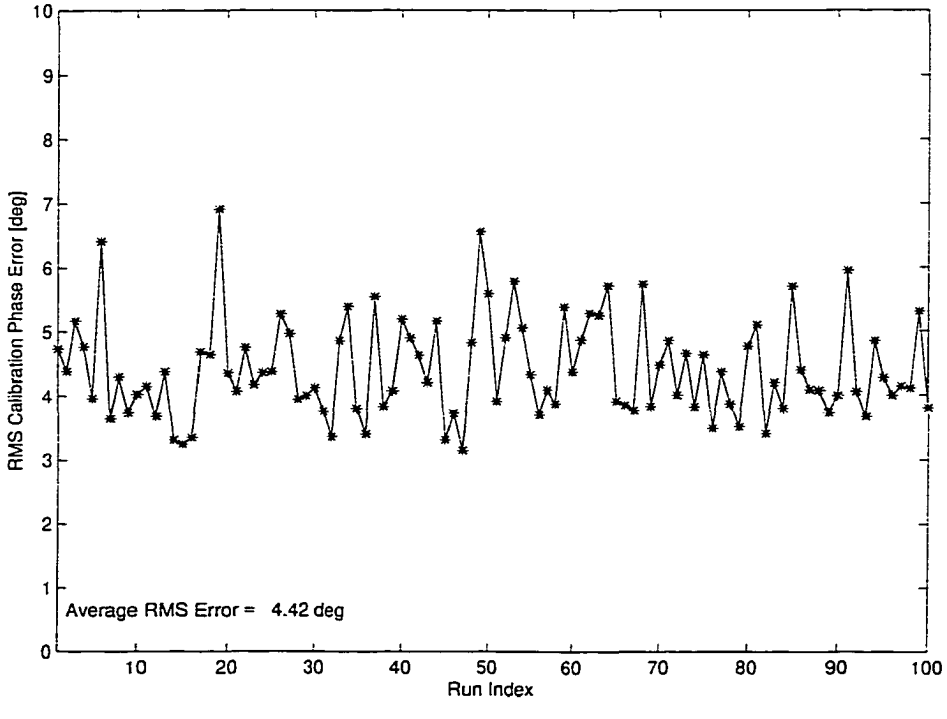

Figure 4.4 RMS error of phase estimate for 100 runs at 20 dB SNR

5 Evaluation Tests Using EARS

5.1 Overview

On 16 October 1995, a low angle tracking experiment was conducted by Defence Research Establishment Ottawa (Canadian Department of National Defence) at Osborne Head, Nova Scotia using the Experimental Array Radar System (EARS). In the data to be analyzed here a Sea King helicopter hovered at an altitude of either 30.5 and 61 m (100 or 200 ft) at a range of approximately 8 km. Data was collected at 8.9 and 9.4 GHz for both altitudes. Using the Toeplitz calibration technique of the last chapter the EARS data is used to compare the performance of the d-MUSIC and MUSIC algorithms.

Owing to the low altitude of the helicopter at such a close range, the center of the direct and multipath source cluster ϕ is not known in advance. As such, this series of tests will use the second version of d-MUSIC that steps through a fixed grid of ϕ values. The grid point where the d-MUSIC estimate best fits the input signal vector is selected as the solution. The discussion begins with a description of the EARS system and the Osborne Head data.

5.2 The EARS Radar

The normal operating range of the EARS system is from 8.9 to 9.4 GHz (X-band) with a 5 MHz bandwidth. A picture of the EARS system with its outer cover removed and the Sea King helicopter is shown in Figure 5-1. A Close-up of the receive array is shown in Figure 5-2.

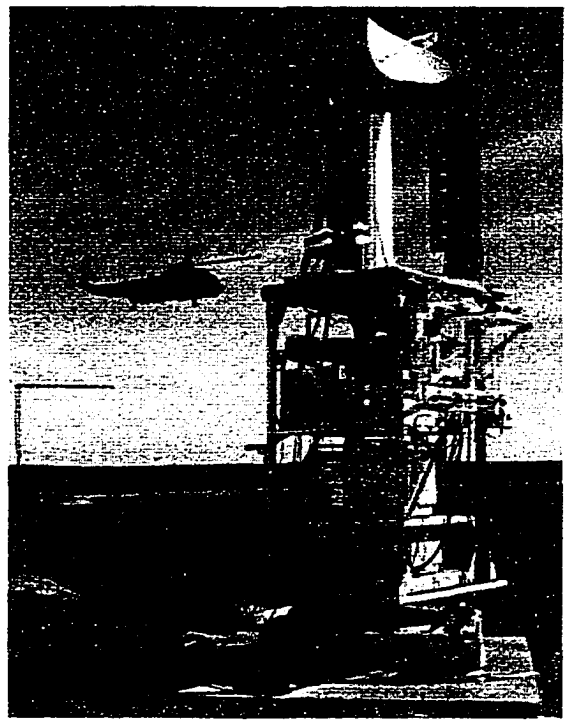

Figure 5.1 EARS radar plus Sea King helicopter

EARS has separate transmit and receive antennas, both horizontally polarized. The parabolic transmit antenna sits on top of the structure and floodlights a large elevation sector but has a narrow azimuth beamwidth. The receive array is an 8 channel vertical linear array of horns facing a parabolic cylinder reflector for increased gain (see Figure 5-2).

The spacing between horns is 12.5 cm (nearly 4 wavelengths). The large spacing is easily justified as the first grating lobe appears at an elevation angle of 15°. As the vast majority of aircraft cannot reach this elevation unless close to the radar (e.g., an aircraft at a line-of-sight range of 50 km flying at 35,000 feet), the increased aperture obtained by a near 4 wavelength spacing easily outweighs any concern regarding grating lobes.

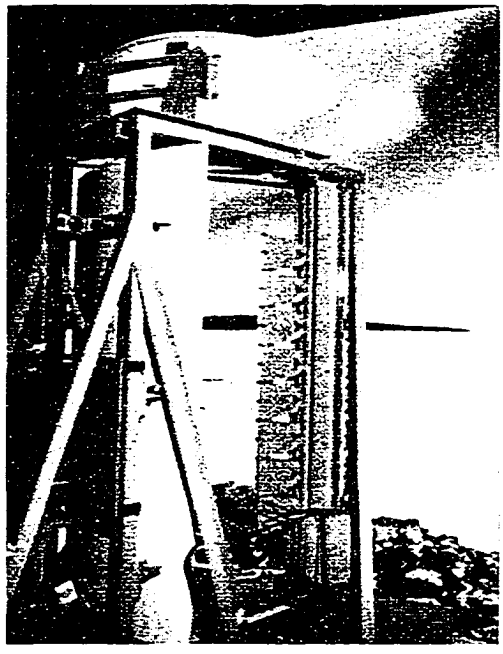

Figure 5.2 EARS 8-element vertical receive array of horns aimed at a cylindrical reflector

Each receive antenna has its own receiver. Sampling is performed at an intermediate frequency (IF) of 5 MHz and the data is digitally mixed down to baseband in-phase (I) and quadrature (Q) signals using a set of sine and cosine multipliers. The high speed A/D converters employed here perform 12 bit sampling at a rate of 20 MHz. Hence, the IF samples have a range spacing of 7.5 m. The data employed here were collected at a pulse repetition frequency (PRF) of 1000 Hz. The transmit waveform consisted of single frequency rectangular pulse with a nominal width of 10^{-6} seconds (20 range samples wide at IF).

After matched filtering (data is convolved with a rectangular window matching the ideal shape of the transmit pulse envelope) the range response of a target will have a triangular shape with a width of 300 m at the base. Hence, the Rayleigh range resolution of the system is 150 m.

5.3 Osborne Head Experiment

5.3.1 Experiment Setup

The Osborne Head data analyzed here is for a Sea King Helicopter hovering over the sea at a range of about 8 km from the EARS radar. The array height above sea level was 27.8 m and the system sat at the top of a 20 m high cliff. Conditions were stormy with winds gusting from 40 to 60 kph. Channel 2 had an IF preamplifier failure during this phase of the experiment. To simplify

matters for both the d-MUSIC and MUSIC algorithms only the bottom 6 channels of the array (channels 3 to 8) were employed for this test. The list of data files is presented in Table 5-1. These 4 files were collected over a span of 12 minutes with each file representing 1900 pulses of data (1.9 second data collection) for 132 range samples between 7.5 to 8.5 km.

Table 5-1 List of EARS Data Files

Data File	Frequency [GHz]	Target Height [m]	Target Range [m]
fort.6	9.4	30.5	8055
fort.7	8.9	30.5	8085
fort.18	9.4	61	7927.5
fort.19	8.9	61	7897.5

The helicopter hovered at a height of either 30.5 m or 61 m. Assuming a 4/3 effective earth radius refraction model this resulted in a direct path and multipath signal separation of 0.42° and 0.85°, respectively. The 6 channel array has a Rayleigh beamwidth (distance from peak to first null) of 2.57° at 8.9 GHz and 2.44° at 9.4 GHz. A spacing of 0.42° and 0.85° represents 16% and 33% of a beamwidth at 8.9 GHz and 17% and 35% of a beamwidth at 9.4 GHz.

An important concern in analyzing the Osborne Head data is the high sea clutter level and the complicated target echo response. The next two sections present an examination of the Osborne Head data to characterize the general properties of the sea clutter and the target echo for this experiment. File fort.7 (8.9 GHz, 30.5 m altitude) will be used for this demonstration.

5.3.2 Range Response

One of the interesting features of sea clutter is its ability to produce a target-like response. The following series of diagrams divides the 1900 pulses of fort.7 into 19 non-overlapping blocks of 100 pulses each, and plots the average power of each block versus range for the raw IF data (Figure 5-3) and the I/Q data after matched filtering (Figure 5-4).

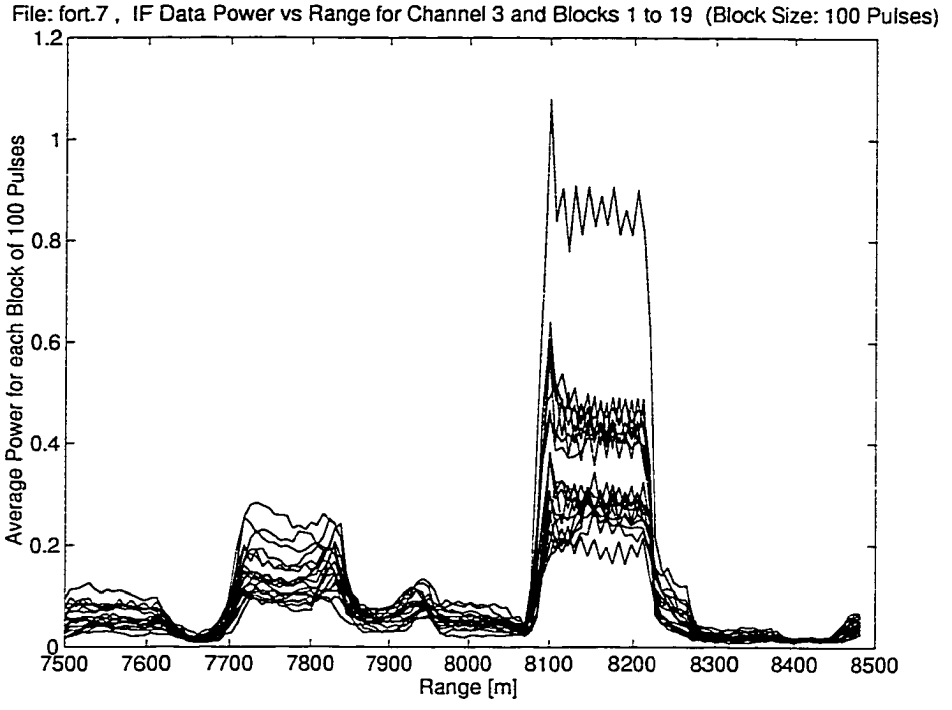

Figure 5.3 Range plot of channel 3 IF data power for each 100 pulse block of file fort.7

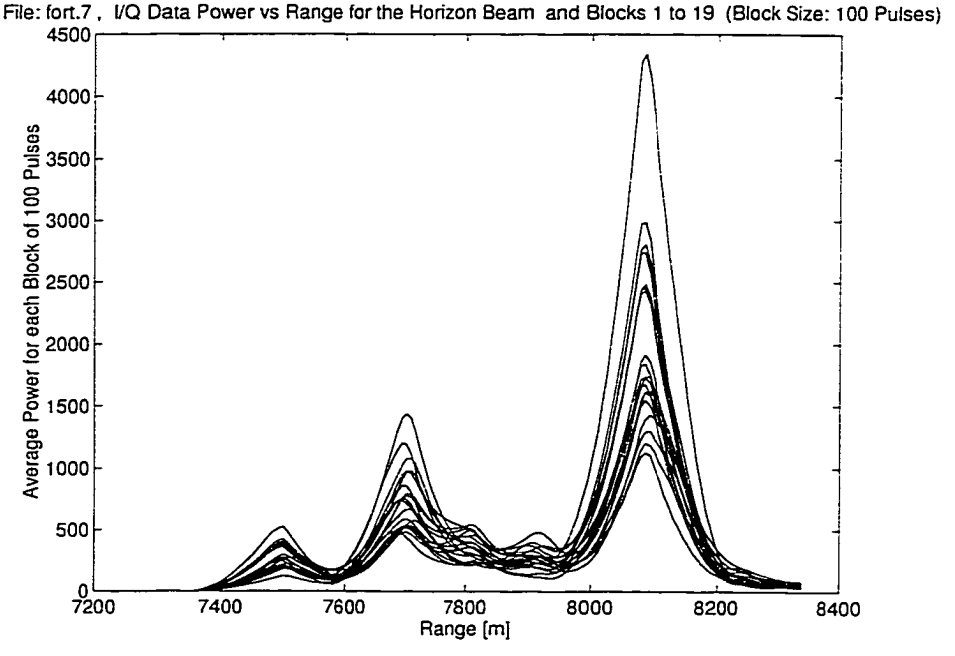

Figure 5.4 Range plot of I/Q data power of the 0° beam for each 100 pulse block of file fort.7

The 19 curves of the IF range plot of Figure 5-3 show 3, possibly more, distinct rectangular structures in the shape of the transmit pulse envelope. The largest rectangular shape of this set corresponds to the known range of the helicopter target, the other pulses are due to ocean clutter. The leading edge of the pulse denotes the true target range. In this case the target appears at a range close to 8085 m. The next largest reflection (sea clutter) has its leading edge at a range of about 7702.5 m. Figure 5-4 is the range plot for the I/Q data after envelope matched filtering. The 19 curves clearly distinguish the helicopter target as a triangular shaped peak centered at a range of 8085 m. The next highest peak (sea clutter) occurs at a range of 7702.5 m.

The apparent target-like response of sea clutter is a common problem in applications involving low incidence angles. Though clutter for the most part is noise-like, it sometimes resolves itself into distinct point-like target echoes with low signal levels occurring between peaks [42, pg. 178]. The placement of these peaks is essentially random though it may hold its position for a long time. These clutter peaks can be distinguished from a constant velocity target echo by its broad velocity signature.

5.3.3 Doppler Analysis

A Doppler analysis will be used to confirm that the helicopter target has been correctly located and to demonstrate the difference in the velocity signature of the helicopter target from the clutter background. The set of 100 pulses for each data block of fort.7 was processed using a FFT to obtain a Doppler versus range response. Figure 5-5 is a plot of the Doppler/range grid of data block 19 of file fort.7. The 6 channels were combined to form a 0° elevation beam (the horizon beam). The helicopter target is clearly distinguished in Figure 5-5 as the large peak at a velocity of near 0 m/s centered at a range of 8085 m (range bin 98).

The velocity spectrum of the target range bin is plotted in Figure 5-6. The peak is the reflection from the helicopter body. The helicopter moved forward with a small velocity to maintain stability. The nearly flat continuum surrounding the peak is not noise, but in fact the reflection from the helicopter blades. Though the blades rotate with a constant angular velocity the tangential velocity of each blade segment increases with increasing distance from the centre, resulting in a spread velocity signature 20 dB down from the main peak. The spread velocity signature for the helicopter blades is easily identified in Figure 5-5, after one recognizes the fact that most of the negative radial velocities are contaminated with ocean clutter.

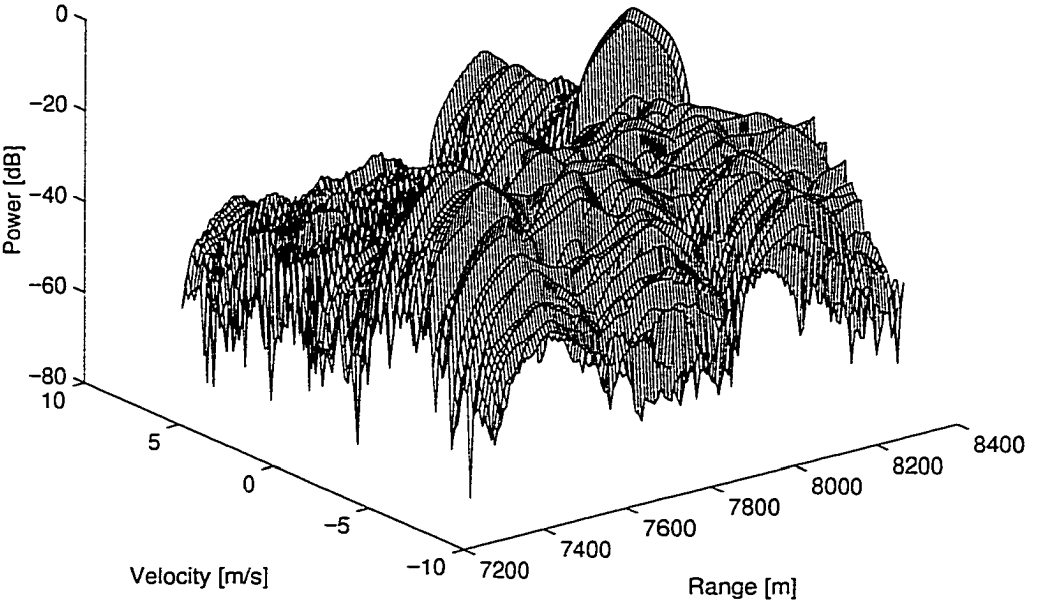

Figure 5.5 Doppler versus range of the 0° beam for block 19 of file fort.7

Figure 5-7 plots the velocity spectrum of range bins 37 to 57 normalized to the target peak of bin 98. Range bin 47 or 7702.5 m is the location of the second largest range peak. These spectra display the classic feature of ocean clutter in high sea state conditions. The 3 dB width of the clutter is roughly 2.5 m/s which is equivalent to a width of 148 Hz in terms of Doppler frequency. An empirical expression for the clutter bandwidth is [3, eqn 7.40]

$$\Delta f_{\text{Hz}} = 3.6 f_{0\,(\text{GHz})} S_D \tag{5-1}$$

where Δf_{Hz} is the 3-dB bandwidth of the clutter in Hertz, $f_{0\,(\text{GHz})}$ is the radar frequency in gigaHertz and S_D is an integer denoting the Douglas sea state numerical scale [3, chap.6]. A value of 1 for S_D is for a smooth sea, 2 is slight, 3 is moderate, 4 is rough, 5 is very rough, etc. Field observers report the sea state as $S_D = 4$ or rough. In this case $\Delta f_{\text{Hz}} = 3.6 \times 8.9 \times 4 = 128.2$ Hz which agrees fairly well with the radar observations.

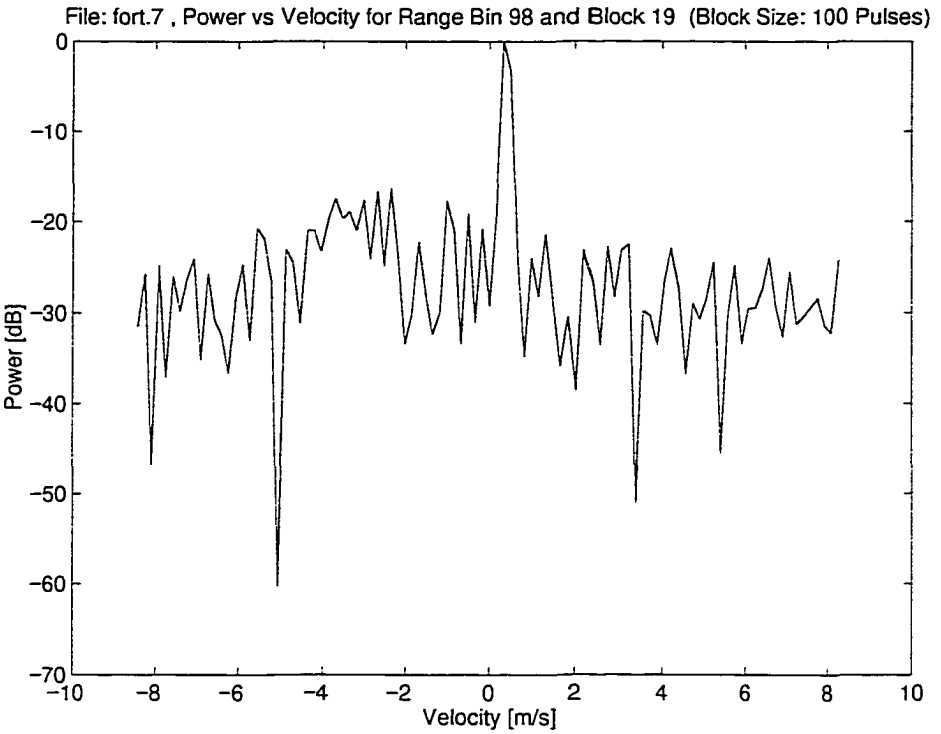

Figure 5.6 Velocity (Doppler) spectrum of range bin 98 (target)

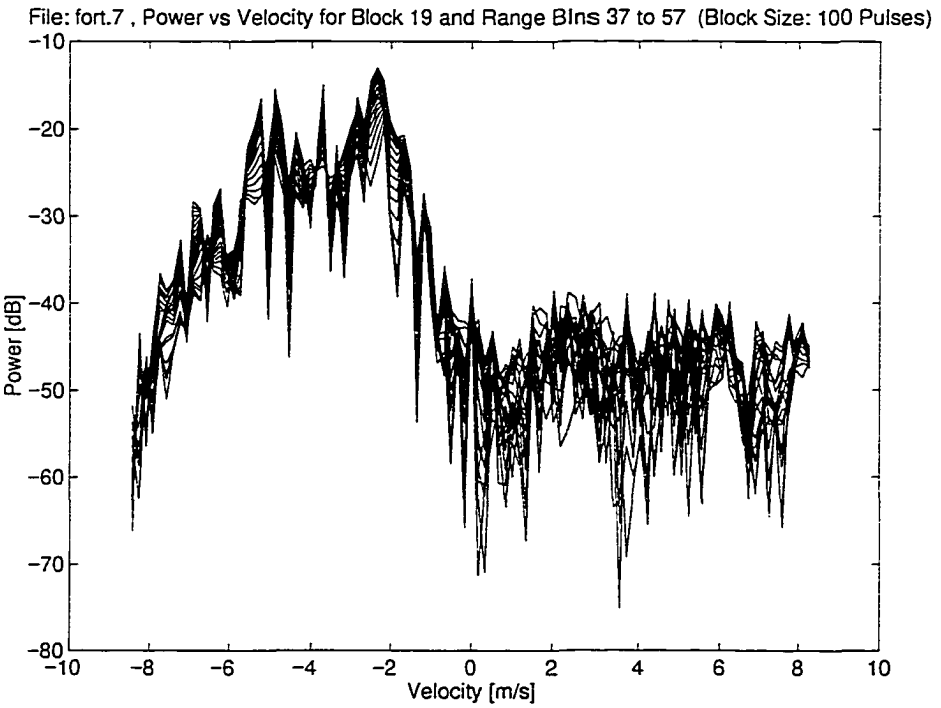

Figure 5.7 Velocity (Doppler) spectrum of range bins 37 to 57 (clutter)

From Figures 5-5 and 5-7 we can conclude that the broad clutter band is confined deep within the negative velocity region for this set of wind conditions. Comparing Figure 5-6 to 5-7 we see that the +0.4 m/s target velocity places it well outside the clutter region. As the positive velocities are suspected to be primarily noise, the SNR of the helicopter is roughly estimated at 40 dB for 100 samples. In other cases the helicopter peak is closer to the clutter region, though still far removed from the clutter peak. In this problem the target strength cannot be accurately judged via an SNR value but rather by a signal-to-clutter ratio (SCR). In many of the examples to be processed here the target peak has an SCR of better than 30 dB.

5.4 Calibration Analysis

5.4.1 Need for Caiibration

Normally, the EARS array is well calibrated. The system was transported to Nova Scotia specifically for this experiment (permanent base is Ottawa) and whether due to environmental factors or equipment problems, the array appeared to fall out of calibration (the Toeplitz calibration technique predicted a RMS phase error of nearly 31°). To illustrate the point the 1900 pulses of the fort.7 file were divided into 19 blocks of 100 pulses each and the phase of the principal eigenvector of the covariance matrix for each block is plotted in Figure 5-8.

Figure 5-8(a) plots the phase of the principal eigenvector versus channel. The first channel (channel 3) is used as a reference. Note that there is a dramatic change in phase from channel to channel, more than would be expected from such closely spaced sources. Though not guaranteed, the weighted sum of two closely spaced steering vectors (e.g., $k_1\, a(\theta_T) + k_2\, a(\theta_R)$) will often result in a vector with a near linear phase response. Clearly, this is not the case here and there is a strong suspicion that the array has a large phase error.

Figure 5-8(b) plots the phase of the principal eigenvector of each channel for each of the 19 data blocks. The phase of each channel undergoes a substantial amount of variation. This could be due to a number of factors, including array motion, fluctuating propagation conditions, sea clutter and changes in the radar cross section of a complicated target for small changes in aspect. It does demonstrate that there is a substantial variation in the target response over time,

In the first attempt to analyze this data no array calibration was applied and both d-MUSIC and MUSIC consistently failed to resolve the two sources. Given the high SNR of the data this is a surprising result, increasing the suspicion that a large calibration error is present. Only after

some form of array calibration was employed did the two algorithms produce any useful results. Time varying calibration errors (e.g., array motion) may be present but we conclude that the greatest component of the error seems to be due to a set of fixed receiver and/or antenna mismatches. As such, we stand a good chance to recover from this error.

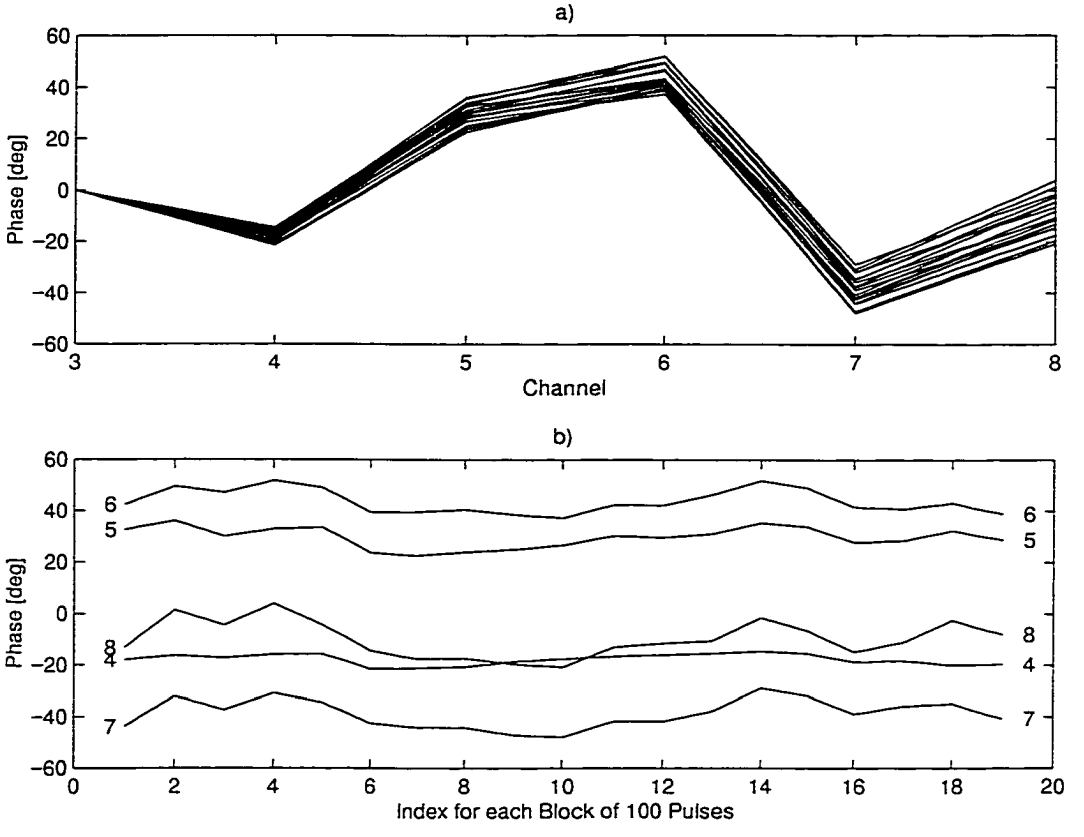

Figure 5.8 Phase of the principal eigenvector of file fort.7 for blocks of 100 pulses

How the array fell out of calibration is not known. Temperature and humidity effects can be a factor. The cause of the pre-amp failure for channel 2 may have had a system wide effect or possibly the transport of the system from Ottawa to Halifax may have affected it somehow. The problem was not detected during the field trials, after which the system was disassembled and shipped back to Ottawa, so we may only speculate as to the cause.

5.4.2 Calibration Issues

As mentioned in chapters 1 and 4 the issue of array calibration is a tricky business, and this experiment highlights many real life problems in this regard. Conceivably, if one knew the direction of arrival of all sources and had an accurate model for the propagation path including the surface reflection coefficient, one should be able to calibrate the array exactly. Unfortunately,

the number of unknowns in this experiment is large. One issue is the exact height of the helicopter. The helicopter is equipped with an altimeter but over a heaving sea the height measurement will experience a significant amount of fluctuation. Also, the conditions were stormy and it must have been difficult for the crew to maintain stability. As the array was subjected to wind gusts of between 40 to 60 kph and conditions were windy all day, the array may experience a significant amount of "wobble". As array motion was not measured it is not possible to draw a firm conclusion regarding its impact. However it is reasonable to assume that such effects are present.

Another problem is that of changing propagation conditions. For a rough sea the surface reflected field is in a constant state of flux due to non-specular or "diffuse" reflection. The specular component will likely still dominate [3, chap. 6] but as the diffuse component arises from a much wider patch of ocean, and adds incoherently to the combined direct and specular field, it will cause the wavefront to take on an irregular shape. The diffuse multipath component typically fluctuates in amplitude with a Rayleigh probability distribution, and fluctuates in phase with an uniform density over 2π radians [3, chap 6].

Both the MUSIC and d-MUSIC algorithms assume that each source arrives from a distinct bearing. When diffuse multipath is present the surface reflected rays will arrive from a band of directions clustered around the specular multipath ray. The presence of such a propagation mechanism will corrupt both the calibration and direction estimation process. However, as the diffuse component is clustered about the specular component and the specular component is likely to be dominant, it may not necessarily lead to an estimate bias but will likely increase the variance of the estimate.

A danger in using a target for array calibration in place of a beacon source is that the radar cross section of the target may fluctuate, especially that of a complicated body with moving parts (rotor blades and tail rotors). Note the near 4 dB fluctuation of the helicopter response in Figures 5-3 and 5-4 over an interval of 1.9 seconds. Part of that is due to the random nature of the multipath signal. Another factor is that a small change in target aspect may produce a large change in radar cross section (RCS), especially that arising from the rotor blades. With 6 degrees of freedom in motion a helicopter may easily pitch forward or back, roll to the left or right, or rotate about its axis (yaw) in a span of 1.9 seconds, especially if buffeted by strong winds. The rotor blades produce a significant RCS. If the helicopter were perfectly level and at the same

height as the array (files fort.6 and fort.7) the radar will only see the blades edge-on. If the helicopter tilts in any direction the radar will see the flat surface of all blades.

The fact that the helicopter moves with a small velocity (for the sake of stability) is not likely an important factor here. At such a small velocity the relative phase between the direct and surface reflected signals will change slightly, even over a 1.9 second interval. For example, the 0.4 m/s velocity of the 8085 m distant helicopter in Figure 5-6 will result in a displacement of 0.76 m in range for a 1.9 second interval resulting in a net phase change of about 0.22° between the direct and specular multipath signals. Assuming a 4/3 effective earth radius model for atmospheric refraction.

The above discussion points to the problem of array calibration in real life. For precise work one must take into account the variability of all parameters. Including array motion, changing propagation factors or target aspect. This is difficult to do in practice and is normally not attempted under stormy weather conditions. For the purpose of estimating a "coarse" calibration vector we can probably treat the calibration error as steady for a short time segment and estimate a correction for each data block.

5.4.3 Calibration Results

The Toeplitz calibration technique of [30] adapted for use here in Chapter 4 will be employed to calibrate the EARS data. This algorithm is attractive in that it is real-time (in keeping with the real-time theme of d-MUSIC) and that no *a priori* information for the source directions is required. The drawback of this technique is that it does not provide a unique solution. However, the number of unknowns in this experiment prevents us from deriving an exact solution to the calibration problem.

The results of the calibration analysis reveal some interesting information regarding the nature and size of the calibration error. The EARS data for each of the 4 data collections was divided into 19 blocks of 100 pulses each and an estimate for the calibration error was made for each block. The error magnitude and phase for the 4 files is plotted in Figures 5-9 to 5-12. The a) portion of each plot is the error magnitude in dB as a function of channel (one curve for each 100 pulse block). The b) portion of each plot is the phase error of each channel versus data block. Both the phase and magnitude error is referenced to the first channel (channel 3).

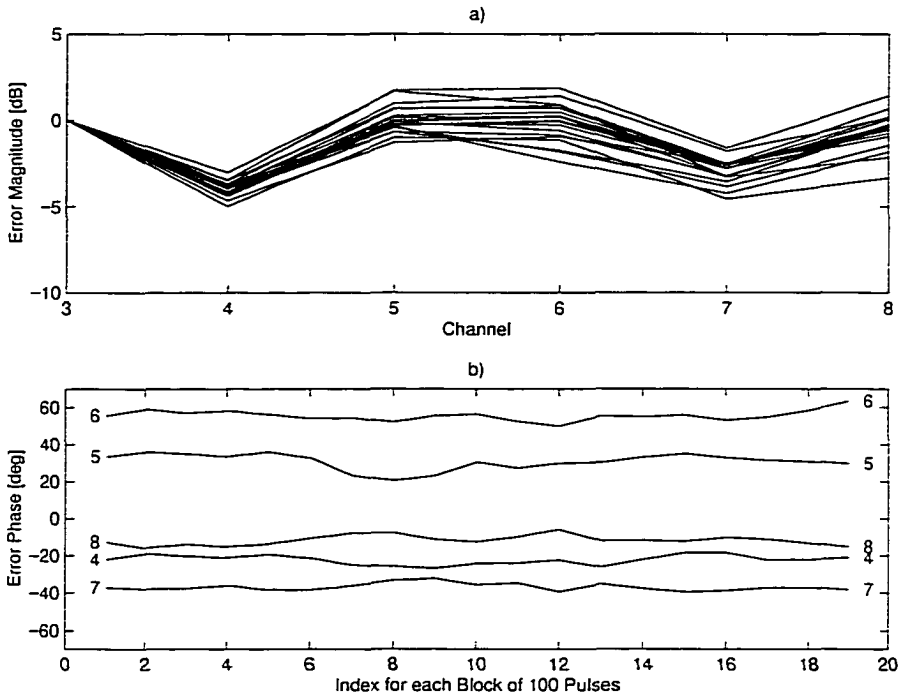

Figure 5.9 Estimate of array errors for file fort.6: a) magnitude versus channel for each data block (19 curves); b) phase versus data block for channels 4 to 8 (5 curves).

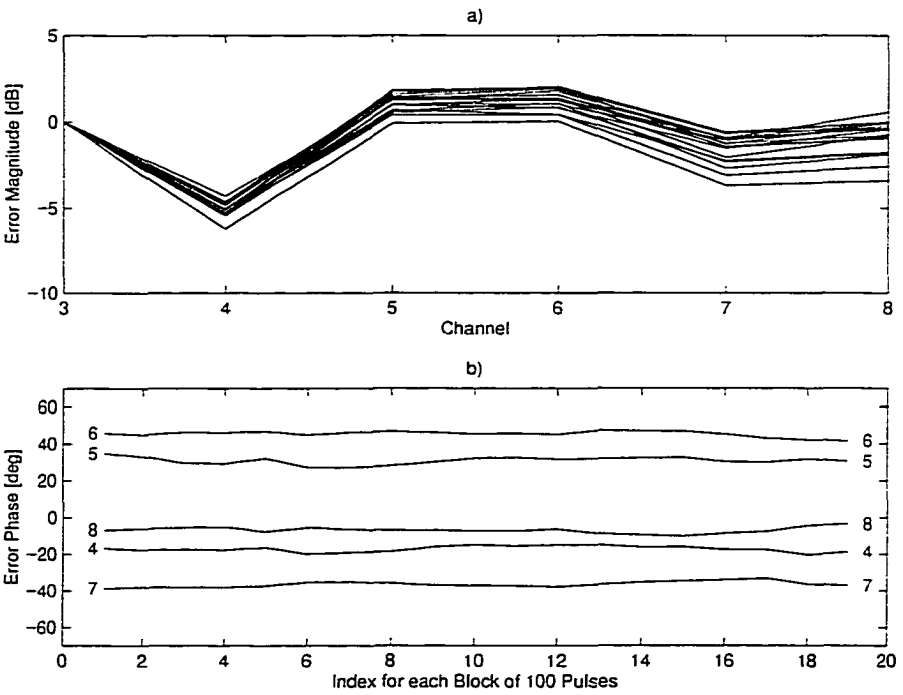

Figure 5.10 Estimate of array errors for file fort.7: a) magnitude versus channel for each data block (19 curves); b) phase versus data block for channels 4 to 8 (5 curves).

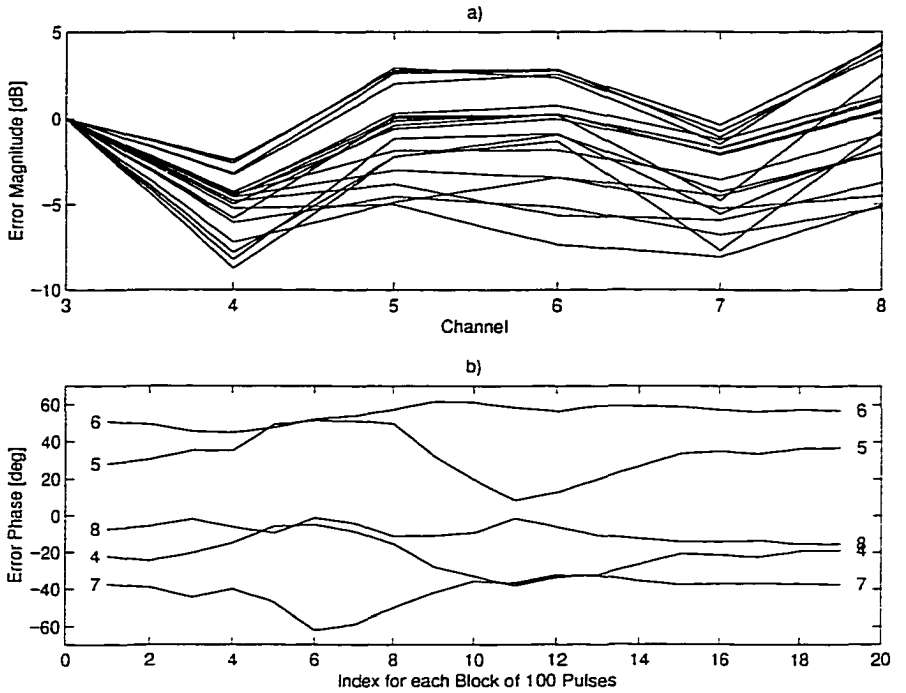

Figure 5.11 Estimate of array errors for file fort.18: a) magnitude versus channel for each data block (19 curves); b) phase versus data block for channels 4 to 8 (5 curves).

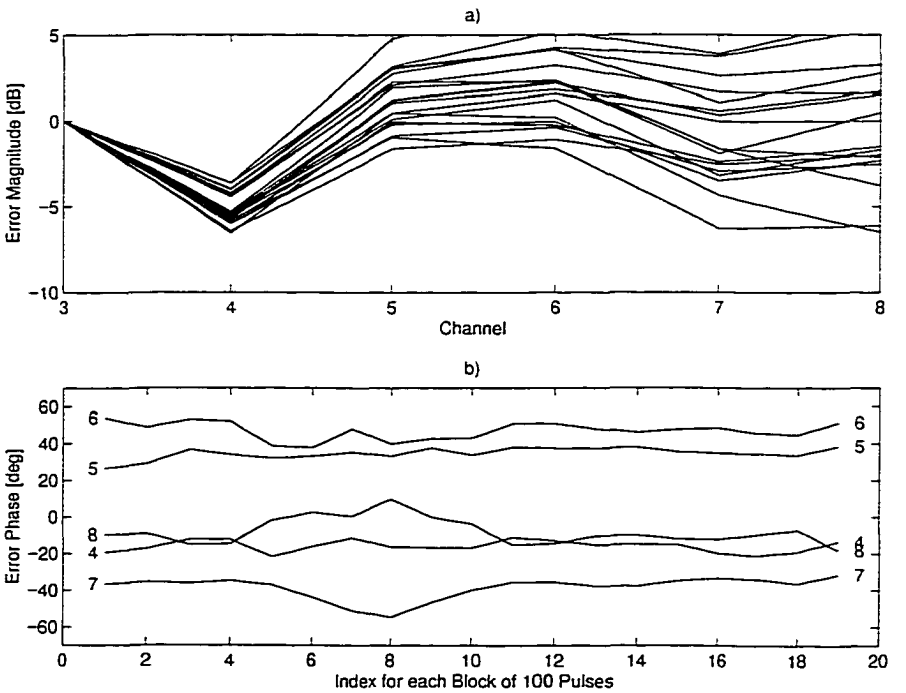

Figure 5.12 Estimate of array errors for file fort.19: a) magnitude versus channel for each data block (19 curves); b) phase versus data block for channels 4 to 8 (5 curves).

The estimate for both the calibration error and magnitude displays a substantial amount of variation over the 19 blocks of 100 pulses. Part of this variability can be attributed to the fact that the calibration method does not provide a unique solution. Other sources of variation are array motion, fluctuating helicopter RCS, sea clutter and diffuse multipath. Without extra information it is difficult to isolate the relative contribution of each.

A summary of the RMS magnitude and phase errors for the 4 files is presented in Table 5-2. The average RMS phase error of 30.76 degrees can be considered extremely high. Our confidence that this estimate reflects reality is based on the good results predicted by both the d-MUSIC and MUSIC algorithms after applying this correction.

Table 5-2 RMS Calibration Errors

File	RMS Magnitude Error [dB]	RMS Phase Error [deg]
fort.6	1.64	31.83
fort.7	2.12	28.01
fort.18	2.98	33.40
fort.19	4.22	29.78
Average	2.74	30.76

A final word of caution regarding the above estimates. As already mentioned the calibration technique will be responsive to errors other than array mismatches. It will undoubtedly include effects such as the "naturally" occurring phenomena of a fluctuating target RCS and diffuse multipath. The method will also be affected by sea clutter and no attempt was made to suppress sea clutter signal in this work. However, the target strength is strong relative to both the clutter and noise. Given all these problems and the fact it does not provide a unique solution this method works surprisingly well. Many of the issues affecting this algorithm are common to many calibration problems. Lacking any other information the Toeplitz calibration technique will suffice for this initial test of the d-MUSIC algorithm.

5.5 d-MUSIC and MUSIC Analysis

Owing to the variation of the errors a calibration estimate will be computed for individual data blocks. In this test each 1.9 second long data collection is divided into 19 non-overlapping blocks of 100 pulses each (updates of 0.1 seconds). As the calibration method operates on the covariance matrix it will be convenient to estimate the input vector to the d-MUSIC algorithm as

$$\mathbf{v} = \mathbf{R}_C \mathbf{1} \tag{5-2}$$

where $\mathbf{1}$ is a $N \times 1$ vector of ones and $\mathbf{R}_C$ is the calibrated covariance matrix. The vector $\mathbf{v} = \mathbf{R}_C \mathbf{1}$ represent the projection of the covariance matrix onto the broadside beam. It is preferred to use the peak of the Doppler spectrum as the input vector to d-MUSIC (after calibration) but there is in fact very little difference in results. In a practical field deployment the d-MUSIC algorithm may be required to use the Doppler peak or a single snapshot. In this experiment we have the luxury of computing the covariance matrix and we shall exercise this option for the sake of extracting a calibration vector.

A root-MUSIC procedure is used for both algorithms to locate the sources after constructing the noise space projector. The two roots closest to the unit circle are selected as the root-MUSIC solution. The spacing between sources is the main quantity of interest here. As the target range is known, the source spacing uniquely defines the altitude of the aircraft [3, chap. 6]. Given the uncertainty in measuring/monitoring the tilt angle of an array in either a mobile platform or a fixed platform subject to wind forces, this quantity represents a practical tool for height measurement. The d-MUSIC and MUSIC source spacing estimates at 0.1 seconds updates for the 4 data collections are presented in Figures 5-13 to 5-16. The dashed line in each plot represents the expected source spacing.

For this set of 76 measurements, the d-MUSIC algorithm successfully resolves the two sources most of the time. In contrast, the MUSIC algorithm displays more scattered results. In many instances MUSIC appears to have failed to resolve the two sources, especially for the 9.4 GHz files fort.6 and fort.18 (Figures 5-13 and 5-15). The best MUSIC results were obtained for the 8.9 GHz files fort.7 and fort.19 (Figures 5-14 and 5-16). In these instances MUSIC produced fairly good results. A summary of the RMS errors for this experiment is listed in Table 5-3.

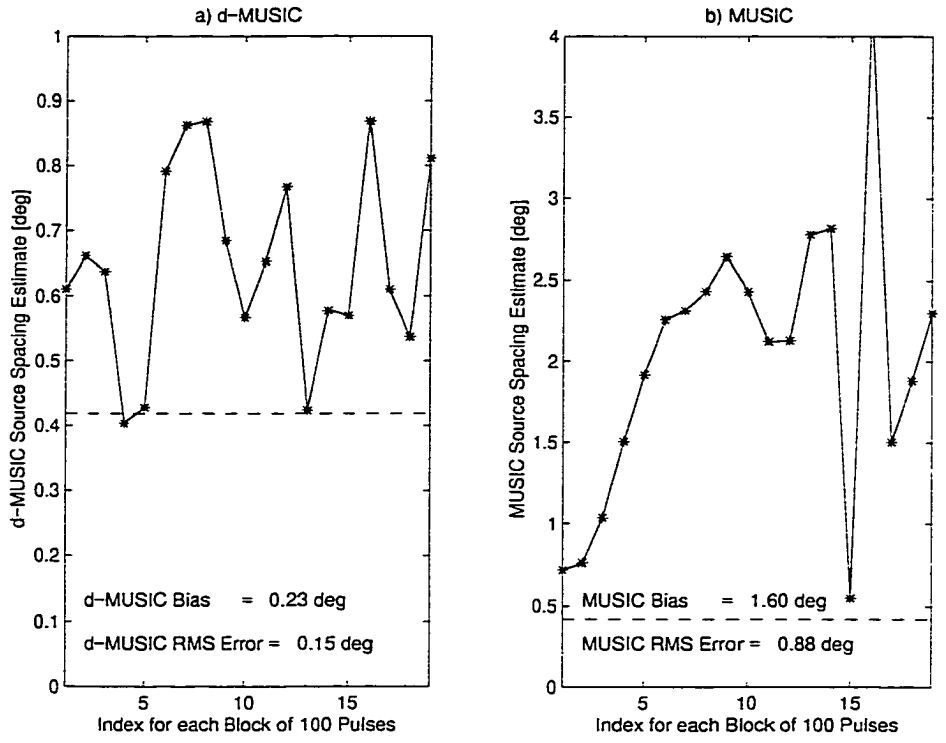

Figure 5.13 Source spacing estimates for file fort.6: a) d-MUSIC; b) MUSIC.

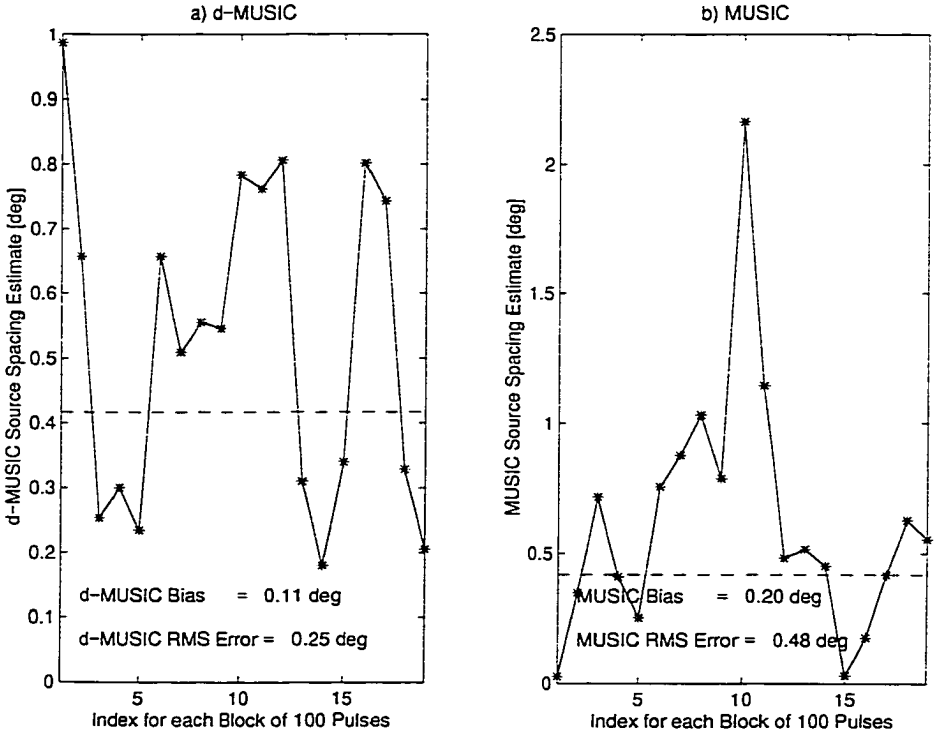

Figure 5.14 Source spacing estimates for file fort.7: a) d-MUSIC; b) MUSIC.

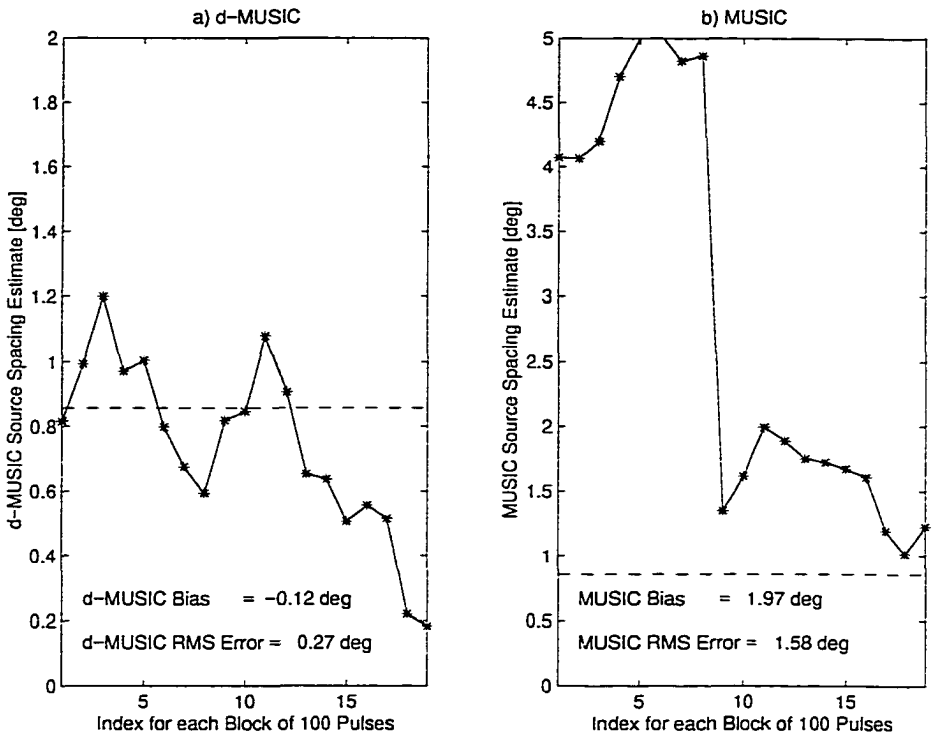

Figure 5.15 Source spacing estimates for file fort.18: a) d-MUSIC; b) MUSIC.

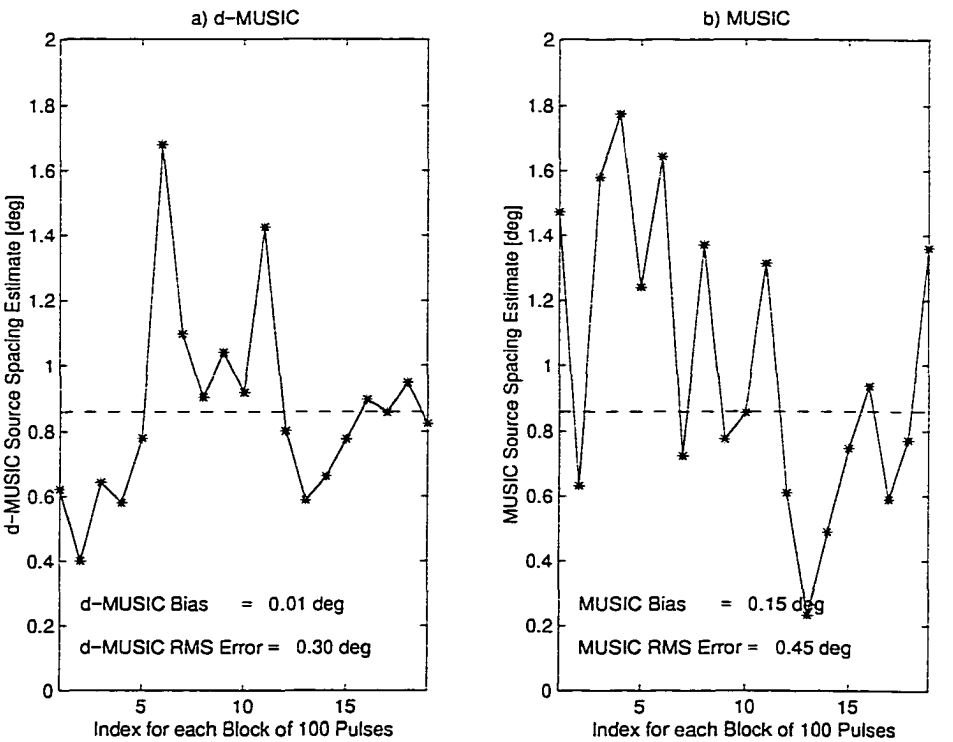

Figure 5.16 Source spacing estimates for file fort.19: a) d-MUSIC; b) MUSIC.

Table 5-3 d-MUSIC and MUSIC error summary (% BW denotes % of a beamwidth)

	d-MUSIC		MUSIC	
File	Bias [% BW]	RMS error [% BW]	Bias [% BW]	RMS error [% BW]
fort.6	9.4	6.1	65.6	36.1
fort.7	4.3	9.7	7.8	18.7
fort.18	-4.9	11.1	80.7	64.8
fort.19	0.4	11.7	5.8	17.5
Average using all 4 files	2.3	9.6		
Average using fort.7 and 19			6.8	18.1

Bias is defined as the mean of the errors (angle estimate minus the expected value). RMS error is the standard deviation of the errors. The abbreviation %BW represents a percentage of a Rayleigh beamwidth. Recall that the Rayleigh beamwidth for EARS for only 6 sensors is 2.57° at 8.9 GHz (files fort. 7 and fort.19) and 2.44° at 9.4 GHz (files fort.6 and fort.18).

In computing the statistics for the cumulative MUSIC result of Table 5-3 the 9.4 GHz files fort.6 and fort.18 were ignored. A small portion of the data for these two cases do seem to produce some useful results, but after weighting the results by the number of blocks that were excised, it has little impact on the overall result.

All in all, the d-MUSIC algorithm performed quite well. The mean bias is 2.3 % of a beamwidth and the RMS error is 9.6 % of a beamwidth using all four cases, whereas MUSIC had a mean bias of 6.1% and a RMS error of 18.1% for the two 8.9 GHz files. Considering the close spacing of the sources (between 16 % to 35 % of a Rayleigh beamwidth), this initial test of the d-MUSIC algorithm can be deemed a success. It demonstrated both a greater reliability and

greater accuracy than MUSIC. A RMS error in the order of 10 % of a beamwidth can be considered a fairly good result.

In all fairness to the MUSIC algorithm a large number of questions are left unanswered from this exercise. Perhaps the most important issue is the accuracy of the calibration method under these conditions and its impact on both algorithms. It is reassuring however that MUSIC did produce good results for at least 2 of the 4 data collections. Given the small amount of data, the severe weather conditions and the large array errors it will be difficult to draw a firm conclusion on the relative merit of d-MUSIC over MUSIC. That the algorithm worked this well is gratifying and may be indicative of its resiliency.

As a first test of the d-MUSIC algorithm this experiment at least establishes that together with the Toeplitz calibration method, it can produce practical height measurements. What is now needed is more real data testing, preferably under more controlled conditions.

6 Conclusions

6.1 Summary

d-MUSIC estimates the direction-of-arrival of two closely spaced sources using a single array snapshot. The input vector may either be a single array sample, the coherent sum of several snapshots (e.g., Doppler processing in radar/sonar systems), the signal space eigenvector of a rank deficient covariance matrix involving two coherent signals, etc. To make the problem full rank for a pair of sources d-MUSIC utilizes additional information, specifically the derivative of the input vector. The combined vector set is mutually orthogonal and can be directly applied to construct a rank two signal space projector to resolve the two sources. To construct this projector an estimate for the center of the signal cluster is required. This is necessary in order to equalize the gain of the two source direction vectors via an $\mathbf{I} + \mathbf{J}$ forward-backward averaging operation. In many radar low angle tracking problems involving distant aircraft the center of the target plus multipath cluster is known *a priori* (flat earth approximation [3]). Otherwise, d-MUSIC estimates the source bearings for a grid of center angles and selects the grid point where the signal space of

the solution is most consistent with the input vector. As d-MUSIC does not require a complex matrix factorization technique such as an eigenvector decomposition or a SVD and all remaining operations are highly vectorized, it is well suited for an inexpensive software implementation in a real-time setting.

As d-MUSIC employs a single space vector and uses additional information to construct a second signal space vector, it is relatively insensitive to the problem of correlated signals. The second vector the algorithm constructs is $\mathbf{a}(\theta_T) - \mathbf{a}(\theta_R)$, the difference between the direct path and multipath direction vectors. If the input is already $\mathbf{a}(\theta_T) - \mathbf{a}(\theta_R)$ then d-MUSIC can not resolve the two sources. The case of two signals 180° out of phase is a moot point however, as the SNR of the combined signal will be a minimum and the probability of detection is low.

Following the approach of Stoica and Nehorai [10], a theoretical estimate for the d-MUSIC error variance is derived and compared to the Cramér-Rao bound for the case of a known cluster centroid (typical air traffic control problem). The algorithm nearly attains the Cramér-Rao bound, displaying a low sensitivity to the problem of signal correlation. A number of Monte Carlo tests are also performed to compare the performance of MUSIC to the two d-MUSIC algorithms (cluster center known or unknown). These tests demonstrate that both versions of d-MUSIC is highly resilient to the problem of signal correlation.

The linear array Toeplitz calibration technique of [30] is adapted for use here to calibrate the Osborne Head data. The method is attractive in that it can be readily employed in a real-time setting but suffers from the drawback of an non-unique solution as the constraint that the phase errors sum to zero is not appropriate for the Osborne Head data. Simulation tests demonstrate that the non-unique solution results in a substantial residual error. But the Osborne Head data suffers from a high calibration error to begin with (the RMS phase error is estimated as 31°) and the application of this technique has led to a substantial improvement in data quality, crucial to the success of the experiment. This method has potential and if additional information can be applied to make the problem full rank it can form the cornerstone of an adaptive auto-calibration scheme.

The algorithm is field tested using data from the X-band EARS radar tracking a near-range low flying helicopter. As the flat earth approximation is not appropriate to this experiment the grid search version of d-MUSIC is employed (unknown cluster center). With a spacing of 16% and 35% of a beamwidth between the direct and multipath signals, the d-MUSIC RMS error for

the source spacing is 9.6% of a beamwidth for the 4 data collections. MUSIC resolved the two signals for 2 of the 4 cases with a RMS error of 18.1%.

6.2 Achievements

In light of the large calibration errors in the Osborne Head data this first field test of the grid search version of d-MUSIC can be considered a success. The algorithm performed better than MUSIC, resolving the two signals for all four data collections with a substantially lower RMS error. The small amount of data and large calibration errors prevents us from drawing a firm conclusion regarding the grid search version of d-MUSIC for this experiment. But this result along with the Monte Carlo tests is encouraging and does establish that the algorithm is a serious contender for the general low angle tracking problem.

Based on the good performance of the algorithm in nearly reaching the Cramér-Rao bound the flat earth version of d-MUSIC (known cluster center) has established itself as a strong presence for the flat earth, low angle tracking problem. Given its low sensitivity to the problem of signal correlation, the fact that it uses only one snapshot and its ease of implementation in a real-time scenario, this algorithm offers a system designer a powerful tool for aircraft height measurement.

6.3 Recommendations

An algorithm is discussed in chapter 2 that can be applied to the multi-source problem in a multipath environment if the flat earth approximation is appropriate for all sources. In that event each signal plus multipath source cluster will all have a common center. In this problem more than one input vector is required and the method creates a companion set of vectors using derivative information. The combined vector set can be processed using a SVD to create an orthogonal basis set to construct a MUSIC signal space projector. The method is not guaranteed to produce a full rank projector but is likely to increase the span we know. Though interesting, this strategy for the multi-source problem is not fully explored here, but is a logical extension to the d-MUSIC algorithm that should be a part of future work in this area.

A theoretical error analysis for the case of an unknown cluster center is a future priority. This option was not pursued at this time owing to the complexity of the problem. This complexity stems from the spatially correlated noise resulting from the $\mathbf{I} + \mathbf{J}$ forward-backward operation and the fact that the noise of the derivative vector is correlated with the input vector.

As such, the number of the error terms generated by the analysis will be large, even if we retain terms to second moment only. If the cluster center is treated as another random variable the number of error terms, already large, would dramatically increase. The Stoica and Nehorai approach [10] is appropriate for the problem of a known cluster center but it may be necessary to derive an alternate approach to the error analysis for the case of an unknown center. In the interim we can stake a claim that the method is worthy of further study based on its improved performance over MUSIC in the Monte Carlo tests and the Osborne Head experiment.

Another research topic of interest is a beamspace version of the algorithm. Most radar systems do not collect data from individual sensors but rather form a set of beams [39-41]. Modern phased-array radars [39] may employ hundreds or possibly thousands of transmit/receive (TR) antenna modules to form a narrow transmit/receive beam using a complex antenna feed network. As the target plus multipath signal may reside on only a few overlapping beams the restriction of two sources for d-MUSIC is much less of an obstacle in this case. A large body of work exists on beamspace processing [e.g., 43-45] and beamspace statistical performance [14, 46-47]. It is hoped to draw inspiration from this work to carry d-MUSIC into the beamspace domain.

Appendix A lays the foundation for a planar array d-MUSIC algorithm. As pointed out in Appendix A there is not a critical need at this time to develop a 2-D algorithm, for the low angle multipath problem at least, as the direct and multipath signals arrive from the same azimuth so the signals are separated in one dimension only. In other problems there may be two closely spaced signals separated in both azimuth and elevation (e.g., two aircraft flying in formation) and a 2-D algorithm is required.

Another concern of the d-MUSIC algorithm is that it only applies to uniformly spaced arrays (due to the $\mathbf{I} + \mathbf{J}$ forward-backward averaging operation). Arrays with an arbitrary sensor placement are common and in any event the uniformity of an array can be compromised by equipment failures, leaving gaps in the array (e.g., the failure of channel 2 in the Osborne Head trials). The generalization of the d-MUSIC algorithm to non-uniform arrays is another worthy research topic.

Finally, more experiment data is required to test the two d-MUSIC algorithms developed here. This is the true test of any algorithm.

Bibliography

[1] R. O. Schmidt, "Multiple emitter location and signal parameter estimation," in *Proc. RADC Spectral Estimation Workshop*, pp. 243 - 258, Griffiths AFB, New York, 1979. This paper is reproduced in *IEEE trans. Antennas Propagat.*, vol. 34, pp. 276 - 280, 1986.

[2] S. Haykin, *Adaptive Filter Theory, 2nd Ed.*, Prentice-Hall, 1991

[3] L. Blake , *Radar Range-Performance Analysis*, Lexington Books, 1980.

[4] H. B. Lee, "Eigenvalues and eigenvectors of covariance matrices for signals closely spaced in frequency," *IEEE Trans. Signal Proc.*, Vol. 40, No. 10, pp. 2518 - 2535, 1992.

[5] M. Viberg, B. Ottersten, and A. Nehorai, "Performance analysis of direction finding with large arrays and finite data," *IEEE Trans. Signal Proc.*, Vol. 43, No. 12, pp. 469 - 477, 1995.

[6] B. M. Radich and K. M. Buckley, "Single-snapshot DOA estimation and source number detection," *IEEE Signal Proc. Letters.* , Vol. 4, No. 4, pp. 109 - 111, 1997.

[7] Q. S. Ren and A. J. Willis, "Extending MUSIC to single snapshot and on line direction finding applications," in *Radar 97,* Edinburgh, UK, pp. 783 - 787, 1997.

[8] R. L. Kirlin, E. Su, and B. Hedstrom, ``The scorefunction approach to bearing estimation: phase-lock loops and eigenstructure", Chapter 4 in *Advances in Spectrum Analysis and Array Processing*, Vol. 3, S. Haykin, ed., Prentice Hall, Englewood Cliffs, N.J., 1995, pp. 135-170.

[9] H. B. Lee and F. Li, "An eigenvector technique for detecting the number of emitters in a cluster," *IEEE Trans. Signal Proc.*, Vol. 42, No. 9, pp. 2380 - 2388, 1994.

[10] P. Stoica and A. Nehorai, "MUSIC, maximum likelihood, and Cramér-Rao Bound, " *IEEE Trans. Acoust., Speech, Signal Processing*, vol. 37, no. 5, pp. 720-741, 1989.

[11] S. Weimin, N. Jinlin, L. Guosui and Z. Guangyi, "The effect of channel mismatch on the spatial spectrum and resolution capability of the MUSIC algorithm. " in *Proc. CIE International Conf. of Radar*, pp. 96-99, Beijing, China, 1996.

[12] B. Friedlander, "A sensitivity analysis of the MUSIC algorithm," *IEEE Trans. Signal Proc.*, vol. 38, no. 10, pp. 1740-1751, 1990.

[13] A. Swindlehurst and T. Kailath, "A performance analysis of subspace-based methods in the presence of model errors, Part I: The MUSIC Algorithm," *IEEE Trans. Signal Proc.*, vol. 40, no. 7, pp. 1758-1774, 1992.

[14] F. Li and H. Liu, "Statistical analysis of beam-space estimation for direction-of-arrival," *IEEE Trans. Signal Proc.*, vol. 42, no. 3, pp. 604-610, 1994.

[15] A. J. Weiss and B. Friedlander, "Effects of modeling errors on the resolution threshold of the MUSIC algorithm," *IEEE Trans. Signal Proc.*, vol. 42, no. 6, pp. 1519-1526, 1994.

[16] K. Wong, R. Walker and G. Niezgoda, "Effects of random sensor motion on bearing estimation by the MUSIC algorithm," *Proc. Inst. Elec. Eng.*, vol. 135, pt. F., no. 3, pp. 233-250, 1988.

[17] F. Li and R. J. Vaccaro, "Statistical comparison of subspace-based DOA estimation algorithms in the presence of sensor errors," in *Proc. 5th IEEE ASSP Workshop on Spectrum Estimation & Modeling*, Rochester, pp. 327-331, 1990.

[18] M. Viberg and A. L. Swindlehurst, "Analysis of the combined effects of finite samples and model errors on array processing performance," *IEEE Trans. Signal Processing*, vol. 42, no. 11, pp. 3073 - 3083, 1994.

[19] B. Friedlander and A. J. Weiss, "Effects of model errors on waveform estimation using the MUSIC algorithm," *IEEE Trans. Signal Processing*, vol. 42, no. 1, pp. 147 - 155, 1994.

[20] S. Haykin, V. Kezys, and E. Vertatschitsch, "Maximum likelihood for angle-of-arrival estimation in multipath," Chapter 3 in *Advances in Spectrum Analysis and Array Processing*, Vol. 2, S. Haykin, ed., Prentice Hall, Englewood Cliffs, N.J., 1995, pp. 123-143.

[21] D. Carhoun, "Constrained adaptive beamforming with an uncalibrated array," in Proc. 8th IEEE Signal Processing Workshop on Statistical Signal and Array Processing, Corfu, Greece, pp. 276-278, 1996.

[22] D. R. Fuhrmann, "Estimation of sensor gain and phase," *IEEE Trans. Signal Processing*, vol. 42, no. 1, pp. 77 - 87, 1994.

[23] A. P.-C. Ng, "Direction of arrival estimates in the presence of wavelength, gain, and phase errors," *IEEE Trans. Signal Processing*, vol. 43, no. 1, pp. 225 - 323, 1995.

[24] M. Viberg and A. L. Swindlehurst, "A Bayesian approach to auto-calibration for parametric array signal processing," *IEEE Trans. Signal Processing*, vol. 42, no. 12, pp. 3495 - 3507, 1994.

[25] V. C. Soon, L.Tong, Y. F. Huang, and R. Liu, "A subspace method for estimating sensor gains and phases," *IEEE Trans. Signal Processing*, vol. 42, no. 4, pp. 973 - 976, 1994.

[26] C-Y Tseng, D. D. Feldman, and L. J. Griffiths, "Steering vector estimation in uncalibrated arrays," *IEEE Trans. Signal Processing*, vol. 43, no. 6, pp. 1397 - 1412, 1995.

[27] A. J. Weiss and B. Friedlander, " "Almost blind" steering vector estimation using second-order moments", *IEEE Trans. Signal Processing*, vol. 44, no. 4, pp. 1024 - 1027, 1996.

[28] M. C. Dogan and J. M. Mendel, "Application of cumulants to array processing - Part I: Aperture extension and array calibration," *IEEE Trans. Signal Processing*, vol. 43, no. 5, pp. 1200 - 1216, 1995.

[29] W.-K. lai and P.-C. Ching, "A novel blind estimation algorithm," *IEEE Trans. Signal Processing*, vol. 45, no. 7, pp. 1763 - 1769, 1997.

[30] M. P. Wylie, S. Roy, and H. Messer, "Joint DOA estimation and phase calibration of linear equispaced (LES) arrays," *IEEE Trans. Signal Processing*, vol. 42, no. 12, pp. 3449 - 3459, 1994.

[31] R. Kumarsen and D. W. Tufts, ``Estimating the angles of arrival of multiple plane waves," *IEEE Trans. Aerospace Electron. Syst.*, vol. AES-19, pp. 134 - 139, 1983.

[32] R. Roy. R., A. Paulraj, and T. Kailath, ``ESPRIT — A subspace rotation approach to estimation of parameters of cisoids in noise," *IEEE Trans. Acoust., Speech, Signal Processing*, vol. ASSP-34 (Oct.), pp. 1340 - 1342, 1986.

[33] L. L. Scharf, *Statistical Signal Processing: Detection, Estimation, and Time Series Analysis*. Addison-Wesley Publishing Co., New York, 1991

[34] D. Bhaskar, D. R. and K. S. Arun, ``Model based processing of Signals: A state Space Approach," *Proc. IEEE*, vol. 80, no. 2, pp. 283 - 309, 1992.

[35] J. E. Evans, J. R. Johnson and D. F. Sun, "High resolution angular spectrum estimation technqies for terrain scattering analysis and angle of arrival estimation," in Proc. 1st ASSP Workshop on Spectral Estimation, Hamilton, Ontario, Canada, pp. 134-139, 1981.

[36] T. J. Shan, M. Wax and T. Kailath, "On spatial smoothing for direction-of-arrival estimation for coherent signals," *IEEE Trans. Acoust., Speech, Signal Processing*, vol. 33, pp. 860-811, Aug. 1985.

[37] W. Du and R. L. Kirlin, "Improved spatial smoothing techniques for DOA estimation of coherent signals," IEEE Trans. Signal Processing, vol. 39, no. 5, pp. 1208 - 1210, 1991.

[38] J. Yang and C. Tsai, "A further analysis of decorrelation performance of spatial smoothing technique for real multipath sources," *IEEE Trans. Signal Processing*, vol. 40, no. 8, pp. 2109 - 2112, 1992.

[39] M. I. Skolnik (ed.), *Radar Handbook, 2nd ed*, McGraw-Hill Inc., New York, 1990.

[40] E. Brookner (ed.), *Aspects of Modern Radar*, Artech House, 1988.

[41] D. Barton, *Modern Radar Systems Analysis*, McGraw-Hill, 1988.

[42] M. W. Long , *Radar Reflectivity of Land and Sea, 2nd Ed.*, Artech House, 1983.

[43] G. Bienvenu and L. Kopp, "Decreasing high-resolution method sensitivity by conventional beamformers processing," in *Proc. IEEE ICASSP '84*, pp. 33.2.1 - 33.2.4, 1984,

[44] H. B. Lee and M. S. Wengrovitz, "Resolution threshold of beamspace MUSIC for two closely spaced emitters," *IEEE Trans. Signal Processing*, vol. 38, no. 9, pp. 1545 - 1559, 1990.

[45] M. D. Zoltowski, S. D. Silverstein and C. P. Matthews, "Beamspace root-MUSIC for minimum redundancy linear arrays," *IEEE Trans. Signal Processing*, vol. 41, no. 7, pp. 2502 - 2507, 1993.

[46] A. J. Weiss and B. Friedlander, "Preprocessing for direction finding with minimal variance degradation," *IEEE Trans. Signal Processing*, vol. 42, no. 6, pp. 1478 - 1485, 1994.

[47] P. Stoica and A. Nehorai, "Comparative performance study of element-space and beam-space MUSIC estimators," *Circuits, Syst., Signal Processing*, vol. 10, pp. 285 - 292, 1991.

A Application to Planar Arrays

A.1 Problem Outline

To locate a source in 3-D space an array is required that spans at least two spatial dimensions, for example, a planar array. A conceptually simple planar structure is an M × N rectangular grid of sensors. Figure A.1 illustrates the geometry of a rectangular grid, rectangular boundary planar array. As it is essentially a collection of linear arrays many of the d-MUSIC ideas can be extended to include the rectangular array problem.

This appendix builds on the linear array d-MUSIC framework to analyze the properties of planar array vectors and their derivatives for the case of two closely spaced sources in a multipath environment. The focus is chiefly tutorial. The planar array theory presented here is not applied to develop new beamforming algorithms, although much of the building blocks for such an algorithm will be developed. Future algorithms may be developed along this line however.

There is no critical need to develop a general planar array technique at this time for the low angle tracking problem. This problem can be efficiently solved using the linear array method. The key point to note is that the direct and surface reflected rays arrive from the same azimuth. As such, each row of the array can be summed to form a zero elevation beam directed at the target azimuth (exact match with the true azimuth is not a strict requirement, though desired). The beamformed output of all rows will correspond to a vertical linear array composed of sensors with a narrow beamwidth in azimuth. The linear array d-MUSIC algorithm can then be applied to measure the two elevation angles.

Planar arrays are widely used, but almost always include some form of up-front beamforming to reduce the dimension of the data and null out interference signals arriving from other directions [39-41]. The beams are usually scanned electronically but sometimes employ mechanical rotation to perform a volume search. If contending signals arrive from other directions, both the row weights and column weights can be adjusted to steer a null along these directions. The beamformer output should include at least 3 identical beams arranged in a column in order to implement the d-MUSIC algorithm.

A.2 Rectangular Planar Array Geometry

Figure A.1 represents a general M × N rectangular planar array of sensors. For convenience, the center of the array will be taken as the phase reference point. The rectangular grid,

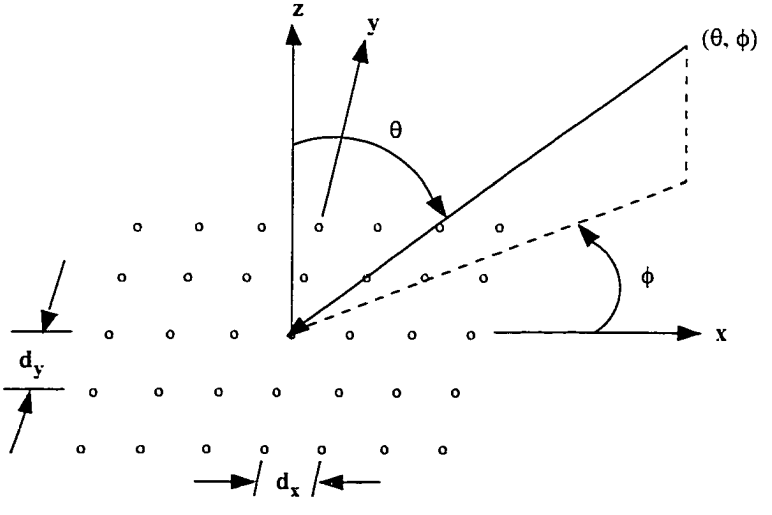

Figure A.1 Rectangular planar array geometry

rectangular boundary planar array can be viewed as a collection of 1-D linear arrays. The set of N-element linear arrays parallel to the x-axis will be designated as a row of the planar array. The top row of Figure 5.1 is designated as row 1 and the bottom row is row M. Elements 1 to N of each row run from right to left (positive x-axis to negative).

The set of M-element linear arrays parallel to the y-axis of Figure A.1 are the columns of the array. The rightmost column is column 1, the leftmost is column N. Elements 1 to M of each column run from top to bottom (positive y-axis to negative). This makes the Northwest corner of the array element (1,1).

The output of the MN sensors are arranged into an MN × 1 vector on a column-by-column basis (starting from column 1). The response of the array for a signal arriving along direction (θ, ϕ) can be expressed as the MN × 1 direction vector

$$\mathbf{a}(\theta,\phi) = \mathbf{a}_x(\theta,\phi) \otimes \mathbf{a}_y(\theta,\phi) \tag{A-1}$$

where $\otimes$ denotes the Kronecker product. For example,

$$\mathbf{p} \otimes \mathbf{q} = \begin{bmatrix} p(1)\mathbf{q} \\ p(2)\mathbf{q} \\ \vdots \\ p(N)\mathbf{q} \end{bmatrix} \tag{A-2}$$

The vectors $\mathbf{a}_x$ and $\mathbf{a}_y$ are linear array direction vectors representing the x- and y-axes responses:

$$\mathbf{a}_x(\theta,\phi) = e^{ju(N-1)/2}\left[1 \;\; e^{-ju} \; e^{-j2u} \cdots e^{-j(N-1)u}\right]^T \tag{A-3}$$

$$\mathbf{a}_y(\theta,\phi) = e^{jv(M-1)/2}\left[1 \;\; e^{-jv} \; e^{-j2v} \cdots e^{-j(M-1)v}\right]^T \tag{A-4}$$

u and v denotes the sensor-to-sensor phase shift of the signal along the x- and y-axes, i.e.,

$$u = \frac{2\pi d_x}{\lambda} \sin\theta \cos\phi \tag{A-5}$$

$$v = \frac{2\pi d_y}{\lambda} \sin\theta \sin\phi \tag{A-6}$$

Like linear array vectors, a rectangular planar array vector is centro-Hermitian symmetric, i.e.,

$$\mathbf{J}\,\mathbf{a}(\theta,\phi) = \mathbf{a}^{*}(\theta,\phi) \tag{A-7}$$

Other useful symmetries include

$$\mathbf{J}\,\mathbf{a}(\theta,\phi) = \mathbf{a}^{*}(\theta,\phi) = \mathbf{a}(-\theta,\phi) \tag{A-8}$$

$$\mathbf{a}(\theta,\phi) = \mathbf{a}(\theta+\pi,\phi+\pi) \tag{A-9}$$

The physical interpretation of the angles θ and ϕ depends on the frame of reference and the orientation of the array. If the coordinate system of the array is selected as the reference frame, than θ and ϕ will correspond to the elevation and azimuth angle of the source. In practice it is more convenient to reference everything to the surface of the earth directly beneath the array.

Two important cases will be considered here. The first is when the array is parallel to the surface at a height h above it (y- and x-axes of array are parallel to those of the surface frame). The second case is when the array is perpendicular to the surface with the array center at height h. That configuration is often used for low angle tracking. Without any loss of generality, assume that the array y-axis is perpendicular to the surface and the array x-axis is aligned with the surface x-axis.

Using the convention that a ray parallel to the surface has a elevation angle of zero, the source elevation angle (El) and azimuth (Az) with respect to the surface is

Array Parallel to Surface:

$$\begin{aligned} &\text{Azimuth:} \quad Az = \phi \\ &\text{Elevation:} \quad El = \theta - \pi/2 \end{aligned} \tag{A-10}$$

y-axis of Array Perpendicular to Surface:

$$\begin{aligned} &\text{Azimuth:} \quad Az = \tan^{-1}(\tan\theta\cos\phi) \\ &\text{Elevation:} \quad El = \sin^{-1}(\sin\theta\sin\phi) \end{aligned} \tag{A-11}$$

A.3 The Rectangular Planar Array Direction Vector Derivative

The derivative of $\mathbf{a}(\theta, \phi)$ with respect to either u or v is

$$\dot{\mathbf{a}}_u(\theta,\phi) = \frac{d\,\mathbf{a}(\theta,\phi)}{d\,\mathrm{u}} = \mathbf{D}_u\,\mathbf{a}(\theta,\phi) \tag{A-12}$$

$$\dot{\mathbf{a}}_v(\theta,\phi) = \frac{d\,\mathbf{a}(\theta,\phi)}{d\,\mathrm{v}} = \mathbf{D}_v\,\mathbf{a}(\theta,\phi) \tag{A-13}$$

where

$$\mathbf{D}_u = \mathrm{diag}\{\mathbf{d}_N \otimes \mathbf{1}_M\} \tag{A-14}$$

$$\mathbf{D}_v = \mathrm{diag}\{\mathbf{1}_N \otimes \mathbf{d}_M\} \tag{A-15}$$

$$\mathbf{d}_P = j(P-1)/2 - j[0, 1, \cdots P-1]^T \tag{A-16}$$

and $\mathbf{1}_P$ is a P × 1 column vector of ones.

The higher-order derivatives of $\mathbf{a}(\theta,\phi)$ may be defined by multiplying $\mathbf{a}(\theta,\phi)$ by either $\mathbf{D}_u$ or $\mathbf{D}_v$ an appropriate number of times. The second derivatives are

$$\ddot{\mathbf{a}}_u(\theta,\phi) = \frac{d^2\mathbf{a}(\theta,\phi)}{du^2} = \mathbf{D}_u\,\mathbf{D}_u\,\mathbf{a}(\theta,\phi) \tag{A-17}$$

$$\ddot{\mathbf{a}}_v(\theta,\phi) = \frac{d^2\mathbf{a}(\theta,\phi)}{dv^2} = \mathbf{D}_v\,\mathbf{D}_v\,\mathbf{a}(\theta,\phi) \tag{A-18}$$

$$\ddot{\mathbf{a}}_{u,v}(\theta,\phi) = \frac{d^2\mathbf{a}(\theta,\phi)}{du\,dv} = \mathbf{D}_u\,\mathbf{D}_v\,\mathbf{a}(\theta,\phi) \tag{A-19}$$

Note that the odd order derivatives are anti-symmetric whereas $\mathbf{a}(\theta,\phi)$ and the even order derivatives are symmetric. As a consequence the odd order derivatives are orthogonal to $\mathbf{a}(\theta,\phi)$. For example,

$$\mathbf{a}^H(\theta,\phi)\dot{\mathbf{a}}_v(\theta,\phi) = \mathbf{a}^H(\theta,\phi)\dot{\mathbf{a}}_u(\theta,\phi) = \mathbf{0} \tag{A-20}$$

where $\mathbf{0}$ is a MN × 1 vector of zeros and $(\cdot)^H$ denotes the complex conjugate transpose.

If the sources are closely spaced we may use the following Taylor series expansions to relate the two direction vectors:

$$\begin{aligned}\mathbf{a}(\theta_T,\phi_T) = \mathbf{a}(\theta_R,\phi_R) &+ \delta_u \dot{\mathbf{a}}_u(\theta_R,\phi_R) + \delta_v \dot{\mathbf{a}}_v(\theta_R,\phi_R) \\ &+ \frac{1}{2}\left(\delta_u^2 \ddot{\mathbf{a}}_u(\theta_R,\phi_R) + \delta_v^2 \ddot{\mathbf{a}}_v(\theta_R,\phi_R)\right) \\ &+ \delta_u\delta_v \ddot{\mathbf{a}}_{u,v}(\theta_R,\phi_R) + O\left(|\delta|^3\right)\end{aligned} \tag{A-21}$$

$$\begin{aligned}\mathbf{a}(\theta_R,\phi_R) = \mathbf{a}(\theta_T,\phi_T) &- \delta_u \dot{\mathbf{a}}_u(\theta_T,\phi_T) - \delta_v \dot{\mathbf{a}}_v(\theta_T,\phi_T) \\ &+ \frac{1}{2}\left(\delta_u^2 \ddot{\mathbf{a}}_u(\theta_T,\phi_T) + \delta_v^2 \ddot{\mathbf{a}}_v(\theta_T,\phi_T)\right) \\ &+ \delta_u\delta_v \ddot{\mathbf{a}}_{u,v}(\theta_T,\phi_T) + O\left(|\delta|^3\right)\end{aligned} \tag{A-22}$$

where

$$\delta_u = u_T - u_R = \sin\theta_T \cos\phi_T - \sin\theta_R \cos\phi_R \tag{A-23}$$

$$\delta_v = v_T - v_R = \sin\theta_T \sin\phi_T - \sin\theta_R \sin\phi_R \tag{A-24}$$

Subtracting the two Taylor series expressions yields

$$\begin{aligned}\mathbf{a}(\theta_T,\phi_T) - \mathbf{a}(\theta_R,\phi_R) = &\frac{\delta_u}{2}\left(\dot{\mathbf{a}}_u(\theta_T,\phi_T) + \dot{\mathbf{a}}_u(\theta_R,\phi_R)\right) + \frac{\delta_v}{2}\left(\dot{\mathbf{a}}_v(\theta_T,\phi_T) + \dot{\mathbf{a}}_v(\theta_R,\phi_R\right. \\ &+ \frac{\delta_u^2}{4}\left(\ddot{\mathbf{a}}_u(\theta_R,\phi_R) - \ddot{\mathbf{a}}_u(\theta_R,\phi_R)\right) + \frac{\delta_v^2}{4}\left(\ddot{\mathbf{a}}_v(\theta_R,\phi_R) - \ddot{\mathbf{a}}_v(\theta_R,\phi_R\right. \\ &+ \frac{\delta_u\delta_v}{2}\left(\ddot{\mathbf{a}}_{u,v}(\theta_R,\phi_R) - \ddot{\mathbf{a}}_{u,v}(\theta_T,\phi_T)\right) + O\left(|\delta|^3\right)\end{aligned} \tag{A-25}$$

For closely spaced sources δ_u and δ_v is small. In that event terms second order and higher may be discarded resulting in the approximation

$$\mathbf{a}(\theta_T,\phi_T) - \mathbf{a}(\theta_R,\phi_R) \approx \frac{\delta_u}{2}\left(\dot{\mathbf{a}}_u(\theta_T,\phi_T) + \dot{\mathbf{a}}_u(\theta_R,\phi_R)\right) + \frac{\delta_v}{2}\left(\dot{\mathbf{a}}_v(\theta_T,\phi_T) + \dot{\mathbf{a}}_v(\theta_R,\phi_R)\right) \tag{A-26}$$

A.4 Low Angle Specular Multipath

A.4.1 Array Parallel to Surface

For low angle specular multipath received by an array parallel to the surface at a height h, we have

$$\begin{aligned} Az_T &= Az_R = \phi_T = \phi_R \\ El_T &= \theta_T - \pi/2, \quad El_R = \theta_R - \pi/2, \quad El_T \neq El_R \end{aligned} \tag{A-27}$$

For this case δ_u and δ_v reduces to

$$\delta_u = u_T - u_R = \cos(Az)\left\{\cos(El_T) - \cos(El_R)\right\} \tag{A-28}$$

$$\delta_v = v_T - v_R = \sin(Az)\left\{\cos(El_T) - \cos(El_R)\right\} \tag{A-29}$$

Note that

$$\delta_u = \delta_v \tan(Az) \tag{A-30}$$

Hence, The Taylor series of equation (A-26) reduces to

$$\mathbf{a}(\theta_T,\phi_T) - \mathbf{a}(\theta_R,\phi_R) \approx \frac{\delta_v}{2}\left\{\tan(Az)\left(\dot{\mathbf{a}}_u(\theta_T,\phi_T) + \dot{\mathbf{a}}_u(\theta_R,\phi_R)\right) + \left(\dot{\mathbf{a}}_v(\theta_T,\phi_T) + \dot{\mathbf{a}}_v(\theta_R,\phi\right.\right. \tag{A-31}$$

As it is a relatively simple matter to estimate the azimuth of the multipath signal, the weight factor tan(Az) required to combine the column and row derivatives to form $\mathbf{a}(\theta_T,\phi_T)$ - $\mathbf{a}(\theta_R,\phi_R)$ is known *a priori*. The problem, though multidimensional, reduces to a form similar to the linear array problem.

Given a signal space vector $\mathbf{p}$ we can use the known target azimuth Az, the centro-Hermitian property of equation (A-7) along with the Taylor series expression of equation (A-31) to convert the vector $\mathbf{p}$ to $\mathbf{a}(\theta_T,\phi_T)$ - $\mathbf{a}(\theta_R,\phi_R)$, in a matter identical to the linear array case. The bisector between the two elevation angles could be found as part of a d-MUSIC grid search as before, or in the special case that the target height and range is much greater than the height of the array, the bisector is zero with the result that $El_R = -El_T$.

A.4.2 Array Perpendicular to Surface

For low angle specular multipath received by an array at a height h above the surface with its y-axis perpendicular to the surface and the array x-axis parallel to that of the surface frame we have

$$\begin{aligned} &Az_T = Az_R \\ &El_T \text{ and } El_R \text{ are both small} \end{aligned} \tag{A-32}$$

It follows from (A-11) that

$$\begin{aligned} &\tan\theta_T \cos\phi_T = \tan\theta_R \cos\phi_R \\ &\sin(El_T) = \sin\theta_T \sin\phi_T, \quad \longrightarrow El_T \approx \sin\theta_T \sin\phi_T \quad \text{is small} \\ &\sin(El_R) = \sin\theta_R \sin\phi_R, \quad \longrightarrow El_R \approx \sin\theta_R \sin\phi_R \quad \text{is small} \end{aligned} \tag{A-33}$$

In order for (A-33) to hold we require that $\theta_T \approx \theta_R$ and that both ϕ_T and ϕ_R are small (necessary in order for the sources to nearly lie in the x-z plane). In that event we can use the approximation

$$\begin{aligned} &u_T \approx u_R \\ &\delta_u = u_T - u_R \approx 0 \end{aligned} \tag{A-34}$$

The Taylor series of equation (A-26) reduces to

$$\mathbf{a}(\theta_T,\phi_T) - \mathbf{a}(\theta_R,\phi_R) \approx \frac{\delta_v}{2}\left(\dot{\mathbf{a}}_v(\theta_T,\phi_T) + \dot{\mathbf{a}}_v(\theta_R,\phi_R)\right) \tag{A-35}$$

and the problem only depends on the column derivatives.

Like the previous case of an array parallel to the surface, the problem of converting a signal space vector $\mathbf{p}$ to $\mathbf{a}(\theta_T,\phi_T)$ - $\mathbf{a}(\theta_R,\phi_R)$ is analogous to the linear array problem. We need only use the centro-Hermitian property of equation (A-7), the Taylor series expression of equation (A-35) along with the angle of the source bisector. This bisector could be found as part of a d-MUSIC grid search or in the special case that the target height and range is much larger than the array height, the bisector is zero with the result that $El_R = -El_T$.

B Cramér-Rao Bound Derivation

B.1 Preamble

When the center line between the direct and surface reflected rays is known, the problem reduces to estimating one parameter, the source spacing. Stoica and Nehorai [10] developed a general formulation to estimate the Cramér-Rao Bound (CRB) for the general beamforming problem of estimating the direction-of-arrival of multiple emitters. The problem of estimating the spacing between two sources when the geometric center of the cluster is known is really a special case of this general problem. As such the Stoica and Nehorai formulation is easily modified to calculate the CRB for this problem.

As only a few changes are required to adapt the method of [10] to this problem we will only present a brief review of the technique and list the required modifications. To facilitate reference to [10] we will adopt its notation to derive the CRB. The final step is the conversion of the CRB expression to the notation of this thesis.

B.2 Problem Statement

The following is a partial list of notation used in [10]:

A^T	the transpose of matrix A
A^+	the conjugate of A
A^*	the conjugate transpose of A
$\overline{A}$	the real part of A
$\tilde{A}$	the imaginary part of A
ω	Sensor-to-sensor phase shift
$d(\omega) = da(\omega)/d\omega$	Equivalent to $\mathbf{Da}(\theta)$ in this thesis

In [10] the direction finding problem is formulated as

$$y(t) = A(\theta)x(t) + e(t), \quad t = 1, 2, \cdots, N \tag{B-1}$$

where

N	Number of samples (snapshots)
n	Number of signals
m	Number of sensors
$\theta = [\omega_1 \ldots \omega_n]^T$	$n \times 1$ vector denoting the value of ω for each source
y(t)	$m \times 1$ array snapshot vector
e(t)	$m \times 1$ zero-mean Gaussian noise vector with variance σ
x(t)	$n \times 1$ vector of signal amplitudes
$A(\theta) = [a(\omega_1) \ldots a(\omega_n)]^T$	set of steering vectors

and $P = E\, x(t)\, x^*(t)$ is the signal covariance matrix where E is the statistical expectation operator.

In Appendix E of [10] Stoica and Nehorai developed a general expression for CRB(θ), the Cramér-Rao Bound for θ. In this problem $\theta = [\omega \ -\omega]^T$ and the problem reduces to estimating ω, half the source spacing. Hence, we want to estimate CRB(ω), the Cramér-Rao Bound for ω.

Stoica and Nehorai considered the case of zero-mean Gaussian sensor noise with variance σ and derived an expression for the Fisher information matrix based on the log-likelihood function (ln L). Employing a standard technique to invert a partitioned matrix, the Fisher matrix is inverted to derive CRB(θ). This same technique will be used to derive an expression for CRB(ω).

B.3 List of Modifications to Derive the CRB

Define dA/dω as

$$D_\omega = \frac{\partial A}{\partial \omega} = \left[d(\omega)\, d^{+}(\omega) \right] \tag{B-2}$$

The log-likelihood function derivative of Equation (E.2.d) of [10] is changed to

$$\begin{aligned} \frac{\partial \ln L}{\partial \omega} &= \frac{-1}{\sigma} \sum_{t=1}^{N} \frac{\partial}{\partial \omega} \left\{ \left[y^*(t) - x^*(t) A^* \right] \left[y(t) - x(t) A \right] \right\} \\ &= \frac{1}{\sigma} \sum_{t=1}^{N} \left\{ x^*(t) D_\omega^* e(t) + e^*(t) D_\omega x(t) \right\} \\ &= \frac{2}{\sigma} \sum_{t=1}^{N} \mathrm{Re} \left\{ x^*(t) D_\omega^* e(t) \right\} \end{aligned} \tag{B-3}$$

The next 3 equations are the modifications to equation (E.8) of [10] relating to the entries of the Fisher matrix. Equation (E.8.d) of [10] is changed to

$$\begin{aligned} E \frac{\partial \ln L}{\partial \bar{x}(k)} \frac{\partial \ln L}{\partial \omega} &= E \left(\frac{2}{\sigma} \mathrm{Re} \left[A^* e(k) \right] \right) \left(\frac{2}{\sigma} \sum_{t=1}^{N} \mathrm{Re} \left\{ x^*(t) D_\omega^* e(t) \right\} \right) \\ &= E \left(\frac{1}{\sigma} \left[A^* e(k) + A^T e^{+}(k) \right] \right) \left(\frac{1}{\sigma} \sum_{t=1}^{N} \left\{ x^*(t) D_\omega^* e(t) + e^*(t) D_\omega x(t) \right\} \right) \\ &= E \left(A^* e(k) e^*(k) D_\omega x(k) + A^T e^{+}(k) e^T(k) D_\omega^{+} x^{+}(k) \right) \\ &= \frac{2}{\sigma} \mathrm{Re} \left[A^* D_\omega x(k) \right] \end{aligned} \tag{B-4}$$

Equation (E.8f) of [10] is changed to

$$E\frac{\partial \ln L}{\partial \tilde{x}(k)}\frac{\partial \ln L}{\partial \omega} = E\left(\frac{2}{\sigma}\mathrm{Im}[A^{*}e(k)]\right)\left(\frac{2}{\sigma}\sum_{t=1}^{N}\mathrm{Re}\left\{x^{*}(t)D_{\omega}^{*}e(t)\right\}\right) \tag{B-5}$$

$$= E\left(\frac{1}{\sigma}\left[-iA^{*}e(k) + iA^{T}e^{+}(k)\right]\right)\left(\frac{1}{\sigma}\sum_{t=1}^{N}\left\{x^{*}(t)D_{\omega}^{*}e(t) + e^{*}(t)D_{\omega}x(t)\right\}\right)$$

$$= E\left(-iA^{*}e(k)e^{*}(k)D_{\omega}x(k) + iA^{T}e^{+}(k)e^{T}(k)D_{\omega}^{+}x^{+}(k)\right)$$

$$= \frac{2}{\sigma}\mathrm{Im}\left[A^{*}D_{\omega}x(k)\right]$$

Equation (E.8g) of [10] is changed to

$$E\frac{\partial \ln L}{\partial \omega}\frac{\partial \ln L}{\partial \omega} = E\left(\frac{2}{\sigma}\sum_{t=1}^{N}\mathrm{Re}\left\{x^{*}(t)D_{\omega}^{*}e(t)\right\}\right)\left(\frac{2}{\sigma}\sum_{s=1}^{N}\mathrm{Re}\left\{x^{*}(s)D_{\omega}^{*}e(s)\right\}\right) \tag{B-6}$$

$$= E\left(\frac{1}{\sigma^{2}}\sum_{t=1}^{N}\sum_{s=1}^{N}\left\{x^{*}(t)D_{\omega}^{*}e(t)e^{*}(s)D_{\omega}x(s) + x^{*}(s)D_{\omega}^{*}e(s)e^{*}(t)D_{\omega}x(t)\right\}\right)$$

$$= E\left(\frac{1}{\sigma^{2}}\sum_{t=1}^{N}\left\{x^{*}(t)D_{\omega}^{*}e(t)e^{*}(t)D_{\omega}x(t) + x^{*}(t)D_{\omega}^{*}e(t)e^{*}(t)D_{\omega}x(t)\right\}\right)$$

$$= \frac{1}{\sigma}\sum_{t=1}^{N}\left\{x^{*}(t)D_{\omega}^{*}D_{\omega}x(t) + x^{*}(t)D_{\omega}^{*}D_{\omega}x(t)\right\}$$

$$= \frac{2}{\sigma}\sum_{t=1}^{N}\mathrm{Re}\left[x^{*}(t)D_{\omega}^{*}D_{\omega}x(t)\right]$$

$$= \Gamma$$

One of the notations immediately following equation (E.8) is redefined as

$$\Delta_{k} = \frac{2}{\sigma}A^{*}D_{\omega}x(k) \tag{B-7}$$

Using the same procedure as outlined in equations (E.9) to (E.11) of [10] the partitioned Fisher matrix can be inverted to yield the following expression for CRB(ω)

$$\begin{aligned}
CRB^{-1}(\omega) &= \Gamma - \sum_{t=1}^{N} Re\left\{ \Delta_t^* \left(\frac{2}{\sigma} A^* A \right)^{-1} \Delta_t \right\} \\
&= \frac{2}{\sigma} \sum_{t=1}^{N} \left\{ Re\left[x^*(t) D_\omega^* D_\omega x(t) \right] - Re\left[x^*(t) D_\omega^* A (A^* A)^{-1} A^* D_\omega x(t) \right] \right\} \\
&= \frac{2}{\sigma} \sum_{t=1}^{N} \left\{ Re\left[x^*(t) D_\omega^* D_\omega x(t) - x^*(t) D_\omega^* A (A^* A)^{-1} A^* D_\omega x(t) \right] \right\} \\
&= \frac{2}{\sigma} \sum_{t=1}^{N} \left\{ Re\left[x^*(t) D_\omega^* \left[I - A (A^* A)^{-1} A^* \right] D_\omega x(t) \right] \right\} \\
&= \frac{2}{\sigma} \sum_{t=1}^{N} \left\{ Re\left[x^*(t) H x(t) \right] \right\} \\
&= \frac{2}{\sigma} Re\left[\begin{bmatrix} 1 & 1 \end{bmatrix} \left\{ H \bullet \sum_{t=1}^{N} \left\{ x^+(t) x^T(t) \right\} \right\} \begin{bmatrix} 1 \\ 1 \end{bmatrix} \right]
\end{aligned} \tag{B-8}$$

where A • B denotes the Hadamard (element-by-element) product of matrices A and B and

$$H = D_\omega^* \left[I - A (A^* A)^{-1} A^* \right] D_\omega \tag{B-9}$$

Note that

$$\lim_{N \to \infty} \frac{1}{N} \sum_{t=1}^{N} \left\{ x^+(t) x^T(t) \right\} = P^T \tag{B-10}$$

Thus the asymptotic CRB for sufficiently large N is

$$CRB^{-1}(\omega) = \frac{2N}{\sigma} Re\left[\begin{bmatrix} 1 & 1 \end{bmatrix} \left\{ H \bullet P^T \right\} \begin{bmatrix} 1 \\ 1 \end{bmatrix} \right] \tag{B-11}$$

Finally,

$$CRB(\omega) = \left(\frac{\sigma}{2N} \right) / Re\left[\begin{bmatrix} 1 & 1 \end{bmatrix} \left\{ H \bullet P^T \right\} \begin{bmatrix} 1 \\ 1 \end{bmatrix} \right] \tag{B-12}$$

B.4 Conversion to Thesis Notation

The CRB for the error in estimating γ, half the source spacing is

$$\mathrm{CRB}(\gamma) = \left(\frac{\sigma^2}{2K}\right) / \mathrm{Re}\left[\begin{bmatrix}1 & 1\end{bmatrix}\left\{\mathbf{H} \bullet \mathbf{S}^T\right\}\begin{bmatrix}1\\1\end{bmatrix}\right] \tag{B-13}$$

where K is the number of snapshots, S is the signal covariance matrix, σ^2 is the noise variance and

$$\mathbf{H} = \mathbf{D}_\gamma^H\left[\mathbf{I} - \mathbf{A}(\mathbf{A}^H\mathbf{A})^{-1}\mathbf{A}^H\right]\mathbf{D}_\gamma \tag{B-14}$$

with

$$\mathbf{A} = \left[\mathbf{a}(\gamma)\,\mathbf{a}(-\gamma)\right] \tag{B-15}$$

$$\mathbf{D}_\gamma = \frac{d\mathbf{A}}{d\gamma} = \left[\mathbf{D}\mathbf{a}(\gamma)\,(\mathbf{D}\mathbf{a}(\gamma))^*\right] = \left[\dot{\mathbf{a}}(\gamma)\,(\dot{\mathbf{a}}(\gamma))^*\right] \tag{B-16}$$